DOCTORAL DISSERTATION IN ODONTOLOGY

DAVID SOTO PEÑALOZA

ON EFFECT OF TWO DISTINCT IMPLANT MACRO-DESIGNS ON THE OSSEOINTEGRATION OF BICORTICALLY INSTALLED IMPLANTS IN TWO TOPOGRAPHIC SITES. A HISTOMORPHOMETRIC STUDY IN RABBIT TIBIAE

DOCTORAL PROGRAM IN ODONTOLOGY
STOMATOLOGY DEPARTMENT
FACULTY OF MEDICINE AND DENTISTRY
UNIVERSITY OF VALENCIA

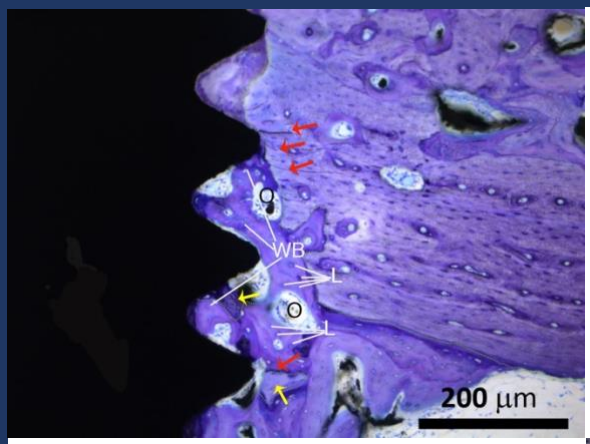

CIRU BUCA
Oral Surgery & Implantology

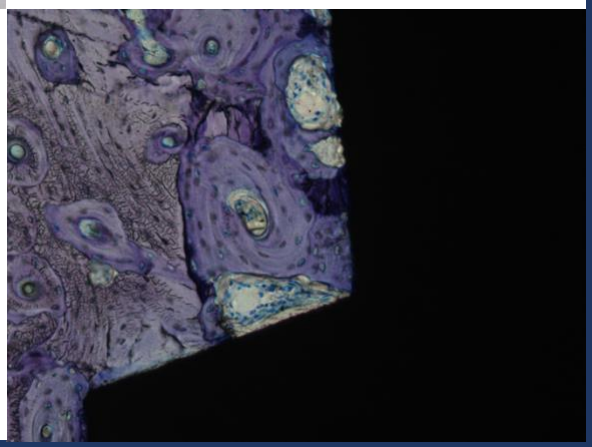

VNIVERSITAT DE VALÈNCIA

DIRECTORS

DR. JOSE VIÑA ALMUNIA
DR. DAVID PEÑARROCHA OLTRA
PROF. DR. JOSÉ JAVIER MARTÍN DE LLANO

Departamento de Estomatología
Facultad de Medicina y Odontología
Universitat de València

EFFECT OF TWO DISTINCT IMPLANT MACRO-DESIGNS ON THE OSSEOINTEGRATION OF BICORTICALLY INSTALLED IMPLANTS IN TWO TOPOGRAPHIC SITES. A HISTOMORPHOMETRIC STUDY IN RABBIT TIBIAE

DOCTORAL PROGRAM IN ODONTOLOGY

(Cod:3143; regulated by RD 99/2011 of January 28th)

DAVID REYNALDO SOTO PEÑALOZA

DIRECTORS

DR. JOSÉ VIÑA ALMUNIA

DR. DAVID PEÑARROCHA OLTRA

PROF. DR. JOSÉ JAVIER MARTÍN DE LLANO

Valencia, July 2019

Departamento de Estomatología
Facultad de Medicina y Odontología
Universitat de València

VNIVERSITAT DE VALÈNCIA

D. David Peñarrocha Oltra, Profesor Ayudante Doctor de Cirugía Bucal de la Facultad de Medicina y Odontología de la Universitat de València.

D. José Viña Almunia, Profesor Asociado de Cirugía Bucal, Departamento de Estomatología de la Facultad de Medicina y Odontología de la Universitat de València.

D. José Javier Martín de Llano, Profesor Titular de la Unidad de Histología, Departamento de Patología de la Facultad de Medicina y Odontología de la Universitat de València.

CERTIFICAN:

Que la presente memoria, titulada "EFFECT OF TWO DISTINCT IMPLANT MACRO-DESIGNS ON THE OSSEOINTEGRATION OF BICORTICALLY INSTALLED IMPLANTS IN TWO TOPOGRAPHIC SITES. A HISTOMORPHOMETRIC STUDY IN RABBIT TIBIAE", corresponde al trabajo realizado bajo nuestra dirección por D. David Reynaldo Soto Peñaloza, para su presentación como Tesis Doctoral en el Programa de Doctorado en Odontología de la Universitat de València.

Y para que conste firma/n el presente certificado en Valencia, a 19 de Julio de 2019

Fdo. José Viña Almunia

Fdo. David Peñarrocha Oltra

Fdo. José Javier Martín de Llano

AGRADECIMIENTOS

El proceso del conocimiento científico, desde la concepción de una idea hasta el poder materializarla y comunicarla es un arduo y dinámico proceso, que sólo puede lograrse con el respaldo de un constante trabajo en equipo y los valores de personas íntegras que aman lo que hacen.

" Si he podido ver más allá es porque me subí a hombros de gigantes" Isaac Newton

-Estos son mis gigantes:

El Prof. Dr. Miguel Peñarrocha Diago, quien ha sido como un padre durante estos últimos años, muchas gracias por su amistad, confianza y respaldo, por su constante motivación y sabias enseñanzas de vida, por ser quien ha sabido sacar de mí el potencial para iniciarme como investigador bajo su tutoría.

El Dr. David Peñarrocha Oltra, por su amistad verdadera, por sus sabias enseñanzas y juicio crítico con cada uno de los avances que he ido realizando, sin duda he sido afortunado de contar con él como tutor científico en los últimos 4 años. Por ser él la primera persona quien me abrió el camino para realizar esta Tesis Doctoral, sin su apoyo nada de esto hubiese sido posible.

El Dr. José Viña Almunia "Pepe", por su gran amistad y sencillez, por compartir conmigo durante todo este período de investigación preclínica el trabajo de campo, por su asesoría científica, por su espíritu crítico casi perfeccionista, que han sabido llevar a buen puerto los proyectos empezados como mucha "sinergia".

El Prof. Dr. José Javier Martín de Llano, por brindarme su amistad, por su sencillez y paciencia durante todo el proceso de este arduo trabajo, sus pautas y enseñanzas han sido esenciales para la correcta interpretación de los resultados, y el éxito de este proyecto, que se basa en los hallazgos del análisis histológico.

El Prof. Dr. José Manuel Almerich Silla, por su amistad y respeto, por ser él quien como Director del Máster de Ciencias Odontológicas me asignó la realización del Trabajo de Fin de Máster en la Unidad de Cirugía Bucal, de no haber sido por este primer evento, quizás nada de lo que hoy es, hubiese sucedido. Muchas gracias por todo.

La Prof.ª Dra. Mª Carmen Carda Batalla, por su amistad y sencillez, por sus pautas y enseñanzas, por todas las facilidades que me ha brindado para poder desarrollar esta Tesis Doctoral en el Departamento de Patología de la Universitat de València. Así como a todo el equipo de esta unidad entre ellos, Lara, Manolo y Rubén por su amistad y apoyo en este proyecto.

El Prof. Dr. Danielle Botticelli de la academia ARDEC, por su amistad, respeto y confianza, por sus enseñanzas en la investigación preclínica desde la etapa inicial de este proyecto, por su soporte científico y perspectiva crítica en el reporte de los resultados, y por compartir momentos de trabajo arduo durante las estancias realizadas en Rimini, su hospitalidad y amistad me hicieron sentir como en casa.

El. Prof. Dr. Marco Caneva, por sus enseñanzas durante la fase experimental de este trabajo, sin duda es un verdadero honor poder contar con su soporte y experiencia.

La Prof.ª Dra. María Peñarrocha Diago, por su valiosa amistad, confianza, cariño y apoyo durante esta importante etapa de mi vida.

La Dra. Berta García Mira, por ser tan cercana, por su amistad y su soporte clínico durante cada una de las mañanas durante la conducción de este trabajo. Muchas gracias por todo.

La Dra. Ana Díaz, y todo el equipo de trabajo de la UCIM de la Universitat de València, por el gran soporte durante los procedimientos quirúrgicos y cuidados pre- y post- operatorios, garantizando en todo momento las buenas prácticas y principios éticos del presente trabajo.

Los profesores y compañeros de la Unidad de Cirugía Bucal: Hilario, Amparo, Paula, Marian, Javi, Juan, Luis, Juancho, Isa, José Balaguer, Regi, Julio, Oscar, Fer, María S, Javier, María D, Juan Carlos, Pablo, Toni, Álvaro, por su amistad y cariño durante estos últimos años. Así como Dña. Rosario, Dña. Inma y Dña. María José, por su apoyo en la organización logística durante el desarrollo del estudio. Así como el Sr. D. Rafael Gálvez de la Secretaría del Departamento de Estomatología por su gran ayuda y orientación en todo momento en las gestiones administrativas.

Mi compañeros y amigos de estudio "*marenostrum*", en especial Priscilla, Manu, Andrés, Daniela y Alex, por su amistad y cariño, y por compartir sus sueños e ideales durante estos años de Doctorado.

- *De forma especial mencionar a mis gigantes emocionales*.

Mis buenos amigos y seres queridos, José, Miriam, Jorge, Richard, Javi, Noe, Zaira, Emilio, Daniel, muchas gracias por su amistad, cariño y todos los momentos que hemos compartido estos años, por hacernos sentir parte de su familia, su constante motivación y cariño.

Galo y Marita, mis tíos queridos, sus sabios consejos y amor han sido determinantes en mi vida. Esther, mi madrina, por su cariño y consejos de superación. Al tío Reynaldo por su cariño y buenos consejos. A mis primos hermanos Micky, María Esther, Leo, Luigi, Reynaldito, Nikolais, Galo, Alexis y María Pía por su amor y verdadera amistad.

El Sr. Pedro y la Sra. Rosario, Pierina, Pedrito, Ariadna, Alessandra y Amir, por su amistad, amor y apoyo durante estos años. Gracias por sus consejos y enseñanzas de vida.

Mi núcleo familiar, las personas mas importantes de mi vida, mis padres Rebeca y Toño, por su amor incondicional, mi aliciente y ejemplo en cada una de las metas trazadas. Mis hermanas Becky y Daniela, por todo su amor, por los valores y ejemplo de superación constantes que de buena forma siempre me han sabido transmitir. A mi hermano José Antonio, por su amistad y cariño.

Jacqueline mi esposa, amiga y compañera, por su paciencia y amor durante todos estos años tan sacrificados al lado de nuestros amados hijos Esteban y Amanda, lo más importante y grande de nuestras vidas, de ustedes he aprendido a ser cada día una mejor persona, gracias por su infinito amor y por estar siempre a mi lado.

Los que ya no están físicamente, sin embargo dentro mí llevo lo mejor de ustedes, gracias por sus enseñanzas de vida y por estar conmigo en el alma y el corazón, ustedes mis amados abuelos Reynaldo y Esther, y queridos tíos Rocío, Ricardo, César, Lucha. Se que estarían muy contentos y orgullosos.

Dedicado

a mis padres

a mi familia

a mi compañera y amiga Jacqueline

a mi razón de ser, Amanda y Esteban

a todos los que confiaron en mí

a los que me ofrecieron su valiosa amistad

a los que estuvieron, y siempre estarán en mi corazón

a todos ustedes

La amabilidad en palabras crea confianza,
La amabilidad en pensamientos crea bondad,
La amabilidad en actos crea amor

Lao-Tsé 490 A.C.

Abbreviations

BIC	Bone-to-implant contact
BMP	Bone morphogenetic protein
BMU	Basic multicellular unit
CaP	Calcium phosphate
DC-Stamp	Dendrocyte-expressed seven transmembrane protein
FGF	Fibroblastic growth factor
GLAST	Glutamate transport by transporters
HA	Hydroxyapatite
HVC	Haversian canal
IGF	Insulin growth factor
LB	Lamellar bone
LL	Lamellae
M-CSF	Macrophage colony-stimulating factor
NFATc1	Nuclear factor of activated T cells 1
OBM	Organic bone matrix
OSCAR	Osteoclast-associated, immunoglobulin-like receptor
PGE2	Prostaglandin-E2
PGI2	Prostacyclin
RANKL	Receptor activator of nuclear factor kappa-B ligand
SLA	Sandblasted/acid etched
Src	Proto-oncogene tyrosine-protein kinase
TGF-B	Transforming growth factor beta
WB	Woven bone
3 integrin	Alpha (v) beta (3) integrin

I. RESUMEN 19
1. INTRODUCTION 33

2. RATIONALE AND STUDY AIMS 37

2.1 RATIONALE 39
2.2 STUDY AIMS 40
2.2.1 MAIN OBJECTIVE 40
2.2.2 SPECIFIC OBJECTIVES 40
THE SPECIFIC OBJECTIVES OF THE PRESENT THESIS WERE: 40

3. STUDY HYPOTHESES 41

4. LITERATURE REVIEW 45

4.1 BASIC BONE BIOLOGY DURING OSSEOINTEGRATION OF TITANIUM DENTAL IMPLANTS 47
4.1.1 THE BONE TISSUE 47
4.1.2 BONE RESPONSE TO DENTAL IMPLANTS 47
4.1.3 BASIC ASPECTS OF BONE BIOLOGY AND ARCHITECTURE 48
4.2 BASIC BONE ANATOMY 49
4.2.1 WOVEN BONE 50
4.2.2 LAMELLAR BONE 50
4.2.3 BONE REMODELING 51
4.2.4 BONE CELLS 52
4.3 THE PHENOMENON OF OSSEOINTEGRATION: STAGES OF THE PERI-IMPLANT HEALING PROCESS 56
4.3.1 CONTACT OSTEOGENESIS: OSTEOCONDUCTION AND *DE NOVO* BONE FORMATION. 57
58
4.3.2 EARLY EVENTS DURING OSSEOINTEGRATION 60
4.3.3 A GLANCE TO DYNAMICS OF OSTEOINTEGRATION OF TITANIUM DENTAL IMPLANTS 62

5. MATERIAL AND METHODS 65

5.1 ETHICAL DECLARATION FOR ANIMAL EXPERIMENTATION 67
5.2 STUDY DESIGN AND EXPERIMENTAL ANIMALS 67
5.3 RANDOMIZATION AND ALLOCATION CONCEALMENT 67
67
5.4 IMPLANT FEATURES 68
5.5 SURGICAL PROCEDURES 68
5.6 POST-OPERATIVE CARE, HOUSING AND HUSBANDRY 69
5.7 EUTHANASIA 70
5.8 HISTOLOGICAL PREPARATION 70
5.9 HISTOLOGICAL EXAMINATION 70
5.10 STUDY VARIABLES 71
5.10.1 NEW OSSEOINTEGRATION VALUES 71
5.10.1 CORTICAL AND MARROW COMPARTMENTS 71
5.11 DATA ANALYSIS 72

6. RESULTS 73

6.1 SEQUENTIAL HEALING DURING OSSEOINTEGRATION OF IMPLANTS WITH RBM SURFACES 75
6.1.1 CLINICAL AND HISTOLOGICAL OUTCOMES 75
6.1.2 WEEK 2 75

76

6.1.3 WEEK 4 77
6.1.4 WEEK 8 78
6.2 THE EFFECT OF IMPLANT MACRO-DESIGN ON OSSEOINTEGRATION 80
6.3 THE EFFECT OF TOPOGRAPHIC SITE ON OSSEOINTEGRATION 82
6.4 THE EFFECT OF IMPLANT MACRO-DESING REGARDING TOPOGRAPHIC SITE ON OSSEOINTEGRATION 85
6.5 THE BONE-HEALING PATTERN AT THE CORTICAL AND MARROW COMPARTMENTS IN THE DIAPHYSIS AND METAPHYSIS OF RABBIT´S TIBIAE 88

7. DISCUSSION 93

7.1 EFFECT OF TWO DISTINCT IMPLANT DESIGN WITH EQUAL RBM SURFACE TREATMENT ON OSTEOINTEGRATION 95
7.2 BONE HEALING PATTERNS AT CORTICAL AND MARROW COMPARTMENT 97
7.3 EFFORTS, LIMITATIONS AND FUTURE TRENDS 99

8. CONCLUSIONS 101

9. REFERENCES 105

10. LIST OF FIGURES AND TABLES 115

10.1 LIST OF FIGURES 117
10.2 LIST OF TABLES 120

11. SCIENTIFIC PUBLICATIONS 121

11.1 SCIENTIFIC DOCUMENTS DERIVED FROM THE PRESENT THESIS 123

12. ENGLISH ABSTRACT 125

RESUMEN

Antecedentes científicos y objetivos de estudio

El uso de implantes dentales como alternativa para la rehabilitación oral ha demostrado su eficacia y mostrando altas tasas de supervivencia. Un aspecto clave de la osteointegración del implante dental está relacionado con la obtención de una estabilidad primaria adecuada, asegurada por el enclavamiento mecánico entre el tejido óseo y la interfaz del implante, la cual depende en parte de la geometría del implante, la rugosidad de la superficie y la técnica quirúrgica para la preparación del lecho implantario. Varios factores están involucrados en la interacción entre la superficie del implante y el hueso nativo circundante durante la osteointegración. Uno de ellos es el macro-diseño del implante, que puede proporcionar diferentes esfuerzos de corte dependiendo de la densidad ósea del sitio de inserción. De acuerdo con sus características, el macro-diseño del implante podría afectar en mayor o menor medida el estrés producido en el hueso, provocando una respuesta del huésped que induce eventos vasculares y celulares, que causan una remodelación ósea interfacial mediada por células. Esta consiste en la reabsorción del "hueso cortical" mineralizado, y por consiguiente, en una "disminución de la estabilidad primaria", que concurre de forma simultánea con una nueva aposición ósea hacia la superficie del implante o aumento de la "estabilidad secundaria" o biológica. Se han propuesto diferentes diseños de rosca de implantes y pasos de rosca para mejorar la osteointegración. En este sentido, la geometría del implante puede afectar los valores de contacto hueso a implante (BIC). La macro-geometría modificada y las diferentes microgeometrías del implante han demostrado tener un efecto estimulante sobre la osteointegración, lo que sugiere que sus características deben estar relacionadas con el microentorno biológico y mecánico. Además, otras características, como el diseño de la cámara de curación y las configuraciones de la zona apical, han demostrado mejorar la osteointegración.

El macro-diseño de los implantes dentales a menudo se complementa con la modificación de la superficie de titanio para mejorar su bioactividad y la capacidad de retención de coágulos durante la osteointegración. Estas modificaciones aumentan de forma tridimensional el área de superficie y confieren diferentes características topográficas para facilitar la atracción de células. La rugosidad de la superficie se cuantifica y se informa como Ra o Sa, dependiendo de si el parámetro se clasifica como bidimensional o tridimensional respectivamente. Esta rugosidad proporciona una activación mejorada de las plaquetas, la adhesión celular y la adsorción de proteínas hacia la superficie del implante, con efectos en el proceso de osteointegración en términos de BIC y estabilidad del implante durante las etapas tempranas de curación a través de un aumento de la actividad

osteogénica y la osteoconductividad del titanio. Se han propuesto varios métodos para el tratamiento de la superficie del titanio (por ejemplo superficies grabadas, superficies pulidas con chorro de arena y grabadas con ácido, superficies recubiertas con hidroxiapatita, superficies pulidas con chorro de arena y ablación con láser, superficies con tratamiento de fluoruro). Entre ellos, la superficie del medio chorreado reabsorbible (RBM) se obtiene a través del arenado de alta velocidad con partículas de fosfato de calcio biocerámico (CaP), en la que el tamaño de partícula determina tanto el grado de rugosidad, como una superficie de titanio libre de partículas. Las superficies RBM han mostrado valores BIC comparables a otras superficies, como el dióxido de titanio (TiO2) u óxido de aluminio (Al2O3), obteniendo mediciones de resistencia biomecánica y torque de extracción similares a los obtenidos en implantes mejorados con calcio y magnesio.

Evidencia científica reciente refuerza el concepto de que la geometría del implante y la densidad del hueso son factores clave involucrados en el grado de estabilidad primaria. Sin embargo, la osteointegración está fuertemente influenciada por la superficie del implante, que desempeña un papel importante durante la fase temprana de la curación del tejido a través de eventos de resorción y aposición ósea. A este respecto, los diferentes sitios topográficos confieren diferentes patrones de curación, como los que ocurren en los compartimentos cortical y medular tanto en los huesos planos (mandíbula de perro) como en los huesos largos (tibia de oveja). Este comportamiento también se observa en tibias de conejo, y a pesar de las diferencias inherentes en los modelos experimentales, se han probado los efectos de geometrías de implantes iguales, pero con diferentes modificaciones en la superficie, y se evidencia el efecto del tratamiento de la superficie en los valores BIC reportados. Por lo tanto, es presumible que tanto los compartimentos corticales como los de la médula ósea tengan características biológicas y físicas distintas en el remodelado interfacial hueso-implante y la aposición ósea directa sobre la superficie de titanio. Su naturaleza delimita la transición de la estabilidad primaria a la estabilidad secundaria o biológica, que concurre de forma simultánea a la caída de la estabilidad primaria del implante durante el proceso de osteointegración. Sin embargo, hay una escasez de datos basados en implantes con diferentes macro-diseños e igual rugosidad de la superficie instalados de forma bicortical, así como también una falta de estudios respecto al patrón de curación ósea sobre la superficie del implante en diferentes compartimentos y entornos óseos. Sobre la base de los aspectos antes mencionados, y la brecha de información a este respecto, el objetivo general de esta tesis es mejorar el entendimiento de los valores de osteointegración (hueso nuevo, hueso viejo, médula ósea y BIC [hueso nuevo + hueso viejo]) de dos macro-diseños de implantes diferentes, con similar tratamiento de superficie RBM en diferentes sitios topográficos en tibias de conejo (diáfisis o metáfisis). Por lo tanto, los siguientes objetivos se

desagregaron de este objetivo principal, para explotar con más detalle la muestra de estudio, como se muestra a continuación:

I. Documentar la curación secuencial durante la osteointegración de implantes con tratamiento de superficie RBM a las 2, 4 y 8 semanas en conejos.
II. Evaluar el efecto de dos macro-diseños de implantes diferentes en los valores de la osteointegración secuencial a las 2, 4 y 8 semanas.
III. Evaluar el efecto de diferentes sitios topográficos en la osteointegración en tibias de conejo.
IV. Evaluar el efecto del macro-diseño de implantes respecto al sitio topográfico en la osteointegración en tibias de conejo.
V. Evaluar el patrón de curación ósea en los compartimentos cortical y medular en la diáfisis y la metáfisis en tibias de conejo.

Material y métodos

El protocolo de estudio fue aprobado por el Comité de Ética de la Universidad de Valencia, Valencia, España (Protocolo ref .: A1432625410189), que siguió las pautas establecidas por la Directiva del Consejo de la Unión Europea (53/2013; 1 de febrero de 2013) para el cuidado de animales y experimentación de acuerdo con las condiciones éticas y legales establecidas por el Real Decreto 223, 14 de marzo y 13 de octubre de 1988.

-Diseño del estudio

El presente estudio experimental preclínico incluyó veintisiete conejos machos albinos de Nueva Zelanda, con 24 semanas de edad media y un peso de 3 a 4 kg. Los animales se asignaron en tres grupos compuestos de 9 animales cada uno, y que fueron sacrificaron a las 2, 4 y 8 semanas, respectivamente. Antes de la cirugía, los animales fueron asignados de forma aleatorizada a uno de los tres grupos en función del período de curación. Los implantes se colocaron siguiendo una asignación aleatoria, lo que resultó en la colocación de cuatro implantes dentales en cada conejo; dos en cada tibia, uno en la diáfisis y la otro en la metáfisis, cada uno con un macro-diseño diferente. La asignación aleatoria fue realizada electrónicamente (www.randomization.com) por un autor independiente que no participó en la selección de los animales ni en los procedimientos quirúrgicos (Danielle Botticelli). Los dos distintos macro-diseños utilizados fueron implantes Ticare® (Mozo-Grau, Valladolid, España) hechos de titanio comercialmente puro de grado IV, tratados con un medio arenado reabsorbible (RBM) (la superficie del implante es chorreada con partículas biocerámicas de fosfato de calcio, lo que resulta en una superficie de rugosidad moderada [Ra = 1.53 ± 0.24]). Los implantes disponen una dimensión de 3,75 mm de diámetro y 8 mm de

longitud, una conexión cónica con un cuello pulido de 45 ° y una capacidad de corte autorroscante en la proximidad del ápice.

Ticare Inhex® : el cuerpo del implante tiene poca conicidad y una gran área de micro espiras en la porción coronal, posee un mayor número de hilos de rosca triangular por unidad de longitud con poca profundidad de hilo respecto al modelo Quattro® . El implante muestra un doble corte autorroscante en la porción apical.

Ticare Inhex Quattro® : el cuerpo del implante tiene una marcada conicidad. Presenta menor cantidad de micro espiras en la porción coronal y un menor número de macro espiras por unidad de longitud en comparación con los implantes Ticare Inhex® . Las espiras son forma cuadrada en la parte media del implante, y se tornan triangulares y profundas hacia la parte apical. El implante muestra un corte autorroscante más agresivo.

-Procedimientos clínicos.

Los conejos se anestesiaron con una inyección intramuscular de ketamina (22 mg/kg) y xilazina (2,5 mg/kg) al 50%, y se les administró una inyección endovenosa de propofol (1,5 mg/kg), la anestesia se mantuvo con isofluorano al 2%. Antes de la cirugía, la piel de la tibia proximal se afeitó y se desinfectó con Betadine. Se administró un antibiótico pre operatorio por vía subcutánea Enrofloxacino 5 mg/Kg (ALSIR® 2,5%, Esteve Veterinaria, Barcelona, España), así como 3 ml de articaína al 2% con 0,01 mg/ml de epinefrina infiltrados por vía intramuscular en la zona quirúrgica de cada pierna. Se realiza una incisión a espesor total en la región proximal de cada tibia (Fig. 1c). Se procede a identificar los dos sitios experimentales en cada tibia (Fig. 1d). Lo sitios de implantación se prepararon empleando fresas de diámetro incremental e irrigando con solución salina estéril acorde a la recomendación del fabricante. Se mantuvo una distancia aproximada de 8-10 mm entre las dos osteotomías. Se instalaron aleatoriamente dos implantes con un macro-diseño diferente en cada tibia, y se sumergieron hasta que el hombro del implante se niveló con la superficie del hueso. La porción apical de los implantes se coloca en contacto directo o dentro del hueso cortical opuesto al compartimiento cortical coronal, con el objetivo de obtener un anclaje bicortical. Los tapones de cierre se atornillaron a los implantes y el colgajo se sutura posteriormente por planos, se emplean suturas reabsorbibles para permitir una curación sumergida (Vicryl 5/0, Ethicon, Sommerville, NJ, EE. UU.) y Nylon 3/0 (Ethilon 3/0). , Ethicon, Sommerville, NJ, EE. UU.).

-Cuidado pre y postoperatorio, vivienda y cría

Todos los animales se mantuvieron en jaulas individuales durante su período de aclimatación antes de la intervención (2 semanas) y durante el cuidado postoperatorio en la Unidad de Servicio de

Almacenamiento de Animales de la Universidad de Valencia, España, en habitaciones especialmente acondicionadas y aclimatadas a 21ºC con 12 h de oscuridad/iluminación. Los animales fueron alimentados con una dieta estándar y tuvieron acceso libre a fuentes de agua. El patrón analgésico consistió en 2,5 mg/kg de morfina intraoperatoria, 0,02 mg/kg de buprenodale, buprex, 0,2 mg/kg de meloxicam (cada 12 horas durante 3 días) y tratamiento antibiótico con enrofloxacina 2,5 mg/kg (ALSIR® 2,5%, Esteve Veterinaria, Barcelona, España) (cada 24 horas durante 7 días) después de la operación.

-Eutanasia

Nueve conejos de cada unos de los tres grupos fueron sacrificados después de 2, 4 y 8 semanas, respectivamente. Se aplicaron los mismos protocolos de sedación y anestesia empleados para la cirugía, la inducción de la eutanasia se realizó con 50 mg/kg de pentobarbital sódico intravenoso. Se usó una pequeña sierra eléctrica para obtener las secciones de la tibia que contienen cada implante.

- Preparación histológica.

Las muestras de implantes se deshidrataron mediante intercambio secuencial de solventes y se incluyeron en metacrilato que contiene poli-(metil metacrilato). Después de agregar peróxido de benzoilo (1g/100 ml), las muestras se polimerizaron, luego se cortaron con un disco de diamante en una máquina de corte de precisión de mesa Accutom-5 (Struers, Copenhague, Dinamarca), estas se lijaron y pulieron con el sistema de pulido LaboPol-21 (Struers, Copenhague, Dinamarca) y láminas de SiC (SiC foils). Se obtuvieron láminas delgadas de aproximadamente 80 μm de espesor. Las muestras se tiñeron a 55ºC con azul de toluidina durante 30 minutos, se lavaron con agua durante 2 minutos y se dejaron secar.

-Evaluación histológica

Las imágenes digitales calibradas superpuestas de los tejidos que rodean toda la superficie del implante (aproximadamente 20 imágenes/implante) se registraron con un microscopio de luz Leica DM4000 B (Leica Microsystems GmbH, Wëtzlar, Alemania) y una cámara digital DFC420 utilizando un objetivo 5x y el programa Leica Applications Suite version 4.4.0. Las imágenes individuales se fusionaron para componer cada lado del implante utilizando el programa Photoshop CS 6 (Adobe Photoshop CC 2015.0.0, Adobe Systems Incorporated, San José, CA, EE.UU., http://www.adobe.com/Photoshop). El programa de procesamiento de imágenes ImageJ 1.48 (National Institutes of Health, Bethesda, MD, EE. UU., http://imagej.nih.gov/ij) se utilizó para realizar las mediciones histológicas. Las líneas se dibujaron a mano en imágenes calibradas que se muestran en la pantalla de la computadora con un aumento de 400x, y fue realizado por un asesor independiente y calibrado que no participa en el estudio. El BIC se evaluó como la suma de hueso

nuevo y viejo, y se calcularon los porcentajes en relación con la longitud de la superficie del implante examinada. La porción apical del implante que se extruyó más allá de hueso cortical se excluyó del análisis.

-Análisis de los datos

Las diferencias entre los diseños de implantes a lo largo de los períodos de cicatrización se analizaron con la prueba U de Mann-Whitney para las variables independientes. Las diferencias entre los implantes colocados en la diáfisis y la metáfisis también se realizaron utilizando una prueba de suma de rangos de Wilcoxon. Se realizó un análisis multivariado de modelo lineal general para explorar la interacción entre las dos variables independientes (diseño/posición) sobre los valores BIC en diferentes etapas de curación. Cada factor tiene dos categorías: diseño (Ticare Inhex®/Ticare Quattro®) y posición (diáfisis/metáfisis). Se eligió este enfoque porque los informes anteriores observaron que las posiciones de los implantes se pueden usar como réplicas independientes con respecto a la variable de resultado, ya que la calidad ósea varía entre los sitios de implantación (sitios topográficos) en el mismo grado que entre las unidades experimentales. El nivel de significancia se estableció en $\alpha = 0.05$.

Resultados

El presente estudio experimental preclínico se realizó siguiendo las directrices de la guía para la conducción de investigación en animales de experimentación (ARRIVE), por lo que la selección y el uso de animales se han considerado cuidadosamente. Para aislar el posible efecto de la macro-geometría del implante en la formación ósea, ambos implantes tuvieron el mismo tratamiento de superficie. Para apreciar el comportamiento de los dos macro-diseños de implantes en dos ambientes óseos diferentes, se colocaron en dos zonas topográficas dentro de la misma tibia, uno con una capa cortical y un contenido medular (diáfisis) similar a un hueso tipo II y la otra con un hueso más trabecular similar a un hueso tipo III (metáfisis).

El propósito del estudio fue evaluar el efecto de dos macro-diseños de implantes diferentes, pero con igual rugosidad de la superficie en la osteointegración secuencial de implantes instalados de forma bicortical en la tibia de conejo. Se analizaron los datos de 27 animales experimentales con cuatro implantes cada uno. Las áreas entre las espiras se rellenaron con hueso tejido (woven bone) a las dos semanas. Se observaron procesos de remodelación después de 4 y 8 semanas de cicatrización, evidenciado por la tinción más clara del hueso lamelar en comparación con la tinción más oscura del hueso tejido.

A las 2 semanas de cicatrización, se observó un grado similar de nueva osteointegración en ambos macro-diseños, siendo 16.0±7.5% para Ticare Inhex® , y 16.3±7.2% para los implantes Quattro® . Los porcentajes de hueso viejo observados fueron de alrededor de 7.4% y 7.6% para los implantes Ticare Inhex® y Quattro®, respectivamente. Con respecto a la posición del implante (diáfisis o metáfisis), no hubo diferencias significativas entre los parámetros evaluados en esta etapa. Se observaron similares valores de BIC entre los macro-diseños de implantes 23.5±14.4% y 23.9±13.3% para los diseños de implantes Ticare Inhex® y Quattro® , y la ubicación topográfica del sitio de implante con valores BIC de 21.5±7.5 y 25.5±14.6 para diáfisis y metáfisis respectivamente. Ninguna de las diferencias tanto para los macro-diseños como sitios topográficos fueron estadísticamente significativas ($p>0.05$).

A las 4 semanas, los valores de hueso nuevo fueron 19.4±7.3% y 18.9± 4.7% para los diseños Ticare Inhex® y Quattro®, respectivamente. Los porcentajes de hueso viejo en esta etapa fueron 2.3±2.2% y 2.4±1.6%, respectivamente. Al agrupar los datos según la posición del implante en la diáfisis y la metáfisis, no hubo diferencias significativas para los valores de hueso nuevo ($p=0.10$). Sin embargo, en esta etapa se encontró una diferencia significativa para los valores de hueso viejo y tejido conectivo ($p<0.05$). Se observaron valores de BIC similares entre los macro-diseños de implantes, pero en relación con la ubicación del sitio topográfico, mejores valores de BIC se observaron en la diáfisis 24,5±6,2% respecto a la metáfisis 18,4±7,7%. Esta diferencia fue estadísticamente significativa ($p=0.05$).

A las 8 semanas, el hueso nuevo aumentó, alcanzando porcentajes de 33.2±7.6% y 33.4±7.7% en los implantes Ticare Inhex® y Quattro®, respectivamente. No se encontraron diferencias estadísticamente significativas entre los dos grupos ($p>0.05$). El hueso viejo todavía estaba presente, sin embargo, en porcentajes muy bajos de 1.2±1.1% y 3.3±1.1% para los diseños de Ticare Inhex® y Quattro®, respectivamente ($p=0.001$). Los porcentajes de hueso nuevo en la diáfisis fueron de 36,4±10,5%, mientras que en la metáfisis de 29.3±6.2%. No se encontraron diferencias estadísticamente significativas ($p>0.05$). Los valores de BIC observados entre los dos macro-diseños de implantes no mostraron una diferencia significativa, a pesar de que se encontraron valores de BIC ligeramente mejores de 36.7±7.7% a favor de Ticare Quattro® en comparación con el diseño de Inhex® con 34.4±7.8. Sin embargo, con respecto a la colocación del sitio topográfico, se observó un mejor valor de BIC en la diáfisis (39.5±11.1%) comparado a la metáfisis (30.6±6.2%), diferencia que fue estadísticamente significativa ($p=0.05$).

En el análisis multivariado se observó que la posición del implante mostró una significancia estadística con respecto a los valores de BIC a las 4 y 8 semanas ($p <0.05$).

Sin embargo, el análisis no detecta una significancia estadística respecto a la interacción del sitio topográfico y los macro-diseños de implantes (diseño * posición) respecto a los valores BIC durante las etapas de curación. Se observa que el implante Ticare Quattro® mostró valores BIC ligeramente mejores los sitios de diáfisis a través de las etapas de curación ($p > 0.05$).

Otro objetivo fue evaluar el patrón de cicatrización ósea en los compartimentos cortical y medular. Se observó patrones de osificación de tipo intramembranoso y aposicional. Este último se pudo observar cuando se produjo un contacto íntimo entre la superficie del implante y el hueso recién formado en el lecho implantario. En promedio, se identificaron mejores valores de osteointegración en los compartimentos corticales, y valores ligeramente más altos pero no estadísticamente significativos en la diáfisis. Respecto al compartimento medular, se observaron mejores tasas de aposición de hueso nuevo a las dos y cuatro semanas en la diáfisis.

A las 2 semanas de cicatrización, no hubo diferencias significativas entre los parámetros evaluados entre los compartimentos cortical y medular en los sitios de diáfisis y de metáfisis. Los valores de BIC fueron de alrededor de 30.0±9.9% versus 23.7±6.4% en la diáfisis y metáfisis, respectivamente en el compartimento cortical ($p=0.09$), y 21.1±12.3 versus 13.9±8.0 en el compartimento medular ($p=0.07$).

A las 4 semanas, se observaron diferencias significativas en los valores de hueso viejo en el compartimiento cortical, y para los valores de hueso nuevo y tejido conectivo en los compartimentos de la médula entre los sitios de diáfisis y metáfisis. No se detectaron diferencias para los valores de BIC en el compartimento cortical, que reportan ser de 25.4±7.8% y 21.4±8.0% en los sitios de diáfisis y metáfisis, respectivamente ($p=0.26$). Sin embargo, se encontró una diferencia significativa en el compartimento medular, que muestra valores BIC de 22.1±6.9 y 13.6±8.5 en la diáfisis y metáfisis, respectivamente. Diferencia estadísticamente significativa ($p=0.01$).

A las 8 semanas, se observaron mejores valores de hueso nuevo y viejo en el compartimiento cortical; se detectó una diferencia significativa entre los compartimentos cortical y medular para estos parámetros en la metáfisis. El contacto mineralizado de hueso a implante en esta etapa no mostró diferencias significativas dentro del compartimento cortical entre los sitios de implantación en la diáfisis y en la metáfisis, con valores de BIC% de 41.1±6.8% y 39.9±9.8%, respectivamente ($p = 0,61$). Se observó una tendencia similar dentro del compartimento medular en los sitios de diáfisis y metáfisis.

Discusión

Objetivo del estudio

El objetivo principal de la presente tesis doctoral fue evaluar el impacto de dos macros diseños de implantes distintos instalados de forma bicortical en dos entornos óseos (diáfisis o metáfisis) en tibias de conejo. Además, se analizaron los patrones de curación ósea en los compartimentos cortical y medular en los sitios de diáfisis y metáfisis.

Resumen de los principales hallazgos

Para aislar el posible efecto de la macro-geometría del implante en la formación ósea, ambos implantes tuvieron el mismo tratamiento de superficie. Para apreciar el comportamiento de los dos macro-diseños de implantes en dos ambientes óseos diferentes, se colocaron en dos zonas topográficas dentro de la misma tibia, una con una capa cortical y un contenido medular (diáfisis) similar a un hueso tipo II y la otra más trabecular similar a un hueso tipo III (metáfisis). En el presente estudio, se encontró que el hueso nuevo después de 2, 4 y ocho semanas de cicatrización fue ligeramente más alto, en los implantes colocados en la diáfisis en comparación con aquellos implantados en la metáfisis, pero sin alcanzar diferencias estadísticamente significativas ($p>0.05$). Los valores de BIC observados entre los macros diseños de implantes no mostraron una diferencia significativa, aunque se encontraron valores BIC ligeramente mejores en los implantes Ticare Quattro® en comparación con el diseño de Inhex® . Sin embargo, con respecto a la colocación del sitio topográfico, se observó mejores valores de BIC en aquellos implantes colocados en la diáfisis a las 4 y 8 semanas de cicatrización ($p=0.05$). Se realizó un análisis multivariado de modelo lineal general para explorar la interacción entre las dos variables independientes (diseño/posición) sobre los valores BIC en diferentes etapas de curación. Se observó que la posición del implante mostró una significancia estadística con respecto a los valores de BIC a las 4 y 8 semanas, a favor de aquellos implantados en la diáfisis ($p<0.05$). Sin embargo, el análisis no detecta diferencias significativas para la interacción entre el macro-diseño y el sitio topográfico (diseño*posición) sobre los valores BIC en todas las etapas de curación. Se observa que el diseño Ticare Quattro® mostró valores ligeramente mejores de BIC en los sitios de diáfisis a través en los distintos periodos de seguimiento ($p> 0.05$).

Por otro lado, se analizó el patrón de curación ósea en los compartimentos corticales y medulares en en los implantes colocados en la diáfisis y en la metáfisis. La nueva formación ósea en el compartimento de la médula mostró valores incrementales levemente mejores del 13.8%, 20.4 y 24.6% a las dos, cuatro y ocho semanas en los sitios de diáfisis, en comparación con el 10,3%, 13% y 25,1% en los sitios de metáfisis. La misma tendencia se observó en el compartimiento cortical con

valores de alrededor de 17.8%, 21.4% y 37% en los sitios de diáfisis, respecto a los 15.1%, 19.7% y 35.5% en los sitios de metáfisis. El hueso viejo se reabsorbió pero todavía estaba presente (<2%) después de 1 mes en ambas zonas topográficas. Los valores de hueso viejo observados fueron ligeramente más altos en la diáfisis a las cuatro y ocho semanas en comparación con la metáfisis en la presente muestra de estudio. Los valores de BIC no mostraron diferencias significativas, excepto en el compartimento medular a las cuatro semanas de cicatrización, mostrando valores de BIC de 22.1±6,9 y 13.6±8,5 (p=0,01) en la diáfisis y metáfisis, respectivamente.

Discusión con literatura previa

El análisis histomorfométrico a las 2, 4 y 8 semanas fue similar para ambos macro-diseños de implantes (p>0.05). Además, al comparar los porcentajes de hueso nuevo en relación con la ubicación topográfica del implante, se encontró que la osteointegración era ligeramente más alta, pero estadísticamente no significativa en los implantes colocados en la diáfisis en comparación con la metáfisis a las 4 y 8 semanas de cicatrización. Estos hallazgos son contrarios a los reportados en un experimento previo en conejos reportado por Caneva y cols. en 2017. Observaciones que podrían atribuirse a varios factores, como el diseño de espira del implante, el tratamiento de superficie utilizados y los protocolos de osteotomía del implante, que difieren entre los estudios. Se sabe que estos factores pueden regular la tensión aplicada al tejido duro en la proximidad del implante. El hueso viejo se reabsorbió, pero todavía estaba presente después de 1 mes de cicatrización (<4%), con mejores valores estadísticamente significativos en el grupo de Ticare Quattro®. Este patrón de curación es comprable con otros estudios realizados en animales y humanos. Cabe mencionar que la morfología ósea en la diáfisis está ocupada predominantemente por un contenido medular en comparación con la metáfisis que presenta un hueso más trabecular. Estos hallazgos están de acuerdo con el supuesto de que la osteointegración es más rápida en zonas donde la aposición ósea no está precedida por la reabsorción ósea como se observó anteriormente en un estudio preclínico en perros reportado por Abrahamsson y cols., en 2003, y confirmado en cerdos miniatura por Buser y cols. en 2004.

Parece probable que la formación de hueso comenzó a partir de los compartimentos corticales (en contacto con hueso nativo mineralizado) y que posteriormente prolifera hacia los compartimentos de la médula. Se sabe que los procesos de resorción se producen antes de una nueva aposición ósea en zonas donde el hueso mineralizado está presente, lo que conlleva un período de curación ligeramente más largo para alcanzar la osteointegración completa.

Los implantes en el presente estudio estuvieron en contacto cercano con el hueso prístino debido a su estabilización bicortical, una condición que favorece la osteointegración en la superficie del

implante. Un patrón de curación previamente documentado para la osteointegración en diferentes modelos pre-clínicos. El hueso viejo "nativo" del lecho implantario es responsable del enclavamiento mecánico, y es relevante durante la pérdida de la estabilidad primaria del implante, donde tiene lugar una remodelación ósea interfacial mediada por células. Por lo general, se describe que esto ocurre en el área de contacto entre la pared ósea prístina y la superficie del implante, donde la remodelación surge en la proximidad de las micro-fisuras seguidas por una aposición ósea en los espacios vacíos, y que resulta una estabilidad secundaria o biológica.

Los resultados del presente estudio están de acuerdo con otros reportes como el de Leonard y cols., en 2009; que demuestra que el macro-diseño no afecta de forma significativa las tasas de BIC en ausencia de carga. Sin embargo, la literatura científica no diferencia las discrepancias con respecto a la posición del implante distintas topografías óseas, específicamente en tibias de conejo, un factor que probablemente puede contribuir a los resultados debido a las discrepancias en la densidad ósea. En este sentido, un informe anterior sugiere que las características del macro-diseño del implante, tales como como el patrón de la espira y el paso de rosca, pueden ser responsables de las diferencias en la cantidad de hueso y el grado de aposición ósea en la superficie del implante. Por lo tanto, la consideración de un macro-diseño de implante específico debe ser en relación con el micro entorno biológico y mecánico, como lo sugiere Vivan-Cardoso y cols., en el 2015.

De acuerdo con las observaciones antes mencionadas, el patrón de curación en los compartimentos corticales y medulares fue analizado en profundidad en dos entornos óseos diferentes (diáfisis y metáfisis) en tibias de conejo. A este respecto, en el presente estudio, la nueva formación de hueso en el compartimento medular mostró valores ligeramente mejores en los sitios de implantación en la diáfisis, mostrando valores del 13,8%, 20,4 y 24,6% a las dos, cuatro y ocho semanas, en comparación con los 10.3%, 13% y 25.1% obtenidos en la metáfisis. La misma tendencia se observó en el compartimiento cortical con valores de alrededor de 17.8%, 21.4% y 37% en la diáfisis, comparados a los 15.1%, 19.7% y 35.5% en la metáfisis. Se observa que los valores de hueso viejo observados fueron ligeramente más altos en la diáfisis a las cuatro y ocho semanas en comparación a la metáfisis en la presente muestra de estudio.

En el contexto de los sitios topográficos de implantación, nuestros resultados fueron contradictorios con los informados en un estudio previo de Caneva et al. en 2017, donde la nueva formación ósea se desarrolló a una velocidad mucho mayor en los implantes colocados en la metáfisis respecto a la diáfisis. Sin embargo, estas diferencias podrían atribuirse a varios factores, como se mencionó anteriormente. Los autores atribuyeron los hallazgos al patrón más denso del hueso trabecular en la metáfisis en comparación con la diáfisis en tibias de conejo.

Por otro lado, la formación ósea que se supone debe ser reforzada por la médula ósea no ocurre, ya que esto apenas contribuyó en la sección media (medular) de los implantes colocados en la diáfisis en comparación con lo que se encontró en las regiones corticales en coronal y apical. Las diferencias metodológicas podrían ser mencionadas para este aspecto. En el estudio de Caneva y cols., en 2017, se demarcaron tres secciones (coronal, media y apical) para probar las diferencias entre los compartimentos en las tibias de conejo. En el presente estudio, las tres secciones se demarcaron de la misma manera, pero el compartimiento cortical se considera como la suma de las regiones corticales y apicales en su conjunto, independientemente del compartimiento medular (centro). Aunque, en ambos estudios, las regiones extremas de los implantes estuvieron en contacto cercano con el hueso prístino debido a su estabilización bicortical.

Por otro lado, es posible concluir que la osteointegración parece favorecerse por la existencia de un coágulo sanguíneo, y perjudicada por la presencia de la médula ósea de grasa amarilla en el modelo de hueso largo, como la tibia de oveja. En este sentido, Morelli y cols., en 2014 realizan dos osteotomías para la instalación de implantes en cada tibia. En los sitios de control, no se realizaron tratamientos adicionales mientras que, en los sitios de prueba, se extrajo la médula ósea del sitio de la osteotomía con una cureta que excedía las dimensiones del implante. Como resultado, la porción apical de los implantes en los sitios de control estaban en contacto con la médula ósea mientras que, en los sitios de prueba, estaba en contacto con el coágulo de sangre. En promedio, la nueva aposición ósea fue mejor en el compartimiento cortical, como se observa en el presente estudio. Además, se observó que la nueva aposición ósea fue más rápida en el grupo con médula ósea grasa en comparación con los grupos con coágulos de sangre en el compartimento medular a las 4 semanas pero sin alcanzar significancia estadística. Sin embargo, los autores concluyen de que los coágulos sanguíneos parecen favorecer la osteointegración, ya que a las 12 semanas de cicatrización, el grupo de prueba mostró mejores valores de hueso nuevo, y que fueron estadísticamente significativos en el compartimento medular, aunque en este estudio los implantes no se colocaron de forma bicortical.

Sin embargo, a pesar de las diferencias inter-especies que impiden las comparaciones directas, no existe certeza hasta qué punto el modelo de tibia de conejo, en su diáfisis, proporciona cantidades de médula ósea grasa que pueden afectar la osteointegración después de las ocho semanas de cicatrización.

Ventajas, limitaciones y recomendaciones para estudios futuros

Este estudio se realizó de acuerdo con las directrices de ARRIVE que fomentan las buenas prácticas y la calidad de los informes en experimentación animal. La novedad del presente trabajo radica en

el hecho de que no hay otro estudio que tenga como objetivo evaluar el impacto de distintos macro-diseños de implantes con similar tratamiento de superficie (RBM de rugosidad moderada) en dos ambientes óseos diferentes sobre los valores de osteointegración y los patrones de curación en los compartimientos corticales y medulares en tibias de conejo. Esto nos permite aislar los efectos del macro-diseño en la osteointegración, lo que nos ayuda a evaluar por separado la dinámica del patrón de curación en distintas densidades óseas. Sin embargo, debido a la ausencia de carga funcional, estos parámetros reflejan la conexión estructural entre el implante y el hueso, y no las propiedades funcionales del hueso a la interfaz del implante.

Existe poca evidencia preclínica con respecto a la curación secuencial de los implantes instalados de forma bicortical con dos macro-diseños y tratamiento de superficie igual, intentando evaluar su interacción en dos sitios topográficos. A pesar de que se evaluó la interacción de los factores, solo el sitio topográfico parece contribuir a los valores de osteointegración a las 4 y 8 semanas. Lamentablemente, es difícil determinar en qué medida cada macro-diseño de implante contribuye a estos hallazgos observados en los sitios de diáfisis o metáfisis. La muestra escasa no permite una adecuada comparación estadística. Cabe mencionar, que los resultados de la interacción son meramente exploratorios y deben interpretarse con cautela. Es de suma importancia tener en cuenta que los resultados actuales solo podrían extrapolarse a implantes con la misma rugosidad de la superficie, su aplicabilidad está fuera del alcance para otros modelos animales debido a las diferencias que se mostraron en los patrones de curación entre las especies (por ejemplo, perros, ovejas, conejos, rata). Se justifican estudios adicionales que comparen el tratamiento de superficies iguales pero con diferentes enfoques de fabricación (p.ej. superficies SLA, anodizadas, etc.), para dilucidar si reproduce los patrones observados en el presente trabajo. Además, no hay datos concretos sobre hasta qué punto el modelo de tibia de conejo, en su diáfisis, proporciona cantidades de médula ósea grasa que pueden afectar la osteointegración después de las ocho semanas de cicatrización. Por lo tanto, sería interesante aislar su efecto en un estudio posterior para confirmar esta hipótesis en el modelo de tibia de conejo. Se requieren estudios adicionales con un tamaño de muestra mayor para responder a estos aspectos, pero este es un desafío difícil, teniendo en cuenta los aspectos éticos y económicos que pueden estar involucrados en la consideración de los criterios de reemplazo, refinamiento o reducción (3R) para el uso animales en investigación.

Conclusiones

En resumen esta tesis concluye que:

I. El patrón de osteointegración secuencial de las superficies RBM en el modelo de conejo fue satisfactorio.

II. Los macros-diseños de implantes no afectan significativamente el proceso de osteointegración en ausencia de carga en las etapas de cicatrización.

III. La morfometría y la densidad ósea pueden afectar la aposición ósea sobre la superficie del implante. Las tasas de aposición fueron ligeramente mejores en la diáfisis en comparación a los sitios topográficos de metáfisis. Los valores de BIC fueron significativamente más altos a las 4 y 8 semanas en la diáfisis.

IV. No hay interacción entre el macro-diseño del implante y el sitio topográfico, como lo muestra el análisis multivariado. Sin embargo, se observó que el macro-diseño de implante Ticare Quattro® mostró valores BIC ligeramente mejores en los sitios de diáfisis a través de las etapas de curación.

V. La nueva aposición ósea fue mejor en el compartimento cortical comparado al compartimento medular. Las tasas de aposición fueron ligeramente mejores tanto en los compartimentos corticales y medulares en la diáfisis comparado a la metáfisis.

1. INTRODUCTION

INTRODUCTION

Osseointegration and the direct bone-to-implant contact (BIC) (Schroeder et al. 1976) are concepts that transformed the maxillofacial reconstruction approaches. Among factors that may exert an effect on bone to implant interfacial remodeling and new bone apposition, the implant material, the surgical technique, the host bed, the implant design and surface, the time and loading conditions showed to affect osseointegration (Albrektsson et al. 1993; Botticelli and Lang 2017).

To achieve implant integration, the primary stability is a key goal required to avoid fibrous encapsulation (Lioubavina-Hack et al. 2006a). The mechanical interlocking that occurs between the surface of the implant and the parent bone in part depends on the implant macro-design, the roughness of the surface, and the surgical preparation of the implant bed (Marco et al. 2005). Further, this primary stability decrease when a remodeling of the surrounding parent bone takes place. It is responsible of implant stability dip, that simultaneously concurs with a secondary or biologic stability gain "osteoconduction" that depends in great extent of the implant surface roughness, and its capacity on fibrin clot retention during healing (Davies 2003; Abrahamsson et al. 2004; Raghavendra et al. 2005).

It is suggested that bone remodeling occurs depending on the degree of mechanical stress (Halldin et al. 2011); So it of utmost importance that the thread design provides a certain level of static strain to the surrounding bone (Chowdhary et al. 2014). Threads are also used to maximize initial contact, improving initial stability and enlarging implant surface area (Ivanoff et al. 1999), that favors dissipation of interfacial stress (Brunski 1988). Different implant thread designs and thread pitches were proposed, aimed to enhance and optimize the osseointegration process, as well in loading conditions (Abuhussein et al. 2010). Implant geometry was reported to affect the BIC ratio and mechanical test values (Steigenga et al. 2004). Also, modified macro-geometry and different microgeometries of implants has shown to have a stimulatory effect on osseointegration (Chowdhary et al. 2014), that impacts the dynamics of implant osseointegration (Vivan Cardoso et al. 2015).

Consequently, it was suggested that macro-design features should be made relative to the biological and mechanical micro-environment (Vivan Cardoso et al. 2015). Nevertheless, other characteristics such healing chamber configuration have proven to facilitate osseointegration (Beutel et al. 2016) and, to a less extent, the apical configurations as well (Gehrke et al. 2017). Preclinical evidence on removal torque values (Ivanoff et al. 1996), and osseointegration at

different titanium surfaces (Caneva et al. 2015), or at implants with different apical configuration design (Gehrke et al. 2017) are available for bi-cortically placed dental implants.

On the other hand, dental implant surface modifications provide different topographical characteristics and increase the tridimensional surface area (Sela et al. 2007). The area is quantified through the surface roughness features, which may be reported as Ra or Sa, depending on whether the parameter is classified as two-dimensional or three-dimensional (Wennerberg and Albrektsson 2009). Modified-surface implants provided enhanced activation of the platelets and the cell adhesion and protein adsorption relating to the implant surface (Park et al. 2001; Sela et al. 2007). These features improve the osseointegration process in terms of BIC and implant stability during the early healing phase (Koh et al. 2009), and may up-regulate osteogenic activity and osteoconductivity (Park et al. 2001; Davies 2003).

The improvement of the bioactivity of dental implants, so they could be able to respond to body fluids, cells, and pathogenic agents, was a result of the different approaches used to produce multifunctional Ti-based surfaces (Spriano et al. 2018). This is a result of the implementation of inorganic coatings, chemical surface modifications, and bioactivation by means of organic coatings (Spriano et al. 2018). Several methods for implant surface treatments (e.g., etched surfaces, sandblasted and acid etched surfaces, hydroxyapatite-coated surfaces, grit-blasted surfaces, laser ablation, fluoride treatment) have been introduced throughout the years (Barfeie et al. 2015). Among them, the resorbable blasted media (RBM) surface is obtained through the grit-blasting of calcium phosphate bioceramic (CaP) particles at high velocity, in which the particle size determines the roughness degree as a particle-free titanium surface (Piattelli et al. 2002; Yeo 2014). A more homogenous honeycomb-like spatial distribution with a lower roughness has been reported for RBM surfaces (Yeo et al. 2008; Coelho et al. 2011). Also, the RBM surfaces showed BIC values that were comparable to other blasting surfaces, such as titanium dioxide (TiO2) or aluminum oxide (Al2O3) (Müeller et al. 2003), and similar biomechanical strength and removal torque measurements were obtained by calcium- and magnesium- enhanced implants (Kang et al. 2018).

Recent evidence reinforces the concept that the implant geometry and the density of the bone are key factors involved in the degree of primary stability (Falco et al. 2018). However, limited evidence is currently available in examining the effect of two distinct implant macro-designs with equal surface treatment installed at different bone densities.

2. RATIONALE AND STUDY AIMS

2.1 RATIONALE

Osseointegration is a dynamic process strongly influenced by the implant surface, which plays a role during the early phase of healing through resorptive and appositional events (Abrahamsson et al. 2004; Botticelli et al. 2005; Botticelli and Lang 2017). Also, recent evidence reinforces the concept that the implant geometry and the density of the bone are key factors involved in the degree of primary stability (Falco et al. 2018).

In osseointegration, healing pattern differences between the cortical and the marrow compartments at both flat (dog jaw) and long bones (sheep tibia) are reported (Rossi et al. 2014a; Morelli et al. 2015). This behavior is observed in rabbit tibiae as well, and despite inherent experimental model differences, it differs from former studies because distinct surface treatments were assessed (Caneva et al. 2015). Indeed, in the study of Caneva et al. 2015 (Caneva et al. 2015), the effects of equal implant geometries have been tested, but at different implant surface modifications.

Therefore, it is presumable that both the cortical and marrow compartments provide distinct biological and physical features at bone-to-implant interfacial remodeling and direct bone apposition toward the implant surface (Abrahamsson et al. 2004; Raghavendra et al. 2005; Gomes et al. 2013). Their nature demarcates the transition from primary to secondary/biological stability after an implant stability dip in the osseointegration process (Raghavendra et al. 2005).

However, data on bi-cortically placed dental implants with different macro-designs and equal surface roughness are still missing and because of the lack of studies regarding bone-healing pattern on implant surfaces at different bone compartments and bone environments, there is a need for further investigation.

2.2 STUDY AIMS

2.2.1 Main objective

The main aim of this experimental pre-clinical thesis was to study the osseointegration values (new bone, old bone, bone marrow and BIC [new bone + old bone]) of two different implant macro-designs, with equal RBM surface treatment in different bone topographic sites (diaphysis or metaphysis).

2.2.2 Specific objectives

The specific objectives of the present thesis were:

I. To document the sequential healing during osseointegration of implants with RBM surface treatment at 2, 4 and 8 weeks in a rabbit model.

II. To evaluate the effect of two different implant macro-designs on the sequential new osseointegration values at 2, 4 and 8 weeks.

III. To evaluate the effect of the topographic site of implants installed at the diaphysis and metaphysis of rabbit´s tibiae on new osseointegration values.

IV. To evaluate the effect of implant macro-design regarding the topographic site at rabbit`s tibiae, on new osseointegration values.

V. To evaluate the bone-healing pattern at the cortical and marrow compartments in the diaphysis and metaphysis of rabbit´s tibiae.

3. STUDY HYPOTHESES

STUDY HYPOTHESES

Using implants with the same RBM surface treatment and bicortically installed in the diphysis or the metaphysis of rabbit tibbiae, the following study hypotheses were formulated :

Null hypothesis I

H_0 There are no differences between new osseointegration values of two implant macro-designs bicortically installed in rabbit tibiae.

Alternative hypothesis I

H_1 Different implant macro-designs will provide different new osseointegration values in bicortically installed implants of rabbit tiabie.

Null hypothesis II

H_0 There are no differences on new osseointegration values between the implants installed at diaphysis or metaphysis topographic sites within rabbit tibiae.

Alternative hypothesis II

H_1 Different topographic sites will provide different new osseointegration values of installed implants at diaphysis or metaphysis of rabbit tiabie.

Null hypothesis III

H_0 There are no differences in new osseointegration values between installed implant macro-design regarding the topographic site in rabbit tibiae.

Alternative hypothesis III

H_1 Different implant macro-design will provide differently new osseointegration values depending on the topographic site in rabbit tibiae.

Null hypothesis IV

H_0 There are no differences in the bone-healing pattern at the cortical and marrow compartments of implants bicortically installed in rabbit´s tibiae.

Alternative hypothesis IV

H_1 The bone-healing patterns at the cortical and marrow compartments of bicortically installed implants are different.

4. LITERATURE REVIEW

4.1 Basic bone biology during osseointegration of titanium dental implants

4.1.1 The bone tissue

In 1892, Julius Wolff postulated that bone is a dynamic tissue that adapts to meet the physical demands of its external environment (Wolff 1986). Nowadays bone is considered a dynamic, vascular, living tissue that changes throughout life and is one of the so-called "connective tissues" of the body and thus comprises cells that become embedded in their own extracellular matrix. Bone tissue has evolved over a far greater period than the half million or so years that we, as Homo Sapiens, have existed on earth. Some believe that the evolution of our cranium can be traced back as far as the emergence of the protofish or cyclostomes some 540 million years ago. Indeed, it is neither trivial nor facetious to point out that the historical timeframe of dental implant development pales into insignificance when compared to the evolution of the tissue into which such implants are placed. Thus it is not unreasonable to assume that, not only do all bony architectures represent highly evolved biological structures, but also that an understanding of normal bone formation and remodeling, through which such architectures are achieved, may well provide an insight into both the healing of bone around implants (Davies 2003).

4.1.2 Bone response to dental implants

Dental implant could be integrated both at hard and soft tissue level. The term osseointegration are related to the long-lasting and functional connection between titanium fixture surface and surrounding bone at implant bed, it is developed across weeks of healing, with or without functional loading. Direct bone-to-implant contact (i.e. osseointegration) was first described by the Swedish scientist Per-Ingvar Brånemark and his coworkers (Adell et al. 1970; Southam and Selwyn 1970) and was first histologically demonstrated by the Swiss scientist Andre Schroeder and his coworkers as 'functional ankylosis' (Schroeder et al. 1976, 1978, 1981), being his group the first to document direct bone-to-implant contact for titanium implants in non-decalcified histologic sections. This intimate relation of implants surface and bone may be due in part to an interaction between titanium oxide-bone via proteoglycans (Listgarten et al. 1992). During follow years, further development of animal studies shed light that various materials and surface configurations become osseointegrated (Schenk and Buser 1998; Salvi and Lang 2001).

Afterwards of years of constant research, efforts reflects significant findings; such as, how the rough-surfaced implants possess a higher bone-to-implant contact and favor biomechanical stability (Berglundh et al. 2003; Abrahamsson et al. 2004; Shalabi et al. 2006; Le Guéhennec et al. 2007).

So, aimed to enhance the understanding of processes implied during bone healing after dental implants placement, this chapter consists in a comprehensive review of the most relevant literature to develop the rationale of basic bone biology and key insights of the sequential healing of titanium dental implants in bone tissue.

4.1.3 Basic aspects of bone biology and architecture

The skeletal system develops from mesenchyme originated from the mesodermal germ layer and neural crest. In view of developmental bone biology, the skeletal system can be divided into four parts: skull, limbs, vertebrae/the ventral column, and ribs/sternum. Bone formation takes place in two ways. In most bones including axial (vertebral column and ribs) and appendicular (limbs) skeletons, a cartilage model first forms and is finally replaced with bone, which is called endochondral ossification. In contrast, most flat bones, such as the majority of bones of the skull, form directly from mesenchymal cells from the first branchial arch without the prior formation of cartilage; this type of osteogenesis is called intramembranous ossification (Maruyama 2011).

Bone it is a specialized connective tissue that works offering support and mechanical stability to the skeleton. It is essential for the protection of internal organs such as those in rib cage (the lungs-, heart-, etc.) and in the cranial (maxillary processes). Also, allows the body load bearing and to do a properly locomotion, the last through a system of levers that multiply the forces that arise from muscle contraction and transduced in body movements (e.g. mandibular excursive movements and occlusal forces). It harbors cavities containing bone marrow where blood cells are formed, which constitute an important source of nutrients (e.g. growth factors, proteins and osteogenic cells precursors). Adding to the above mentioned aspects, the bone tissue works as reservoir of calcium, phosphate and other ions, that can be released or stored in a controlled fashion to maintain the body homeostasis. The diversity of bone functionality is due to its complex structure. This mineralized tissue therefore confers mechanical and metabolic functions to the skeleton. Bone is a specialized connective tissue composed of calcified extracellular material “Bone Matrix” and three major cell types (Osteocytes, Osteoblasts and Osteoclasts). All of them have specific functions for the maintenance of a healthy bone tissue.

Its mineral phase enmeshed with organic fibers (type I collagen fibers embedded in a ground substance consisting of proteoglycans, glycoproteins and inorganic minerals). It is considered that both minerals and collagen fibers are involved in the mechanical resistance of the tissue (Currey

1969a). The collagen fibers form bundles resistant to pulling forces, whereas the mineral provide stiffness to resist bending and compression forces (Currey 1969b). Those minerals mainly in the form of calcium phosphate- (CaP) or hydroxyapatite- (HA) crystals, may associates with collagen fibers, providing a specific hardness to the bone during a progressive and sequential mineralization of bone matrix.

The metabolites embedded inside bone are not capable of diffusing through the calcified matrix, the exchanges between osteocytes and microvasculature structures are mediated by very thin cylindrical spaces of the canaliculi, cytoplasmatic elongations that connect the trapped cells "osteocytes" within mineralized tissue with the surface lining cells in irreversible manner. All bones are lined on both internal and external surfaces, such as "the endosteum" surrounding the marrow cavity and "periosteum" for external surface respectively.

4.2 Basic bone anatomy

Macroscopically the bone may be classified in compact (cortical) bone that represents the 80% of total bone mass, and deeper areas with numerous interconnecting cavities, called cancellous (trabecular or spongy) bone that represents the 20%; the first one consists of concentric layers of matrix surrounding longitudinal vessels, within Haversian systems, interposed between them mainly un-remodeled interstitial bone, that consists a framework of the bone, although weaker than cortical bone, it provides a metabolic support. The compact bone tissue is organized in cylindrical shaped osteonic structures that have concentric layers or lamellae surrounding a central canal or Haversian canal, a source of nutrients, nerve´s and blood supply for bone maintenance.

On the surface of the osteon, the boundary is formed by the cement line resultant of bone remodeling process or the "*De novo"* bone formation a concept drawn from bone fracture healing lessons (Davies 2003). According to classical histology, bone tissue may be classified in relation to the spatial orientation of collagen fibers. Two different types of bone have been recognized through microscopic examination: woven-fibered bone and parallel-fibered bone (non-lamellar or lamellar) (Currey 1969a). Woven bone has a poorly structured matrix that is formed rapidly in response to wounding or hypertrophic adaptation. Parallel-fibered or lamellar bone results from the slower appositional rate, the more highly organized matrix and greater strength of the bone; the degree of mineralization is also related to the stiffness and strength of the bone (Traini et al. 2006).

There is evidence that variances on collagen fibers orientation within bone matrix seem to be associated with both mechanical loading and regimen (Riggs et al. 1993; Traini et al. 2005b). A previous report observes that forces exerted by biting and chewing have a significant effect on the variation in the preferential alignment of c-axis in apatite crystals, as was demonstrated in monkeys (Nakano et al. 2002).

This observation may be in part explained because the bone tissue has a specific anisotropic morphology derived from collagen fiber alignment and the related hydroxyapatite crystal orientation as a bone quality index, and the osteoblasts cell orientation that seems to determine the crystallographic anisotropy of apatite crystals when a new osteoid matrix is developed (Matsugaki et al. 2015). Noteworthy to mention that anisotropy is related to tissue that shows different mechanical characteristics under different strain conditions (different loading vectors direction).

4.2.1 Woven bone

Woven bone (WB) is non-lamellar and characterized by the random disposition of type I collagen fibers and is the first type bone tissue to appear in embryonic development and fracture repair, such as implant bed drilling. This kind of bone is rich in osteocytes which lie in lacunae that vary in size and shape; also, is indicative of rapid uncontrolled bone formation and high bone turnover. It is usually temporary and is replaced by lamellar bone, except in very few places of the body (e.g. near the sutures of the calvaria or in the insertion of some tendons). In addition to the irregular interwoven array of collagen fibers, this type of bone has a lower mineral content being more easily penetrated by X-rays, and has a higher proportion of osteocytes than mature lamellar bone, which reflects the fact that woven bone forms more quickly but has less strength than lamellar bone.

4.2.2 Lamellar bone

Mostly bone in adults, cortical or trabecular, is organized as lamellar bone (LB), characterized by multiple layers or lamellae of calcified matrix, organized either parallel to each other or concentrically around a central canal. In each lamella type-I collagen fibers are aligned in parallel, with the pitch of the fiber’s orientation shifted orthogonally (by about 90 degrees) in successive lamellae.

This highly ordered organization of collagen within lamellar bone is visible under a polarizing light microscope as birefringence; alternating bright and dark layers are due to the changing orientation of collagen fibers in the lamellae “like wood fibers in plywood"; the highly ordered of collagen fibers disposition confers greatly to the strength of lamellar bone.

An osteon is a bone functional unit or “Haversian system”, it refers to the complex of concentric lamellae surrounding a small central canal that contains a blood vessel/nervous/adipose tissues and endosteum. Between each concentric lamellae, there are lacunae, each one with one osteocyte interconnected by canaliculi containing the cells´ dendritic process, connected with neighbored cells process through gap junctions. All cells of an osteon receive nutrients and oxygen from microvasculature in central canal.

This central canal, surrounded by 4-10 concentric lamellae, communicates with marrow cavity, periosteum and another osteons through transverse perforating or Volkmann´s canals, and it may have few, if any, concentric lamellae. All central and perforating canals come into the existence when the matrix is laid down around areas with preexisting blood vessels. Scattered among the intact osteons are numerous irregular shaped groups of parallel lamellae called interstitial lamellae, that are lamellae remaining from osteons destroyed by osteoclasts during growth and remodeling of bone.

4.2.3 Bone remodeling

The bone replacement process in the adult skeleton is known as remodeling. When bone is removed by osteoclasts, new bone is laid down by osteoblasts in the same place, because the load bearing requirement is unchanged. Bone is usually replaced because it is too old to carry out its function, which is mainly mechanical in cortical bone and mainly support for homeostasis and hematopoiesis in cancellous bone. Remodeling always begins on a quiescent bone surface, separated from the marrow by flat lining cells that are one of the two modes of terminal differentiation of osteoblasts. Lining cells are gatekeepers, able to be informed of the need for remodeling, and to either execute or mediate all four components of its activation-selection and preparation of the site, recruitment of mononuclear preosteoclasts, budding of new capillaries, and attraction of preosteoclasts to the chosen site where they fuse into multinucleated osteoclasts (Parfitt 1994).

Both remodeling processes are developed through bone structure, the osteonal remodelling in cortical bone and a hemi-osteonal remodelling in spongious bone, that consists in osteoclastic resorption advancing on the bone "cutting cone", followed by osteoblastic activity making a new bone matrix "closing cone" (Parfitt 1994). Bone remodeling is designed to maintain a mechanically competent skeleton and to repair areas of microdamage. It is achieved by the ongoing process of mature bone removal and replacing by new bone formation, which implicates an osteoclastic cycle recruitment and activation through the subsequent initiation of osteoblast formation, and repair resorption sites. Adult bone is continuously broken down by osteoclasts and rebuilt by osteoblasts, collaborating within 'basic multicellular units' (BMU's). Osteoclasts create a resorption cavity that is subsequently filled with new bone by osteoblasts (van Oers et al. 2008).

4.2.4 Bone cells

4.2.4.1 **Osteoblasts**

Osteoblast are mononuclear, fibroblast-like cells found in a single layer on bone surfaces. An osteoblast forms a volume of matrix equivalent to its own size every day. The bone matrix consists primarily of type I collagen and a number of noncollagenous proteins, such as sialoprotein, osteocalcin, and osteonectin (Rodan and Harada 1997). High concentrations of growth factors, such as TGF-β and insulin growth factor (IGF), are also secreted into the matrix. The control of osteoblast differentiation was poorly understood, because a multiplicity of factors is involved. Adaptation of bone in response to load has been in part elucidated (Rubin and Lanyon 1987). Under compression the cortex is thicker and has an increased osteon density but has smaller osteons and less turn over, while the cortex under tension is thinner and has a higher turnover with larger, less numerous osteons (Skedros et al. 1994b, a).

There are also differences in the degree of skeletal mineralization, with regions of bones that are under tension having a lower mineral density than those under compression (Currey et al. 1996). It is because tensile yield in compact bone is determined by strain, post-yield behavior by mineral content, so the greater the mineral content the less the post-yield work and the less the increase in post-yield stress and strain (Currey 2004).

Cortical porosity has been investigated in relation to the principal loading mode, compression or tension. To maintain any level of bone mass requires a continued, loading-related osteoregulatory stimulus (Lanyon 1996; Liu et al. 2018). Furthermore, differing loading environment exerts an

effect on the orientation of bone collagen fibers inside the bone matrix. Also, around dental implants, bone under compression has oblique transverse collagen fibers, while that under tension has longitudinal collagen fibers (Traini et al. 2005a, b, 2009; Delgado-Ruiz et al. 2015).

4.2.4.2 **Osteocytes**

Osteocytes, the most abundant cells in bone, have been long postulated to detect and respond to mechanical and hormonal stimuli and to coordinate the function of osteoblasts and osteoclasts. The discovery that the inhibitor of bone formation sclerostin is primarily expressed in osteocytes in bone and downregulated by anabolic stimuli provided a mechanism by which osteocytes influence the activity of osteoblasts (Bellido 2014). They are considered former osteoblast that became trapped in the bone matrix during bone formation. They inhabit the lacunar-canalicular system and communicate with other osteocytes and with the surface lining cells, in part via gap junctions. Osteocytes elongate their dendrite processes and develop lacunar-canalicular systems (Fig. 4.1), that play an important role in bone remodeling (Zhang et al. 2006). Bone remodeling, which is essential for the maintenance of skeletal homeostasis, continues throughout life in response to dynamic and/or static loading such as gravity, functional movements, and exercises. Dynamic and static loading on bone tissue are converted to various mechanical stimuli, such as fluid shear stress, hydrostatic pressure and direct cellular deformation (Klein-Nulend et al. 2012), and osteocytes receive these stimuli through their dendrite processes within lacunar-canalicular systems, resulting in activation of signaling pathways that control bone reactions by producing bone formation and/or resorption proteins. Therefore, osteocytes and dendrite processes are crucial components of bone anabolic responses to mechanical loading (Weinbaum et al. 1994; Bellido 2014).

Nowadays, the evidence suggests that osteocytes works as mechanoreceptor, and that they almost certainly sense rates of change of mechanical deformation (strain). They ultra-structurally demonstrated that mechanical loading via bone-integrated implants increased the number of spherical-shaped osteocytes in bone around dental implants, and increased osteocyte dendrite processes in the implant neck. Concluding, that accelerated osteocyte responses to mechanical loading via bone-integrated implants may be associated with increased bone anabolism (Sasaki et al. 2015).

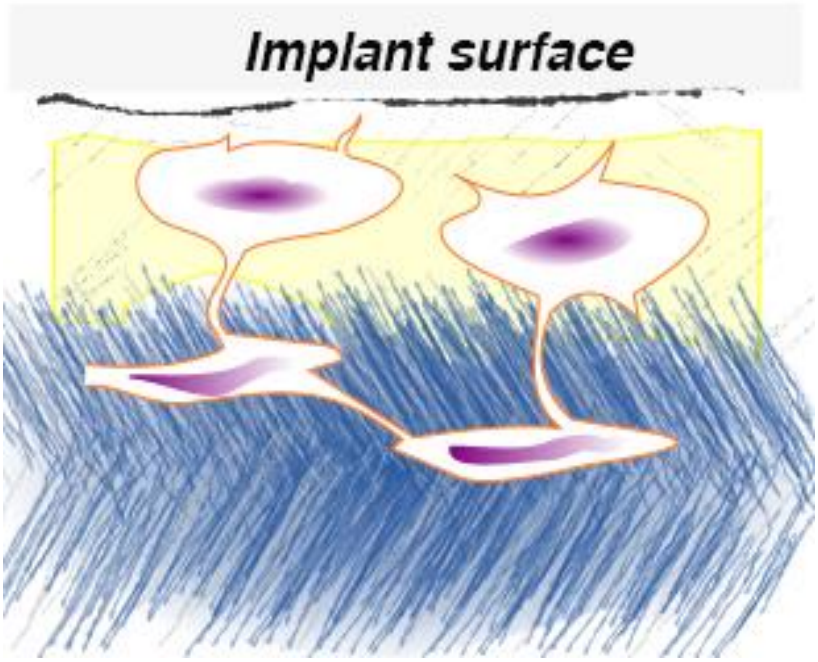

Figure 4.1 Schematic representation of the osteocyte trapped within lacunae in mineralized bone matrix "light blue" linked with surface cells "osteoblasts" through canaliculi. Image Adapted from Davies et al. (Davies 1998).

It occurs through a number of paracrine signals, including prostacyclin (PGI2) and prostaglandin-E2 (PGE2), nitric oxide and insulin growth factor (IGF), are stimulated by osteocytes following changes in skeletal loading. Moreover, the findings that expression of the glutamate transport by transporters (GLAST) with similar weight as in brain, but expressed in plasmatic membrane of osteoblast and osteocytes which is increased following loading, the last one due to the presence of a splice variant, GLAST-1a in bone tissue (Mason et al. 1997; Mason and Huggett 2002). It suggests that excitatory amino acids may play role in the mechano-transduction of the loading strain.

Some studies, raised the intriguing possibility that osteocytes apoptosis may be part of the mechanism whereby osteoclasts are targeted to sites of bone resorption (Noble et al. 1997). Estrogen suppression, a known stimulant of bone resorption, increases osteocytes apoptosis, and changes in bone loading are also associated with osteocyte apoptosis (Skerry et al. 1989).

However, osteocyte apoptosis is spatially and temporally linked to bone fatigue-induced microdamage and to subsequent intracortical remodeling. Specifically, osteocytes surrounding fatigue microcracks in bone undergo apoptosis, and those regions containing apoptotic osteocytes co-localize exactly with areas subsequently resorbed by osteoclasts (Cardoso et al. 2009). Previous observations may be in part explained because osteocytes, not osteoblasts or lining cells, are the

main source of the receptor activator of nuclear factor kappa-B ligand (RANKL) required for osteoclast formation in remodeling cancellous bone as recent reported (Xiong et al. 2015).

4.2.4.3 **Osteoclasts**

Osteoclasts resorb bone by attaching on the bone matrix and forming a sealing zone. Osteoclasts are large, multinucleated cells that can penetrate 50 to 70 μm into compact bone and resorb a volume of bone equivalent to that formed by osteoblasts. Osteoclasts possess numerous mitochondria and an extensive Golgi system but have a sparse endoplasmic reticulum and few ribosomes. Osteoclasts are formed from hematopoietic mononuclear cells of the bone marrow, although the exact nature of the precursor cell is still a matter of debate.

The regulation of osteoclast activity is complex, involving a variety of factors (including systematic hormones, such as parathyroid hormone, 1,25-dihydroxyvitamin D3, and calcitonin as well as numerous local factors). A number of these factors act through the generation of secondary signals by osteoclasts, mechanisms that are believed to couple bone resorption with bone formation. The mechanisms by which bone resorption is terminated includes activation of matrix-derived transforming growth factor β (TGF-β), the presence of calcium sensor and finally osteoclast apoptosis.

To maintain bone homeostasis by resorbing the bone, osteoclasts become differentiated from hematopoietic cells in response to stimulation by RANKL and macrophage colony-stimulating factor (M-CSF) produced by osteoblasts or osteocytes (Takayanagi 2007). RANKL signaling promotes expression and activation of nuclear factor of activated T cells 1 (NFATc1), a transcription factor and master regulator of osteoclastogenesis, which upregulates the expression of various molecules that accelerate osteoclastic differentiation and bone resorption, such as dendrocyte-expressed seven transmembrane protein (DC-Stamp), osteoclast-associated, immunoglobulin-like receptor (OSCAR), 3 integrin, Src, and cathepsin K (Ikeda et al. 2006; Asagiri and Takayanagi 2007; Takayanagi 2007).

During differentiation, osteoclast precursor cells fuse with each other, spread, and form the actin ring, a unique actin structure at the cell periphery (Zaidi et al. 2003; Jurdic et al. 2006; Takahashi et al. 2007). Osteoclasts strongly attach to the bone matrix, demarcate the bone-resorbing area by

sealing it with the actin ring, and form a ruffled border to secrete bone-resorbing factors, such as protons and cathepsin K (Marchisio et al. 1984; Soriano et al. 1991; Boyce et al. 1992; Zaidi et al. 2003; Horne et al. 2005; Jurdic et al. 2006; Takahashi et al. 2007). Thus, the formation of the actin ring and ruffled border is necessary for bone resorption (Marchisio et al. 1984; Soriano et al. 1991; Boyce et al. 1992). The osteoclast structure is depicted in (Fig.4.2).

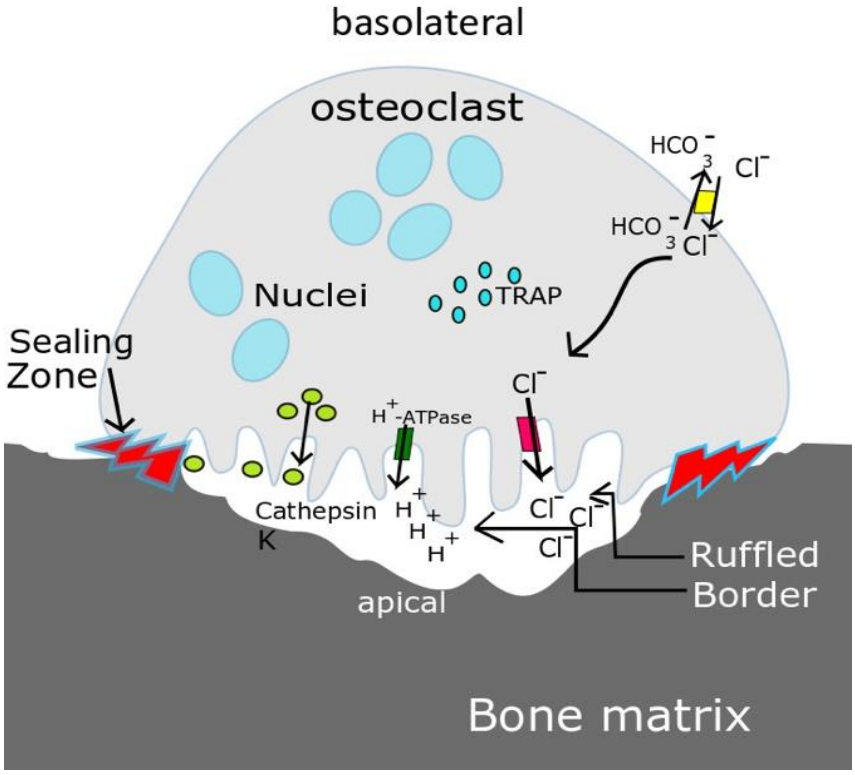

Figure 4.2 Illustration of a functional active osteoclast. Mature osteoclasts are large multi-nucleated cells that cover a big area on the bone to degrade the bone matrix. The apical membrane faces the bone and the sealing zone generates an isolated region. A ring of aggregated F-actin assures the strong attachment of the osteoclast to its substrate. The resorptive area is acidified by secretion of HCL to demineralize the bone matrix. Organic components are degraded by Cathepsin K. Osteoclasts express tartrate-resistant acid phosphatase (TRAP), which is commonly used as a marker for osteoclasts. Image adapted from Kubatzky et al. 2013.

4.3 The phenomenon of osseointegration: Stages of the peri-implant healing process

The osseointegration is a dynamic process either during their establishment and maintenance, characterized by resorption and apposition events, the extent and degree of osseointegration is in part affected by implant surface configuration (Abrahamsson et al. 2004). This process is orchestrated and regulated by the expression of biological cues, proteins and genes related to immune-inflammatory-, skeletogenesis-, angiogenic- and neurogenic- responses (Ivanovski et al. 2011).

Nowadays, osseointegration is considered by international team for implantology (ITI) as any biocompatible material capable to integrate within bone tissue, either commercial pure titanium, titanium alloys or zirconium oxide. Osseointegration is marked by three distinct healing phases, it is transduced in many stages involved, such as haemostasis-, inflammatory-, proliferative- and remodeling- phases, resulting of communication and interaction between cells types (Terheyden et al. 2012).

As addressed experimentally (Davies 1998), it could be appreciated three healing stages during endosseous implant integration: *Osteoconduction, "de novo" bone formation, and bone remodeling*. These are not unique of peri-implant endosseous healing, but also occur, as an outcome of evolutionary development, during both bone remodeling and fracture healing, and can thus be considered as critical hallmarks of bone healing and regeneration. The combination of osteoconduction and bone formation will result in contact osteogenesis. The long-term remodeling of the tissue is influenced by different stimuli, the most important being the biomechanics of the developed healing site, and thus should also be treated separately; Indeed, since trabeculae are damaged during implant site preparation, it is not surprising that bone fracture healing and peri-implant healing exhibit many similarities (Davies 2003).

4.3.1 Contact Osteogenesis: Osteoconduction and *De novo* Bone Formation.

These two healing phases involved, osteoconduction and *de novo* bone formation, result in contact osteogenesis given an appropriate implant surface, bone bonding. This distinction was thoroughly explored by Osborn and Newesley in 1980 (Osborn and Newesley 1980), who described two different phenomena, contact and distance osteogenesis. It refers to the general relationship between forming bone and the surface of an implanted material. Though, their classification was linked to different implant material types, rather than the biologic mechanisms underlying their histological observations, it still provides one of the most useful starting points to understand the mechanism of endosseous integration (Davies 1998).

4.3.1.1 **Osteoconduction: The Key to Contact Osteogenesis**

The first and most important healing phase, osteoconduction, relies on the recruitment and migration of osteogenic cells to the implant surface, through the residue of the peri-implant blood clot (Fig. 4.3). Among the most important aspects of osteoconduction are the knock-on effects

generated at the implant surface, by the initiation of platelet activation, which result in directed osteogenic cell migration through the release of platelet derived growth factors and molecules contained in plasma (e.g. TGF-β1, acid FGF, Trombin, BMP-2, BMP-7) among others. Osteoconduction also occurs during normal tunneling remodeling in bone. In such remodeling, differentiating osteogenic cells are derived from undifferentiated peri-vascular connective tissue cells (pericytes) (Jaworski 1981).

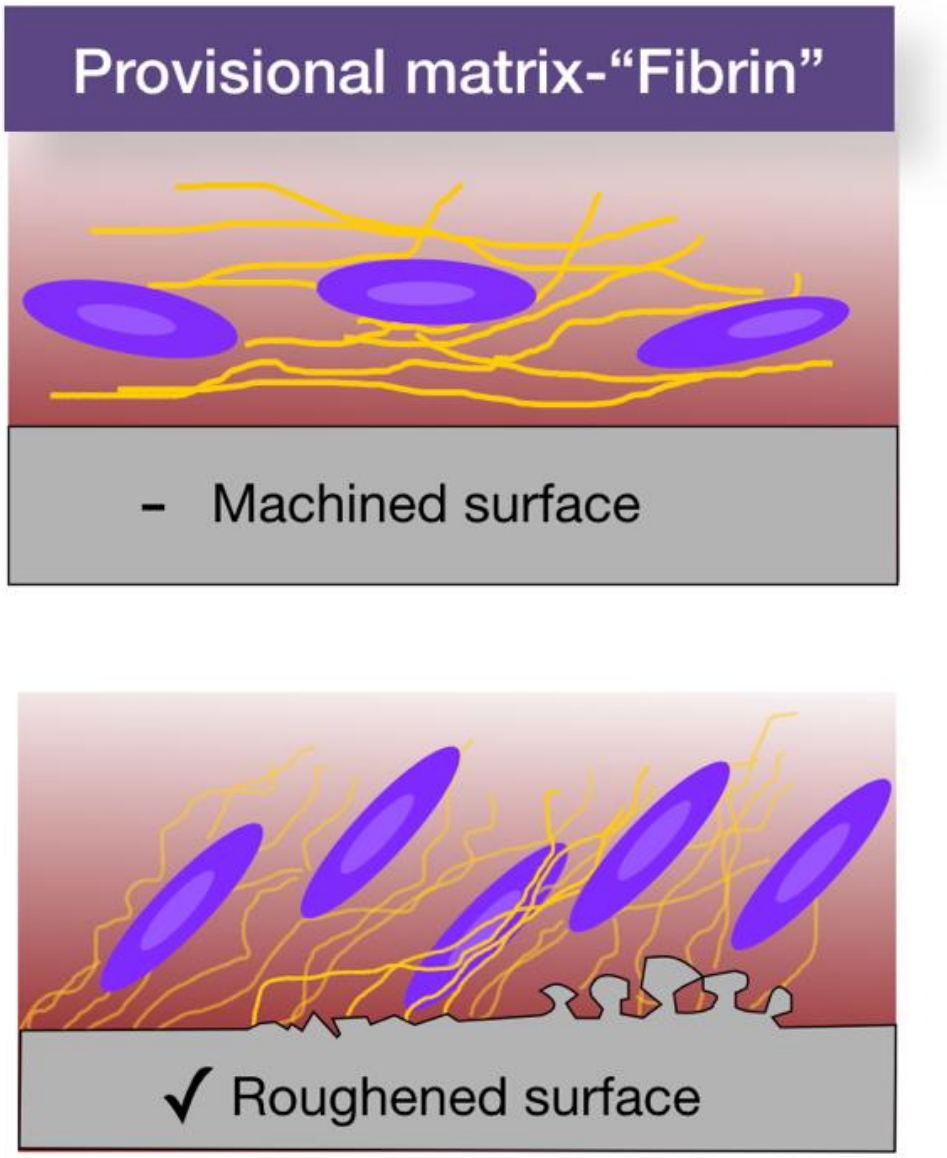

Figure 4.3 Osteoconduction is mainly influenced by the titanium surface treatment. Thus, depending of the degree of roughness, may capable to retain in more or less extent the blood clot and consequently the stabilization of fibrin matrix (yellow fibers) toward the implant surface after platelets (purple spheres) activation. This fibrin matrix does work as a provisional extracellular matrix, that encourages the cell migration, releasing growth factors, fomenting the angiogenesis.

4.3.1.2 *De Novo* Bone Formation

Osborn and Newesley 1980 work is particularly important in understanding contact osteogenesis (Osborn and Newesley 1980). However, their work omitted a critical step, that being the formation of the earliest mineralized matrix by differentiating osteogenic cells before they become mature polarized osteoblasts. This is the very stage at which, in normal bone remodeling sites, the osteogenic population secretes an initial matrix that provides the interface between old bone and new bone. Interestingly this interface was first described 123 years ago by a German histologist, von Ebner, who coined the term "Kittiinien", or cement lines, to describe the mineralized interfacial matrix laid down between old bone and new bone. Although new bone is formed, the term “de novo” bone formation is restricted to describe the cascade of biological events that occurs during bone formation by newly differentiating populations of osteogenic cells (Davies and Hosseini 2000; Davies 2003). The *de novo* bone formation is depicted in (Fig.4.4).

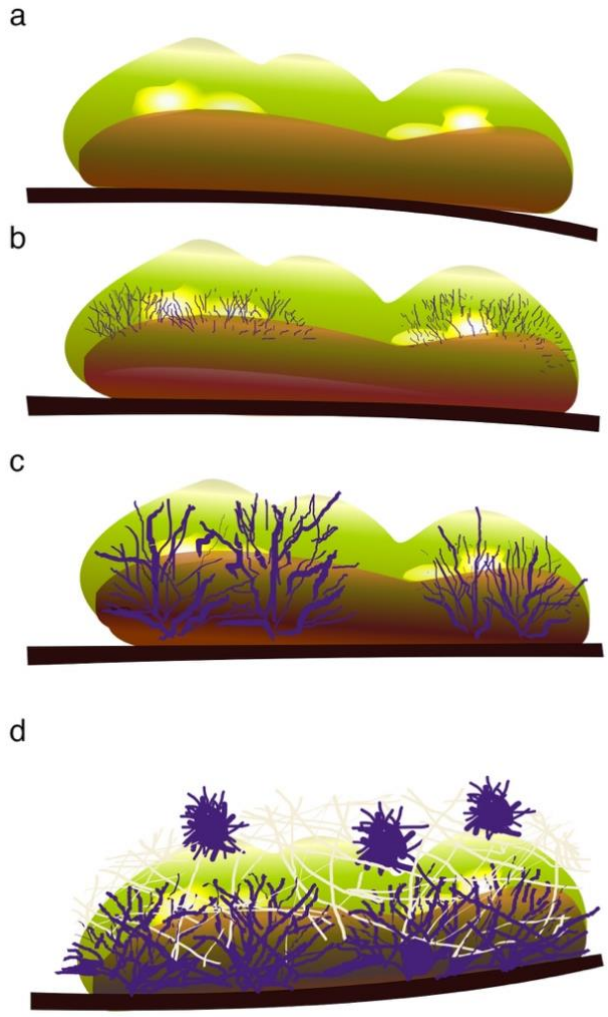

Figure 4.4 The “De Novo” bone formation. (a) Organic matrix secreted by osteoblast without collagen fiber, but rich in bone sialoproteins such osteopontin (OPN) and proteoglycans; OPN is secreted by immune cells like T lymphocytes, macrophages and monocytes. It is early expressed by osteoprogenitors cells, their presence is linked to pre-osteoblast differentiation. The proteoglycans is a fundamental component of extracellular matrix, it “fills” the intercellular spaces, and there are involved with Ca cations union and forms complex links with other proteins as type I collagen. (b) Ca ions nucleation. (c) Collagen synthesis, it is ensembled as woven bone, although at this instance collagen fibers are not completely mineralized. (d) Collagen mineralization, arose the cement line, that differentiate the mineralized from non-mineralized compartment, evidenced by cement line. Adapted from Davies and Hosseini 2000.

4.3.2 Early events during osseointegration

The series of events leading to osseointegration encompassed coagulum formation, granulation tissue formation, development of a provisional matrix, woven bone formation, parallel-fibered bone formation and eventually lamellar bone formation (Salvi et al. 2015). After implant installation, the thread was in contact with pristine bone and the pitches of the threads provided a mechanical anchorage in the pristine bone, providing the primary mechanical stability of the device (Raghavendra et al. 2005; Lioubavina-Hack et al. 2006b). The void between the pitch and the body of the implant established a geometrically well-defined wound chamber (Abrahamsson et al. 2004). This chamber was filled with a blood clot, characterized by the presence of erythrocytes, neutrophils and monocytes/macrophages in a network of fibrin, this tissue contained numerous mesenchymal cells, matrix components and newly formed vascular structures (Davies and Hosseini 2000; Salvi et al. 2015).

4.3.2.1 **Primary stability and interfacial remodeling healing pathway**

Arguably, one of the most important aspects to reach a clinical osteointegration is the primary stability during implant placement (Lioubavina-Hack et al. 2006a). In first instance there is an implant fixture mechanical anchorage provided by parent bone walls of implant bed preparation and the mechanical interlocking with implant threads and pitches during insertion. The extent of primary anchorage is tightly related to native bone characteristics, implant design, patient characteristics and surgical technique respectively (Meyer et al. 2004), all them regulate in more or lesser extent the strain applied to mineralized tissue in the implant proximity (Petrie and Williams 2005; Isidor 2006; Gottlow et al. 2012). Also, strain is directly related to bone interfacial stress and frictional force transferred, clinically interpreted as insertion torque (N/cm) (Huang et al. 2011; Chowdhary et al. 2015). Even though, this is the sole mechanical interlocking between the bone and the implant, there where exists no biological interplay (Halldin et al. 2011; Norton 2013). Therefore, primary stability should not be regarded as osseintegration since it is the result of the osteoconduction of implant system .

Higher primary stability is intuitively and fallaciously perceived as higher value of insertion torque, which is a pre-requisite to clinically indicate procedures such as immediate loading (Esposito et al. 2008; Javed and Romanos 2010). It is due to the fact that primary stability concept arise from theoretical background in which bone mineralized tissue is considered an elastic material, and both

the strain and the implant stability will have a linear relation (Halldin et al. 2011). Though, this implant stability would decrease as consequence beyond the yield strain of the bone due to the excessive microcracks formation and compression necrosis, events that trigger the peri-implant bone remodeling (Chamay and Tschantz 1972; Halldin et al. 2011). Smaller cracks (less than 100 micrometres) can also be detected during implant bed osteotomy preparation (Warreth et al. 2009), and longer cracks are often detected when the implant is placed in undersized implant sites (Bartold et al. 2011). Also, as previous reported osteocyte apoptosis is induced by bone fatigue, this apoptosis is localized to regions of bone that contain microcracks, and osteoclastic resorption after fatigue also coincides with regions of osteocyte apoptosis (Verborgt et al. 2000). It is because, if the high strain applied overpass the physiologic threshold, it results in a plastic deformation with numerous microcracks that alter pristine bone mechanical properties (O'Brien et al. 2005; Halldin et al. 2014); on the contrary an elastic response occurs if strain is below the yield point.

Although, microcrack formation is regarded an important phenomenon for the intracortical remodeling (Bentolila et al. 1998), excessive microcrack formation however has the risk of generate a macrocrack (fracture) through the interconnection of unrepaired microcracks (Burr et al. 1997, 1998). A necrosis by compression take place when the hard tissue around implant is faced with excessive strain with a deleterious effect on capillaries and nerves, damaging its structure (Zizic et al. 1985). Therefore, depending of implant design, surgical technique (instrumentation dimension), a variable degree between implant and parent bone friction and interlocking may occurs leading to higher or lower insertion torque, equivocally interpreted by several clinicians as proportional to implant primary stability, due to the fact that experimental evidence demonstrates that there is an inverse relationship between insertion torque and immediate micromotion; being unrelated in particular for those implants with the least insertion torque (Bashutski et al. 2009; Freitas et al. 2012). Also, a recent study reported that the more implant insertion force was used, the lowest primary stability is obtained through resonance frequency, though different forms of an implant system need different insertion torques to obtain an optimal primary stability (Staedt et al. 2017).

In summary, nowadays high insertion torque should be questioned because since elastic theory predicts that excessive strain may provoke deleterious biologic effects on bone response and its biomechanical stability depending on the implant thread design. This primary stability decreases as consequence of the cell mediated remodeling of surrounding pristine bone toward the implant surface (resorption and apposition), that was theoretically proposed by Raghavendra et al., 2005,

and further corroborated experimentally (Jimbo et al. 2014a), confers from this perspective, the implant stability dip, where high degrees of implant stability go down to a lower levels, and it may occurs when it is reached through a mismatch between implant macro-design and surgical instrumentation dimensions, or because the strain generated by thread tip is slightly higher than physiological limit, and consequently generates a stability lost through a cell-mediated interfacial bone remodeling, thereafter regained through bone apposition (Raghavendra et al. 2005; Jimbo et al. 2014b). Interfacial bone remodeling is depicted in (Fig. 7, 8).

4.3.3 A glance to dynamics of osteointegration of titanium dental implants

The knowledge from which the rationale of the integration of dental implants arises from several research lines in different species, including human studies. The extent of bone remodeling varies among species, being not compatible to be extrapolated across species, despite the biological process represented through optical histology shows qualitatively a similar pattern of bone tissue response. The osseointegration process of a titanium dental implant may depend on a number of variables and hence, results of the various parameters may not be standardized depending on the type of testing system and the factors with potential influence. Consequently, such variables may determine the rate and extent of osseointegration at various time points and in various species (Botticelli and Lang 2017).

These factors have been described; even though their relative significance to the speed and extent of osseointegration have not been studied systematically. It was recognized and suggested that the early osseointegration in an animal model was double as effective as in humans (Lang et al. 2011). To identify relevant factors that may influence the osseointegration phenomenon (e.g. parent old bone, implant geometry, implant surface, species model, timing of surgery, loading conditions), the parameter "*interception point*" was proposed (Botticelli and Lang 2017). This express the point at which two proportional lines of old and new bone illustrating bone resorption and bone apposition on the implant surface intersect which other, and it is defined by the time occurrence and the percentage of osseointegration reached.

4.3.3.1 **Parent old bone**

The parent old bone is related to the primary bone contact, it may vary between 15-32% measured between coronal level and the apex (Rossi et al. 2014a; Mainetti et al. 2015, 2016; Favero et al. 2016b, a). However, if fixture geometry changes were applied, lower BIC% of parent bone was

found after installation 6.3-6.5% compared to standard not modified implants (Berglundh et al. 2003; Abrahamsson et al. 2004). Another factor that may affect the primary bone-to-implant contact is the bone morphology of the recipient site. An experimental study in dogs (Rossi et al. 2014a) compared bone resorption and bone apposition separately at the cortical and at the marrow compartments.

After 5 days of healing, the contact of old bone to the implant surfaces was 66.5% in the cortical, 23.3% in the spongiosa, and 31.6% on the full length of the implant. So, the primary contact varies among the different zones that the implant is crossing and providing a mean value may not properly describe the real situation in the various regions of the implant (Botticelli and Lang 2017).

4.3.3.2 **New bone formation and interception point**

Regarding the new bone formation and interception point, it was observed that many variables influence the time and extent of bone apposition around titanium implants, and the above-mentioned parameter may provide data on efficiency of osteointegration. It was strongly influenced by the presence of old bone; So, in regions not in contact with mineralized tissues bone apposition starts within few days. On the contrary, bone in direct contact with implant surface has to undergo a resorption process before new bone may be formed (Berglundh et al. 2003; Rossi et al. 2014a). Accordingly to the aforementioned observations, a previous report in dogs (Abrahamsson et al. 2004), the trough prepared around the implant reduced the percentage of parent bone primary contact, so that more surface was at disposal for bone apposition. The interception point expressed this situation with 5.1 days and 9% of osseointegration at the SLA surface and 5.3 days and 6% at the turned surfaces.

At implants installed in cortical or spongy bone, different patterns of healing are expected, due to the differences in density of the bone in primary contact with the implant surfaces. Denser bone lead to a delay in bone formation, while spongy bone may allow a rapid bone apposition thanks to the presence of marrow spaces interposed among trabeculae. It was first demonstrated in an experiment in dogs (Rossi et al. 2014a). After 30 days of healing, old and new bone proportions were 43.3% and 34.3% in the cortical region, respectively and 10.9% and 53.4% in the trabecular region. The interception point expressed these results as 36.9 days at 39.4% of osseointegration in the cortical region and 10.6 days and at 15.9% of osseointegration in the trabecular region, respectively.

4.3.3.3 **Implant surface**

Additionally, implant surface characteristics also influenced the processes of osseointegration; Surface topography influences bone response at the micrometre level and some indications exist at nanometer level (Wennerberg and Albrektsson 2009). The earlier the interception point was reached and the higher is slope of the regression line (m), the earlier and faster was bone apposition (Botticelli and Lang 2017). The sequential healing of different surfaces was studied in dogs (Favero et al. 2016b, a). Similar percentages of old bone were present after 7 days and 14 days of healing. The osseointegrative properties of three surfaces may be expressed with the interception point that ranged from 10.2 days, at 16.9% osseointegration with m = 3.4 to 15.4 days and 15.3% of osseointegration m = 1.1. As such, the influence of the surface configuration on the osseointegration speed and extent was the least significant factor.

4.3.3.4 **Species assessed**

The osseointegration appeared to be strongly influenced by the species model, considering that rabbit model was faster compared to the dog model, and the dog model was faster the human model (Botticelli and Lang 2017). The interception point illustrated these results occurring after 4–6 days with 18–19% of osseointegration with an m = 4.1–6.3 for new bone in rabbits (Caneva et al. 2015) as opposed to 25.2 days with 28.4% of osseointegration and m = 1.4 for new bone for the SLA_ surfaces, and 18.1 days with 24.5% and m = 2.4 for new bone for the SLA_active_surfaces in humans (Bosshardt et al. 2011; Lang et al. 2011). So, among the factors involved during osseointegration, it was reported that the greatest influence is the differences in species followed by implant geometry, bone morphology, implant surface configuration, timing of surgery and load. The interception points may provide information on efficacy of early osseointegration.

4.3.3.5 **Basic anatomy of rabbit tibiae**

The rabbit is one of the most common used animals in dental implant research. It is used around 35% of all musculoskeletal research studies (Neyt et al 1998). This model reaches its skeletal maturity at around 6 to 8 months of age (Gilsanz 1988). This can be studied using radiographs from metaphysis. The most common experimental sites are the femoral diaphyseal bone and the tibial bone. The femoral and tibial bone of the rabbits has several advantages. The dimensions and the anatomy of the bone correspond fairly well with the edentulous jaw in humans.

5. MATERIAL AND METHODS

5.1 Ethical declaration for animal experimentation

The study protocol was approved by the Ethics Committee of Valencia University, Spain (Protocol ref.: A1432625410189), which followed the guidelines established by the Council Directive of the European Union (53/2013; February 1, 2013) for animal care and experimentation in agreement with the ethical and legal conditions established by Royal Decree 223, March 14 and October 13, 1988.

5.2 Study design and experimental animals

The present experimental pre-clinical study involved twenty-seven males, albino New Zealand rabbits, 24 weeks of mean age and weighing 3 to 4 kg. The animals were segmented into three groups composed of 9 animals each and sacrificed at 2, 4 and 8 weeks, respectively. Implants were assigned to the animals in a random way, having as a result the placement of four dental implants in each rabbit; two in each tibia, one in the diaphysis and the other one in the metaphysis.

5.3 Randomization and Allocation Concealment

Before surgery, the animals were put in one of the three groups by a random allocation, each group being the representation of a healing period. Two implants with a different macro-design were installed in each tibia. The position of each implant, i.e. diaphysis or metaphysis, was randomly assigned. The aleatory choice was carried out electronically (www.randomization.com) by an independent author neither involved in the selection of the animals nor in the surgical procedures (Danielle Botticelli) **(Fig. 5.1)**.

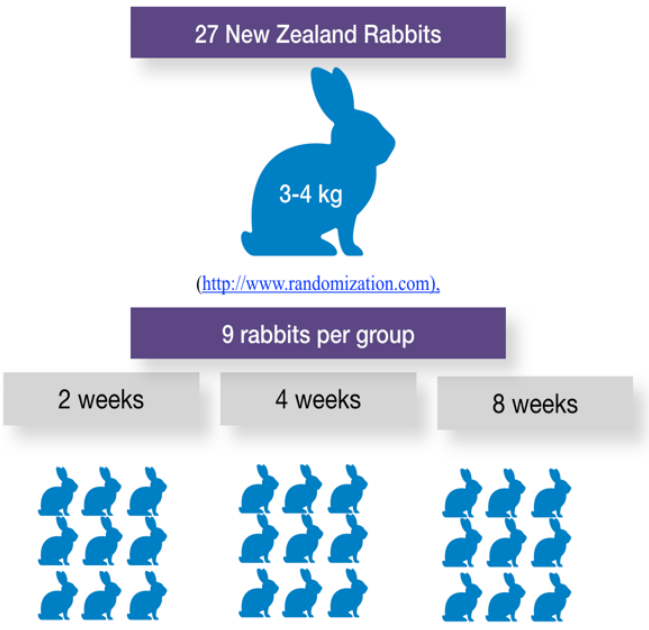

Figure 5.1 Randomization and allocation concealment scheme.

5.4 Implant features

Ticare® implants (Mozo-Grau, Valladolid, Spain) made of commercially pure grade-IV titanium treated with resorbable blast media (RBM) (implant surface blasted with calcium phosphate ceramics, resulting in a moderately rough (R_a=1.53±0.24) surface) were used. All implants had a dimension of 3.75 mm of diameter and 8 mm of length, a conical platform with a 45º polish neck with a self-tapping feature closer to the apex (Fig. 5.2).

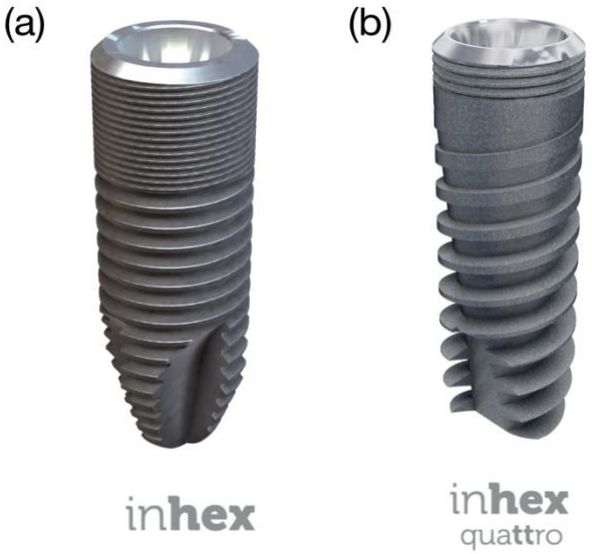

Figure 5.2 Ticare Inhex® (a): the implant body had a little conicity and a large area of micro-threads at the coronal portion, and higher number of triangular threads per unit length and with little thread depth compared to Quattro® model. Moreover, the implant had a double self-tapping at the apical portion. **Ticare Inhex Quattro® (b):** the implant body had a marked conicity. Fewer micro-threads at the coronal portion and a lower number of macro-threads were present compared to Ticare Inhex® implants. The threads were squared in the middle part of the implant and become triangular and deeper at the apex. Aggressive self-tapping at the apex.

5.5 Surgical procedures

The rabbits were induced to anesthesia with Ketamine injection (22 mg/kg) intramuscularly, xylazine (2.5 mg/kg) and intravenous injection of Propofol (1.5 mg/kg) and maintained with 2% of isoflurane. Before surgery, the rabbits' fur that was proximal to the tibia was shaved and disinfected with Betadine. A preoperative antibiotic Enrofloxacin 5 mg/kg (ALSIR® 2,5%, Esteve Veterinaria, Barcelona, Spain) was infiltrated subcutaneously, and 3 ml of articaine at 2% with 0.01 mg/ml epinephrine infiltrative anesthesia was intramuscularly applied in the surgical area of each leg. The skin of both tibiae was incised in the proximal region, the flaps were raised and the bone was shown below the anterior tibial tuberosity (Fig. 5.3a). Both areas, one in the metaphysis and other in the diaphysis were identified as experimental sites. The recipient sites were prepared following the recommendations of the manufacturer using drills with increasing diameter under irrigation with sterile saline (Fig. 5.3b). A distance of about 8-10 mm was maintained between the two osteotomies (Fig. 5.3c). Two implants with different macro-design were randomly installed in each tibia: Ticare Inhex® and Ticare Quattro®. The implants were screwed until the implant shoulder was leveled with the bone surface.

The implant's apex was placed in close contact with or into the cortical bone opposing the coronal cortical compartment, looking forward to obtain a bi-cortical anchorage. Cover screws were placed on the implants, and the flaps were subsequently sutured in layers with resorbable sutures (Vicryl 5/0, Ethicon, Sommerville, NJ, USA), and Nylon 3/0.

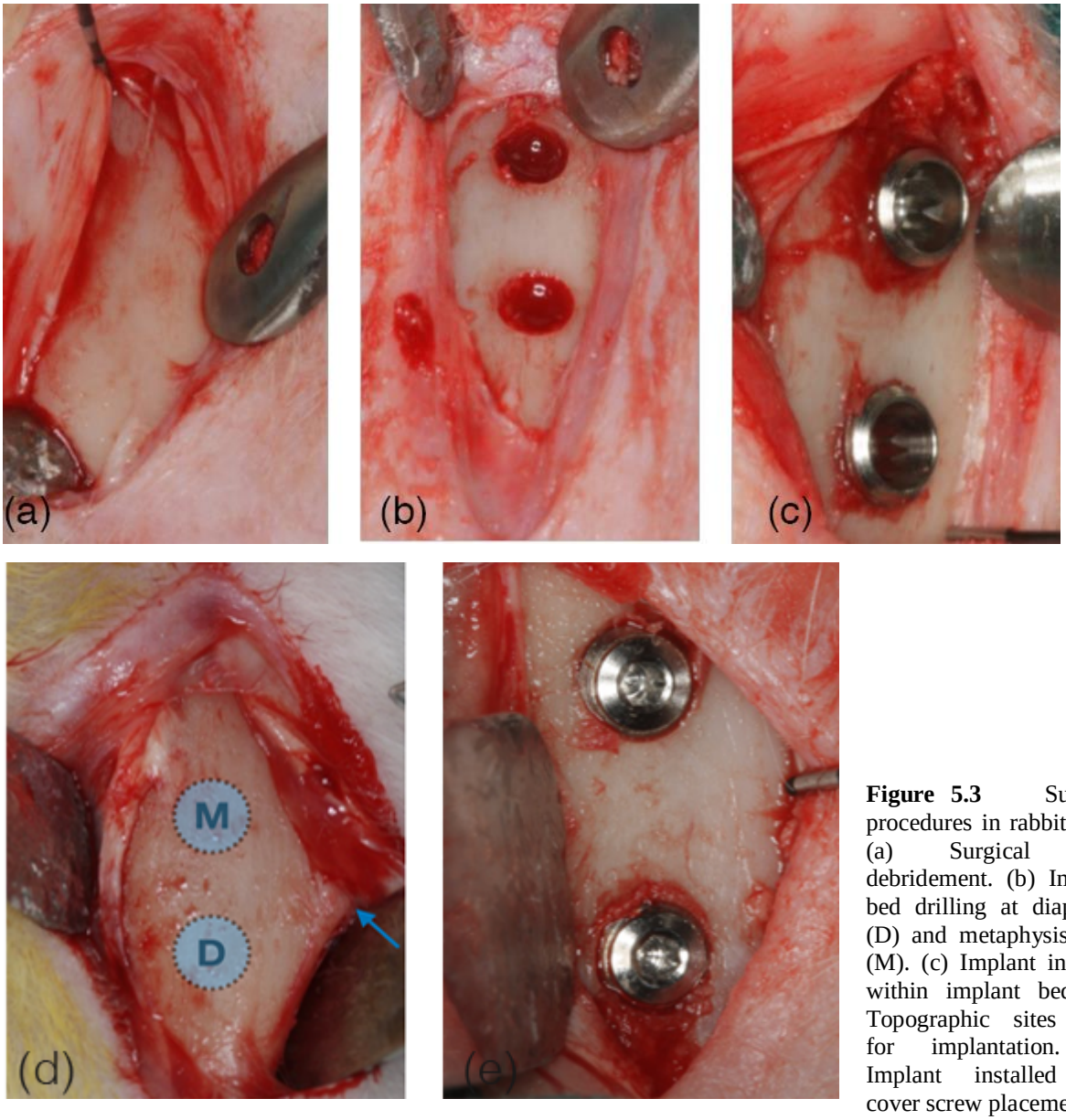

Figure 5.3 Surgical procedures in rabbit tibia. (a) Surgical flap debridement. (b) Implant bed drilling at diaphysis (D) and metaphysis sites (M). (c) Implant inserted within implant bed. (d) Topographic sites used for implantation. (e) Implant installed and cover screw placement.

5.6 Post-operative care, housing and husbandry

Each animal had its own cage; the room in which they were kept was purposely designed so it could have 12 hours of light; and so it was an acclimatized space**.** The animals were fed with a standard diet and had free access to water. The analgesic pattern consisted in 2.5 mg/kg of morphine intraoperative, 0.02 mg/kg buprenodale, buprex, 0.2 mg/kg meloxicam (every 12 hours during 3

days) and antibiotic therapy with Enrofloxacin 2.5 mg/Kg (ALSIR® 2,5%, Esteve Veterinaria, Barcelona, Spain) (every 24 hours during 7 days) post-operatively. Within 2–3 days, the animals continued to act in a normal way, lacking of pain or distress symptoms. Also, after the operation the wounds were constantly inspected and cleaned with Betadine to prevent future complications.

5.7 Euthanasia

The euthanasia of the animals took place at different healing times according to the group; some animals were sacrificed after 2 weeks while others after 4 or 8 weeks. It was performed by using the same protocols used for surgery; 50 mg/kg intravenous sodium pentobarbital was applied to each rabbit. Both animal's tibias were removed, while the adhering soft tissues were dissected. A small electric saw was used to obtain the sections of the tibia containing each implant.

5.8 Histological preparation

Implant samples were dehydrated by sequential solvent exchange and embedded in methyl methacrylate containing poly-(methyl methacrylate). After adding benzoyl peroxide (1 g/100 mL), samples were polymerized at room temperature for several days and were then sawed using a diamond wheel on a precision table top cut-off machine Accutom-5, (Struers, Copenhagen, Denmark) and then were wet ground and polished using a LaboPol-21 system (Struers, Copenhagen, Denmark) and SiC foils. Approximately 80 μm thin sections were obtained using SiC foils of decreasing particle size. The samples were stained at 55 °C with toluidine blue for 30 min, washed with tap water for 2 minutes and let dry.

5.9 Histological examination

Overlapping calibrated digital images of the tissues surrounding the whole implant surface (about 20 images/implant) were recorded with a bright field Leica DM4000 B microscope (Leica Microsystems GmbH, Wëtzlar, Germany) and DFC420 digital camera using a 5× objective and the Leica Applications Suite version 4.4.0 software. Individual images were merged to compose each implant side using the Photoshop program (Adobe Photoshop CC 2015.0.0). The image processing program ImageJ 1.48 (National Institutes of Health, Bethesda, MD, USA; http://imagej.nih.gov/ij) was used for histological measurements. Lines were drawn by hand on calibrated images showed on the computer screen at 400× magnification by an independent and calibrated assessor not involved in study. The following references highlights were traced to identify: (B) the most coronal bone-to-

implant contact and (A) the base of the implant. Three sections with similar length were established to divide the implant within: coronal, middle and apical areas regarding the long axis (Caneva et al. 2015).

5.10 Study variables

5.10.1 New osseointegration values

The percentages of (nb) new bone, (ob) old bone, and (m) bone marrow in contact with the implant surface were measured on the entire implant length as well as on each of the three sections. The BIC was examined as the sum of new and old bone, and percentages in relation to the length of the implant surface examined calculated. The apical portion of the implant that extruded beyond the compact cortical layer was excluded from the analyses (Fig. 5.4)

5.10.1 Cortical and marrow compartments

The percentage of new osseointegration values were assessed at both cortical (coronal and apical sections) and marrow (middle section) compartments. For the study purposes the cortical compartment is considered as a whole (coronal + apical).

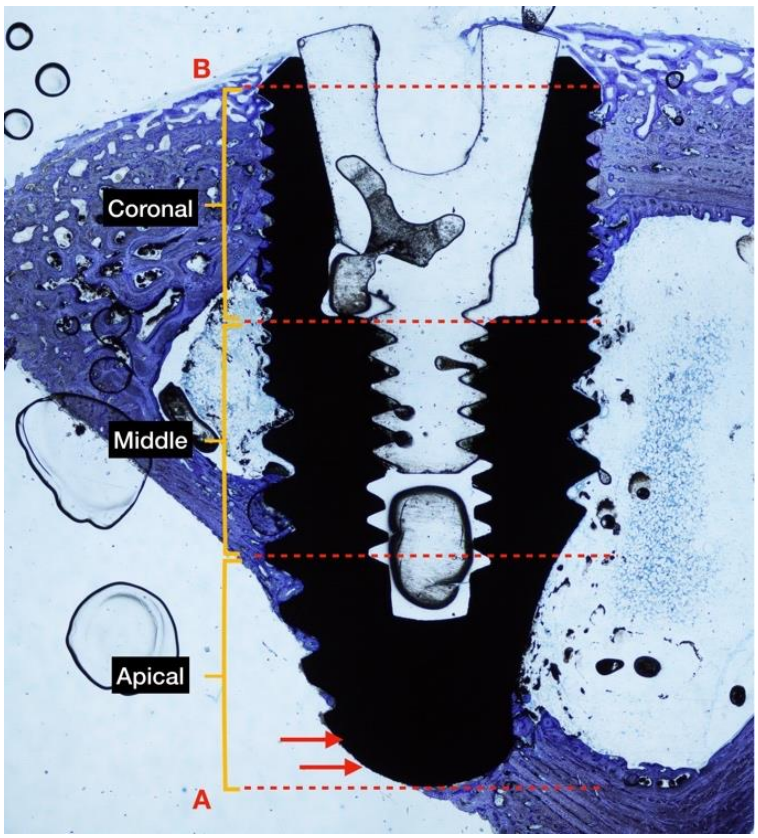

Figure 5.4 Ground section of rabbit tibia in diaphysis position at 4 weeks of healing. The implant is divided in 3 equal sections (coronal, middle, apical) for BIC measurement. Two points were traced: (B) Most coronal part of bone to implant contact. (A) Base of the implant. The Implant surface outside to the cortical bone is not considered in analysis (red arrows). Original magnification x2. Toluidine blue staining.

5.11 Data analysis

Differences between implant designs across the healing periods were analyzed with the Mann–Whitney U-test for independent variables. Differences between implants placed in the diaphysis and metaphysis were also performed using a Wilcoxon rank-sum test. A multivariate general lineal model analysis was performed to explore the interaction between the two independent variables (design/position) over BIC values at different healing stages. Each factor with two categories: design (Ticare Inhex® /Ticare Quattro®) and position (diaphysis/metaphysis). This approach was chosen because previous reports observed that the positions of the implants can be used as independent replicates regarding outcome variable, since bone quality varies between implantation sites (topographic sites) at same degree as between experimental units (Ernst et al. 2015).

6. RESULTS

6.1 Sequential healing during osseointegration of implants with RBM surfaces

6.1.1 Clinical and histological outcomes

This experimental preclinical study is performed in abidance with the Animal Research: Reporting *In vivo* Experiments (ARRIVE) guidelines and animal selection and use have been carefully considered (Kilkenny et al. 2010). No complications occurred during the healing period. All implants seemed adequately integrated into the histological evaluation across each period. Finally, data of 27 experimental animals with four implants each were analyzed. The areas between the threads were filled with woven bone at two weeks. Remodeling processes were observed after 4 and 8 weeks of healing, as shown by the lighter-staining of the lamellar bone compared to the darker-staining of the woven bone.

6.1.2 Week 2

The healing process remains in its initial phase. There is an evident accelerated proliferation of blood vessels and mesenchymal cells embedded inside the provisional granulation tissue that stimulate the formation of an immature peri-implant primary bone, this bone modeling is observed in healing chambers by the presence of a cell-rich immature bone or woven bone (WB) (Fig. 6.1).

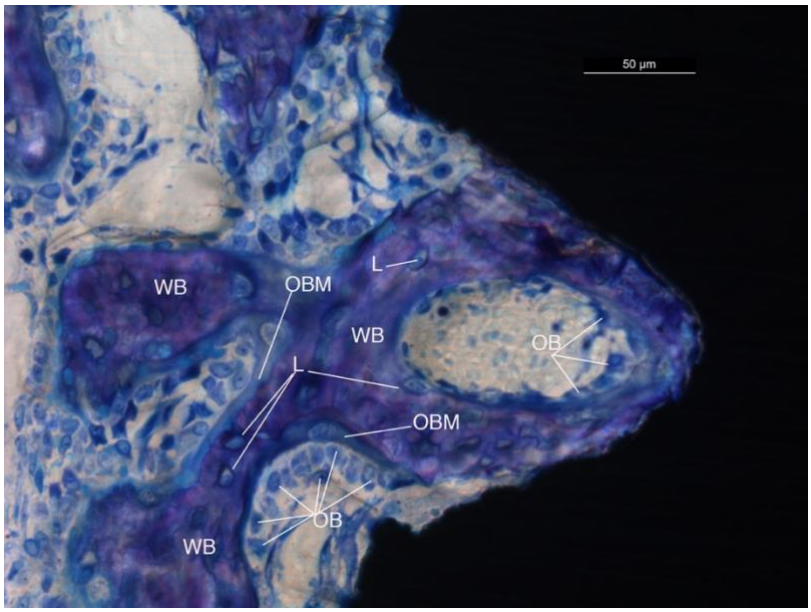

Figure 6.1 Optical micrograph of woven bone (WB) in a rabbit model at 2 weeks of healing. The image depict an uncontrolled and disorganized bone growth as consequence of organic bone matrix (OBM) deposition by osteoblast, note the irregular distribution of fibrous matrix in a diffuse woven bone and the presence of some osteocytes embedded within lacunae (L). Toluidine blue staining.

High magnification evaluation showed woven bone formation throughout the extension of the healing chamber region, with loci of diffuse woven bone and lines of osteoblasts depositing bone matrix. This ‘contact osteogenesis’ is considered to represent the very first phase of

osseointegration, namely direct contact between the roughened implant surface and newly formed woven bone as depicted in (Fig. 6.2).

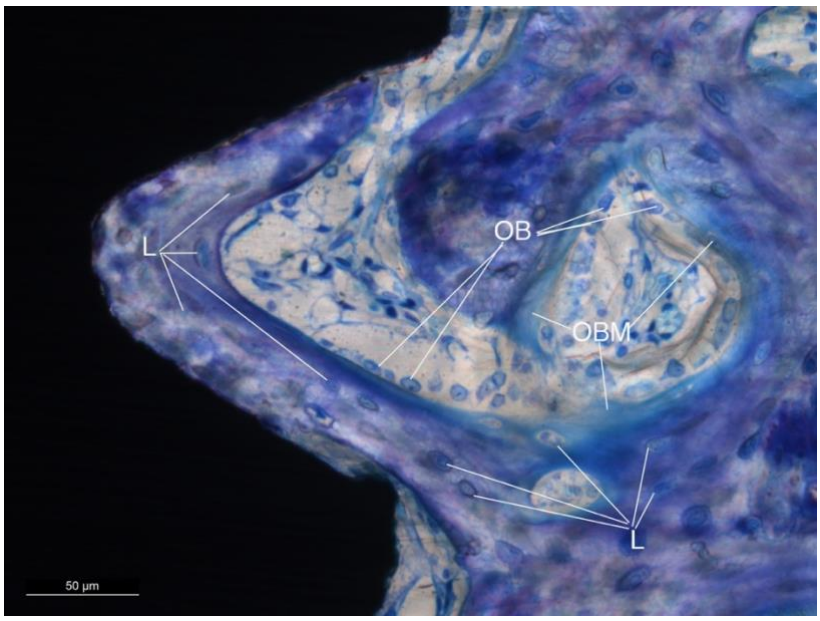

Figure 6.2 Optical micrograph at 2 weeks in-vivo in a rabbit model. It is observed the non-mineralized woven bone (WB) within healing chamber, also some osteoblasts (cube-shaped cells) secreting organic bone matrix perceived by the light blue color (OBM) and some lacunae in the proximity (L) suggesting the presence of osteoblast trapped in bone matrix to become converted as osteocytes. The image depicted at this stage suggesting a high activity of the cellular content. Toluidine blue staining.

Simultaneously, osteoclast formation concurs on the pristine bone, resulting in bone resorption adjacent to the implant surface, especially in areas of pressure of the implant to the bony bed (i.e. pitches of the threads) that provided initial fixation for the implant, had undergone resorption through a cell mediated interfacial bone remodeling around microcrack zones, and were also involved in new bone formation after 2 weeks of healing. Mechanical stability of the implant was replaced by secondary biological stability (Fig. 6.3).

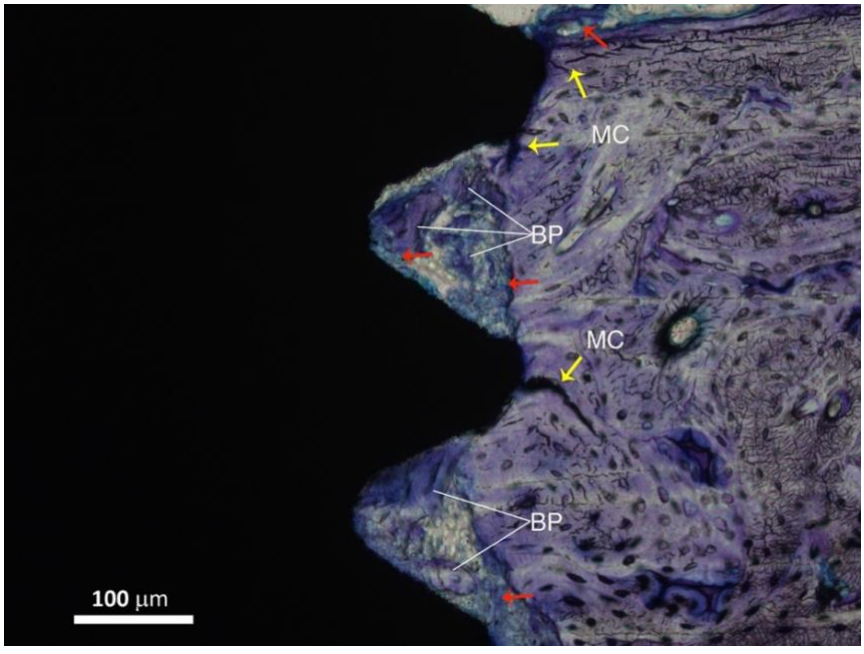

Figure 6.3 Optical micrograph at 2 weeks of healing in a rabbit model. It could be appreciated how the bone-implant interface, advert visually a mechanical interlocking between parent bone of implant site and implant surface, responsible for the primary stability. At this period the presence of a microcrack (MC) in proximity to implant thread (yellow arrow), as well as old bone particles (BP) within healing chamber, shed light that yield of bone strength overpass the physiological limit due to the high stress in this area. It is denoted by an active remodeling establishment within healing chamber and microcrack proximity (red arrow), compatible with an interfacial bone remodeling. Toluidine blue staining.

6.1.3 Week 4

The healing progress at this stage showed the woven bone (WB) replacement by lamellar bone (LB), suggesting an initial remodelling begin. It is evidenced by the presence of primary osteonic structures (O) which elucidate the onset of WB remodeling toward LB configuration surrounding blood vessels. Also, lacunae in LB were present behind the mineralizing bone front, the bone organic matrix is secreted and deposited circumferentially towards osteonic lumen by osteoblastic cells, this osteonic structures constitutes a source of nutrients, blood vessels and mesenchymal cells. The healing at this stage is depicted in (Figs. 6.4 and 6.5).

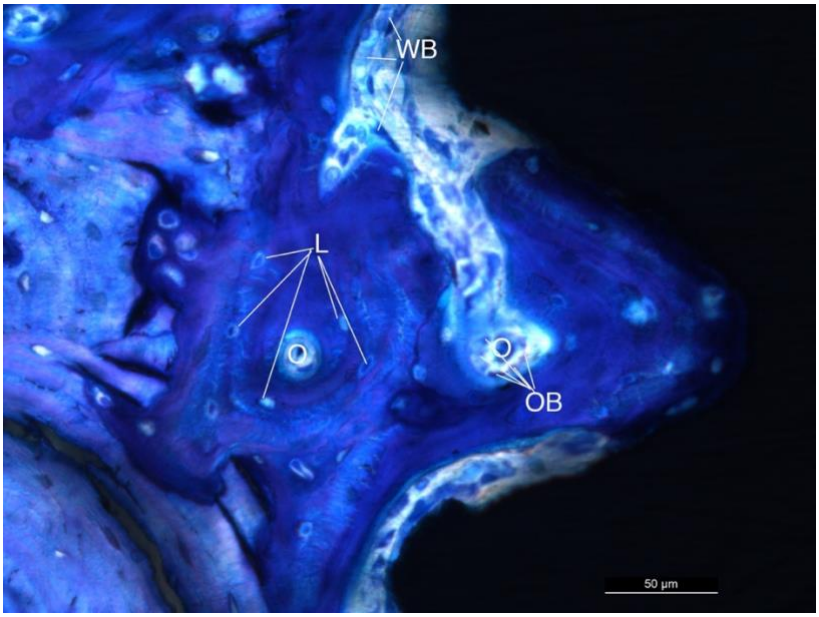

Figure 6.4 Optical micrographs at 4 weeks in-vivo in a rabbit model, it is observed how the woven bone (WB) is progressively replaced by a more organized lamellar bone (LB) surrounding primary osteonic structures (O), also some osteoblast (OB, cube-shaped cells) secreting organic bone matrix within osteon lumen in a circumferential manner. There are some lacunae within lamellar bone distributed in concentric manner (L). Toluidine blue staining.

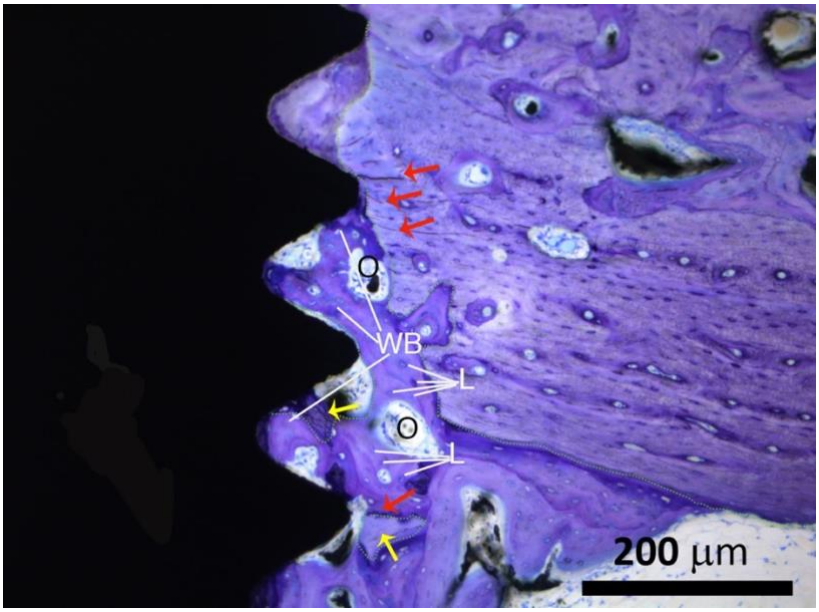

Figure 6.5 Optical micrograph at 4 weeks of healing in a rabbit model. It is evident a remodeling across healing chambers, remodeling sites occurs in the proximity of microcracks (red arrows). The resorbed area will be replaced by woven (WB) bone which reestablishes the contact to implant surface (secondary stability), subsequently to arise the will be the new primary osteons (O) with some osteocytes trapped within lacunae (L). Tissue remodeling has occurred at the interface where cell-mediated processes resorbed the region encompassed between the green dashed line and the implant. Toluidine blue staining.

6.1.4 Week 8

The bone throughout the healing chambers showed clearly a "bone remodeling" process, with the presence of parallel fibered lamellar bone deposition. There was a plenty of bone formed, evidenced by the presence of primary and secondary osteonic structures. It is visible lamellar osteons (Haversian systems) outlined by cement-line boundaries. The bone trabeculae had become reinforced thus providing a structure to cope with the bearing of load (Fig. 6.6a-b). There is a mixed bone morphology with regions of woven and lamellar bone, the remodeling process still occur at this stage (Figs. 6.7 and 6.8).

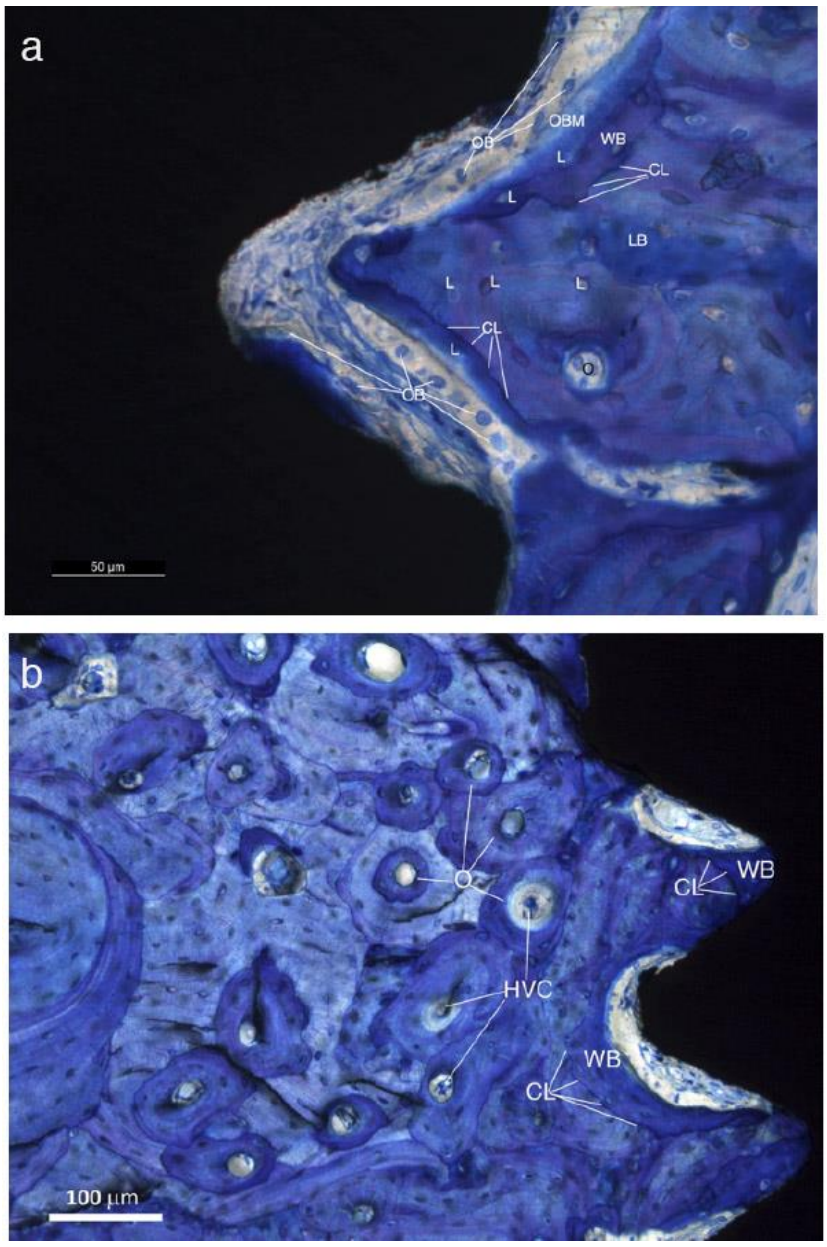

Figure 6.6 Optical micrographs at 8 weeks in-vivo in a rabbit model. **(a)** The bone remodeling still occurs within healing chamber in the proximity of implant surface, it is denoted by the presence of woven bone (WB) with some osteoblasts (OB) depositing organic bone matrix (OBM) characterized by a light blue staining, and lacunae (L) with trapped osteocytes. The WB is surrounded by lamellar bone showing primary osteonic structures (O) which revealed that onset of woven bone remodeling toward lamellar configuration surrounding blood vessels, outlined by reversal "cement lines" (CL) that differentiate the mineralized from non-mineralized compartment. **(b)** It could be clearly observed the presence of primary and secondary osteonic structures (O) with their owns Haversian´s system canals (HVS). At this stage the mature bone its capable to resist load bearing. Toluidine blue staining.

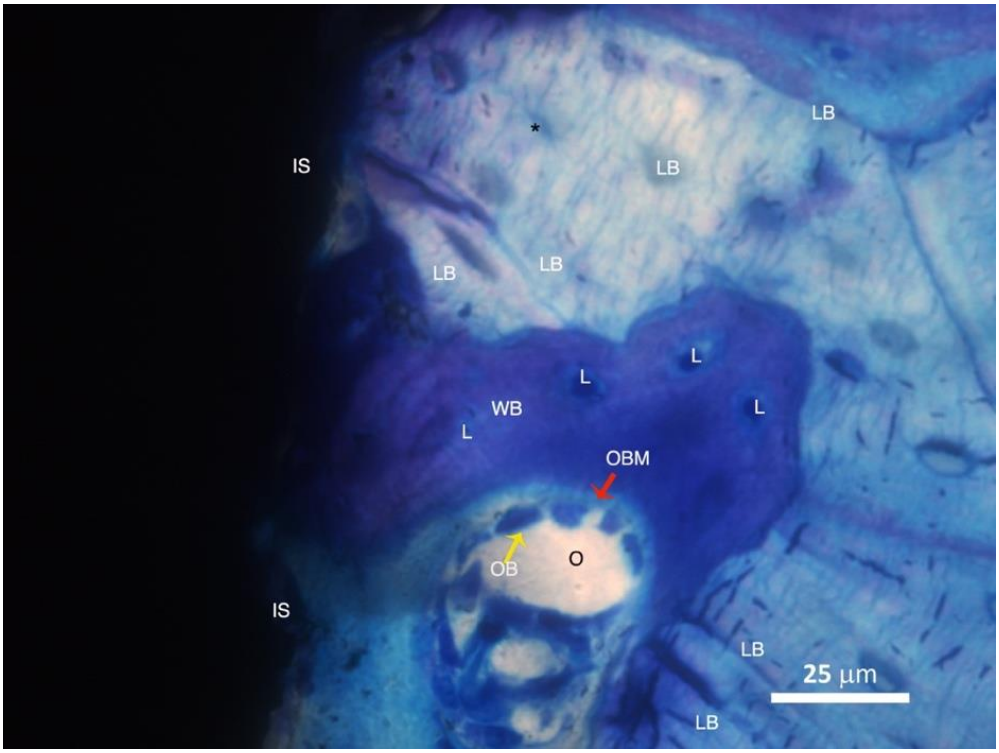

Figure 6.7 Optical micrograph at 8 weeks in-vivo in a rabbit model. It is evidenced a mixed bone morphology with regions of woven (WB) characterized by a "more intense" staining color and lamellar bone (LB) "less intense" staining color, surrounding osteonic structures (O). There is a new bone formation in contact implant surface (IS) at expense of lamellar bone remodeling, it is visible the presence of osteocytes in LB (black asterisk) and trapped in lacunae's (L) as well, behind the organic bone matrix (OBM) deposition by osteoblast cells (OB) disposed circumferentially within osteon lumen (yellow arrow), and denoted by the light blue color (red arrow). Toluidine blue staining.

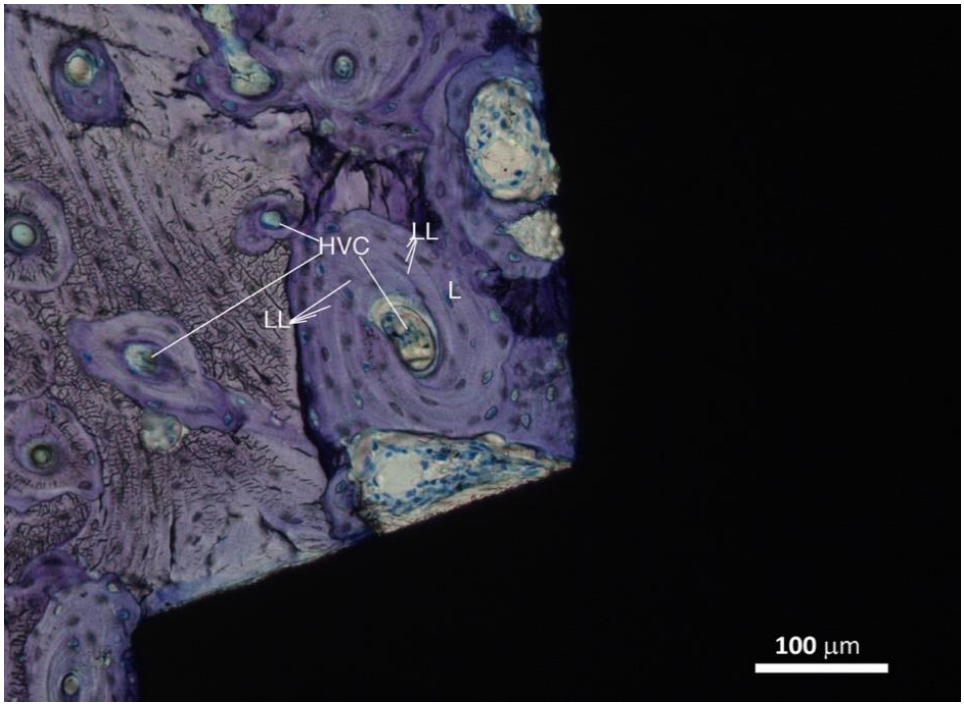

Figure 6.8 Optical micrograph of the lamellar bone (LB) in a rabbit model at 8 weeks of healing. The histological image showed remodeling units "osteons" showing concentric layers of lamellae (LL) around a Haversian canals (HVC) (vascular support).

6.2 The effect of implant macro-design on osseointegration

2-week healing

A similar degree of new bone was observed in both macro-designs at this stage, being 16.0±7.5% for Ticare Inhex® , and 16.3±7.2% for Quattro® implants. The old bone percentages observed were 7.4% and 7.6% for Ticare Inhex® and Quattro® implants, respectively (Fig. 6.9a). Similar BIC values were observed between implant macro-designs and were 23.5±14.4% and 23.9±13.3% for Ticare Inhex® and Quattro® , respectively (Fig. 6.9b). None of the differences for both macro-designs were statistically significant (Tables 6.1 and 6.2).

4-week healing

The values of new bone at this time of healing were 19.4±7.3% and 18.9±4.7% for the Ticare Inhex® and Quattro® designs, respectively. The old bone percentages at this stage were 2.3±2.2% and 2.4±1.6%, respectively (Fig. 6.9a). Similar BIC values (old + new bone) were observed between implant macro-designs (Fig. 6.9.b). None of the differences for both macro-designs were statistically significant (Tables 6.1 and 6.2).

8-week healing

At this stage, new bone increased, reaching percentages of 33.2±7.6% and 33.4±7.7% for Ticare Inhex® and Quattro® implant designs, respectively. Old bone was still present, however at very low percentages, being 1.2±1.1% and 3.3±1.1% for Ticare Inhex® and Quattro® designs, respectively (p=0.001) (Table 6.9a). The BIC values observed between implant macro-designs did not show a significant difference, even though slight better BIC values in favor Ticare Quattro® compared to Inhex® design were found, being 36.7±7.7 % and 34.4±7.8, respectively (Table 6.1; Fig. 6.9b).

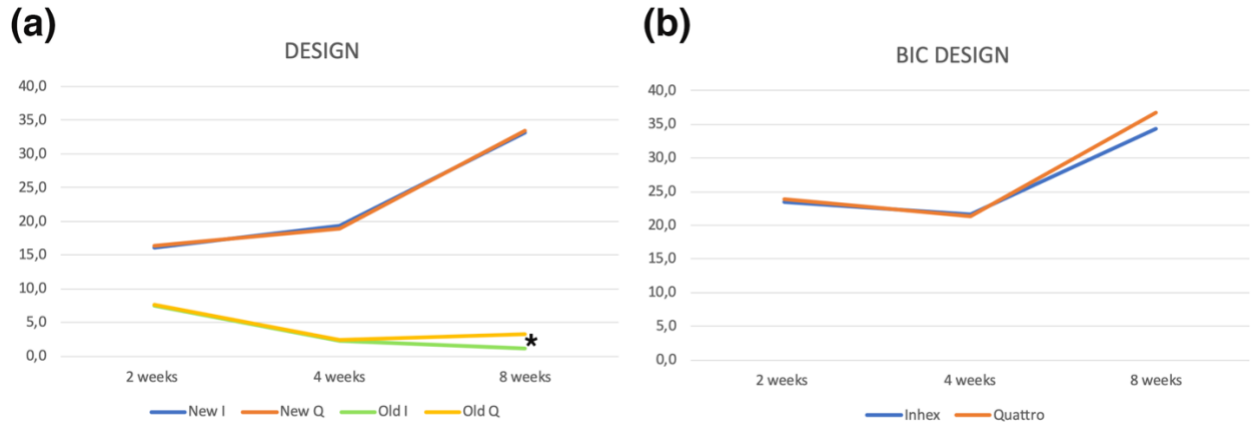

Figure 6.9 The total amount of new bone and old bone (**a**) and BIC values (new+old) according to implant implant macro designs, Ticare Inhex or Ticare Quattro (**b**) at different healing periods. Significant differences between implant macro-designs (*); ($p < 0.05$).

Table 6.1 Summary of proportion (%) of tissues components assessed in contact with the implant surface for both implant macro-designs at the various time periods, n = 9 per each period of healing.

Healing period		Inhex					Quattro			Differences
		New Bone	Old Bone	Soft Tissue			New Bone	Old Bone	Soft Tissue	
2 weeks	Mean	16	7,4	76,5	2 weeks	Mean	16,3	7,6	76,1	NB: p=0,93
	SD	7,5	6,3	7,1		SD	7,2	5,4	6,7	OB: P=0,94
	Median	16,1	4,6	76,1		Median	16,5	6,5	76,9	ST: p=0,89
4 weeks	Mean	19,4	2,3	78,4	4 weeks	Mean	18,9	2,4	77,3	NB: p=0,74
	SD	7,3	2,2	7,8		SD	4,7	1,6	6,3	OB: P=0,58
	Median	20,3	1,4	77		Median	18,4	2,2	79,1	ST: p=0,88
8 weeks	Mean	33,2	1,2*	65,4	8 weeks	Mean	33,4	3,3*	63,3	NB: p=0,92
	SD	7,6	1,1	8,2		SD	7,7	1,1	7,7	OB: P=0,00
	Median	32,6	0,7	64,6		Median	32,4	3,3	64,7	ST: p=0,40

U Mann withney-test: p<0,05
*P < 0.05 between Inhex and Quattro designs.

Table 6.2 Summary of proportion (%) of bone to impant contact (BIC) of implant macro-designs at the various time periods. n = 9 per each period of healing.

Healing period	BIC %			Differences
	Statistic	Inhex	Quattro	
2 weeks	Mean	23,5	23,9	p=0,916
	SD	14,4	13,3	
	Median	23,0	23,0	
4 weeks	Mean	21,6	21,2	p=0,822
	SD	10,0	7,1	
	Median	22,6	20,8	
8 weeks	Mean	34,4	36,7	p=0,626
	SD	7,8	7,7	
	Median	32,2	30,0	

U Mann withney-test: p<0,05
*P < 0.05 between diaphysis and metaphys

6.3 The effect of topographic site on osseointegration

2-week healing

Similar degree of new bone were observed either at diaphysis, 16.4±5.8%, and metaphysis, 16±6.2% (p>0.05). The old bone percentages were around 7.5±4 at diaphysis and 7.6±5.6 in metaphysis sites. There were not significant differences among the assessed parameters at this stage (Fig. 6.10a). Similar BIC values were observed between implantation sites, and were 21.5±7.5 and 25.5±14.6 at diaphysis and metaphysis sites, respectively (Fig. 6.10b). None of the differences for both topographic sites were statistically significant (Tables 6.4 and 6.5). Histological images at this stage are shown in Figure 6.11a,d.

4-week healing

The new bone values were 21.2±5.2% at diaphysis and 17.1±7.9% at metaphysis (p>0.05). The old bone values were 3.3±2.6% and 1.3±0.9% at diaphysis and metaphysis, respectively; this difference proved to be significant (p=0.05) (Fig. 6.10a). A significant difference was observed for soft tissue values at this stage and were around 75.5±6.4% and 81.6±7.7% for diaphysis and metaphysis sites, respectively (p=0.05) (Table 6.4). The BIC values were 24.5±6.2% for diaphysis and 18.4±7.7% for metaphysis at this stage (Fig. 6.10b). This difference proved to be significant (p=0.05) (Table 6.5). Histological images at this stage are shown in Figure 6.11b,e.

8-week healing

A similar degree of new bone were observed at diaphysis, 36.4±10.5%, and metaphysis, 29.3±6.2%, sites (p>0.05). The old bone values were 3.1±2.6% and 1.3±1.1% at diaphysis and metaphysis sites, respectively (p>0.05) (Fig. 6.10a). The BIC values were 39.5±11.1% and 30.6±6.2 % for diaphysis and metaphysis sites (Fig6.10b). The difference proved to be significant at this stage of healing (p=0.05) (Table 6.5). Histological images at this stage are shown in Figure 6.11c,f.

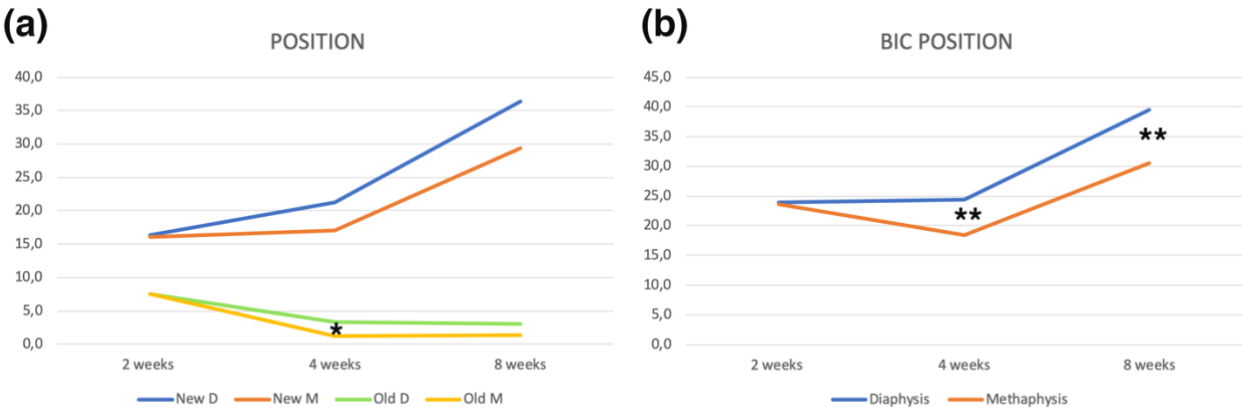

Figure 6.10 The total amount of new bone and old bone (**a**) and BIC values (new+old) according to implant position (diaphysis or metaphysis) at different healing periods. Significant differences between implant macro-designs (*) and between diaphysis and metaphysis (**); ($p < 0.05$).

Table 6.3 Summary of proportion (%) of tissues components assessed in contact with the implant surface according topographic location at the various time periods. n = 9 per each period of healing.

Healing period		Diaphysis					Metaphysis		
		New Bone	Old Bone	Soft Tissue			New Bone	Old Bone	Soft Tissue
2 weeks	Mean	16,4	7,5	76,1	2 weeks	Mean	16	7,6	76,4
	SD	5,8	4	5,1		SD	6,2	5,6	7
	Median	16,2	5,4	76,4		Median	14,1	5,9	75,6
4 weeks	Mean	21,2	3,3*	75,5*	4 weeks	Mean	17,1	1,3*	81,6*
	SD	5,2	2,6	6,4		SD	7,9	0,9	7,7
	Median	22	2,9	73,8		Median	16,6	1,2	82,3
8 weeks	Mean	36,4	3,1	60,5	8 weeks	Mean	29,3	1,3	69,4
	SD	10,5	2,6	11,1		SD	6,2	1,1	6,2
	Median	35,7	1,9	55,4		Median	27,8	1,1	69,5

U Mann withney-test: p<0,05
*P < 0.05 between diaphysis and metaphysis.

Table 6.4 Summary of proportion (%) of bone to impant contact (BIC) according topographic location at the various time periods. n = 9 per each period of healing.

Healing period	BIC %			
	Statistic	Diaphysis	Metaphysis	Differences
2 weeks	Mean	21,5	25,5	p=0,530
	SD	7,5	14,6	
	Median	23,0	19,5	
4 weeks	Mean	24,5*	18,4*	p=0,05
	SD	6,2	7,7	
	Median	29,4	16,5	
8 weeks	Mean	39,5*	30,6*	p=0,05
	SD	11,1	6,2	
	Median	35,9	30,6	

U Mann withney-test: p<0,05
*P < 0.05 between diaphysis and metaphysis.

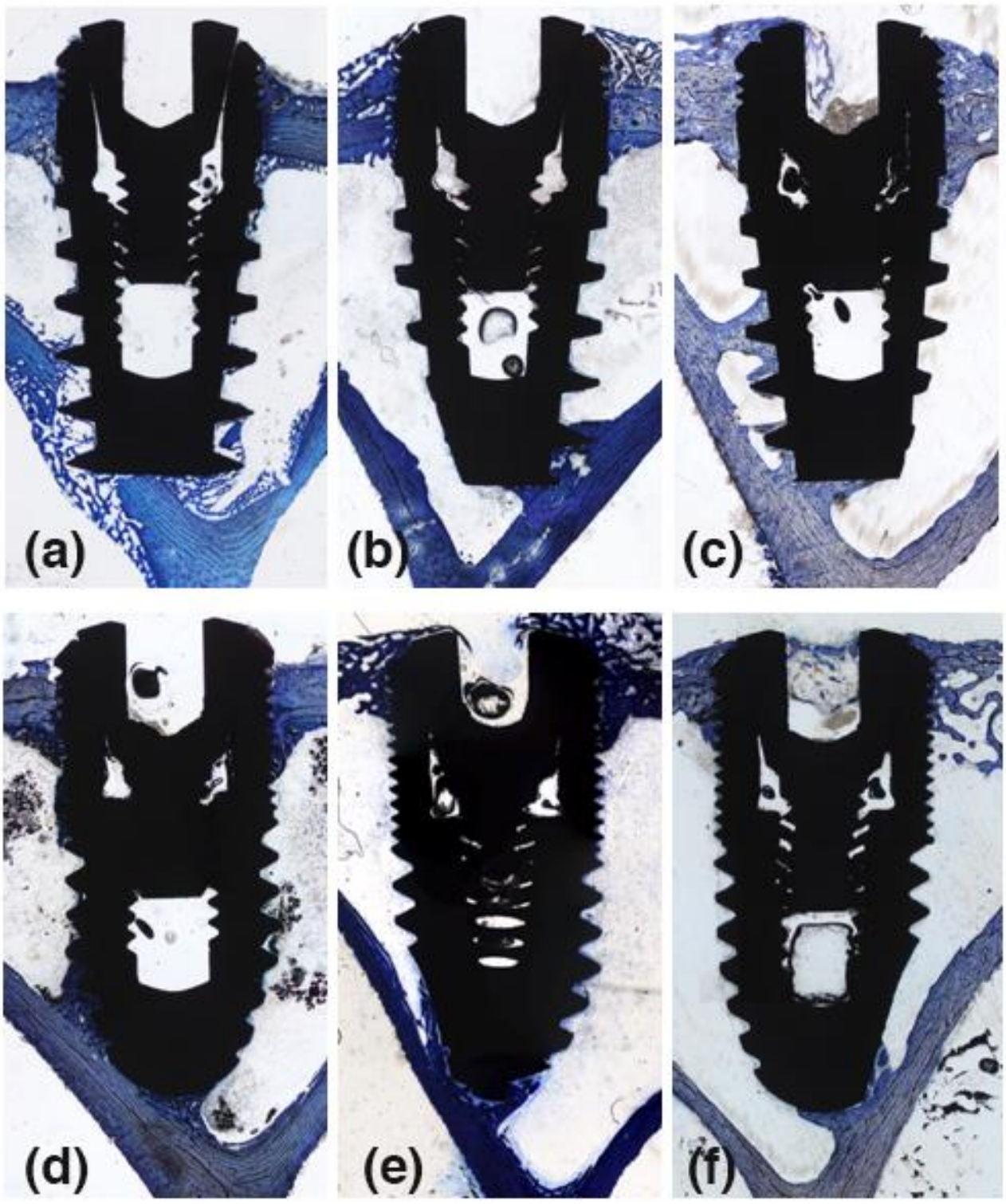

Figure 6.11 Ground sections illustrating the healing of implants installed in the diaphysis (a-c) and metaphysis (d-f) areas after 2, 4 and 8 weeks. Toluidine blue (1.6x).

6.4 The effect of implant macro-desing regarding topographic site on osseointegration

2-week healing

-Ticare Inhex Quattro®

The new bone values were around 18.3±7.9% and 14.4±10.1% at diaphysis and metaphysis sites. The old bone values were 8.0±6.4% and 7.2±5.3% at diaphysis and metaphysis sites, respectively. The soft tissue (bone marrow) values were 77.0±6.2% and 78.4±11.7%. There were no significant differences for these parameters at this stage (Table 6.6).

-Ticare Inhex®

The new bone values were 14.5±8.1% and 17.5±12.7% at diaphysis and metaphysis sites. The old bone values were 7.0±5.0% and 7.9±8.3% at diaphysis and metaphysis sites, respectively. The soft tissue (bone marrow) values were 78.5±7.5% and 74.5±14.6%. There were no significant differences for these parameters at this stage (Table 6.6).

4-week healing

-Ticare Inhex Quattro®

The new bone values were 22.7±4.7% and 18.2±8.3% at diaphysis and metaphysis sites. The old bone values were 3.2±3.1% and 1.2±1.3% at diaphysis and metaphysis sites, respectively. The soft tissue (bone marrow) values were 77.0±4.6% and 80.6±8.8%. There were no significant differences for these parameters at this stage (Table 6.6).

-Ticare Inhex®

The new bone values were 19.6±8.3% and 16±8.9% at diaphysis and metaphysis sites. The old bone values were 3.3±3.5% and 1.3±2.0% at diaphysis and metaphysis sites, respectively ($p<005$). The soft tissue (bone marrow) values were 74.0±9.4% and 82.7±8.9% ($p<0.05$). The difference proved to be significant for old bone and soft tissue parameters (Table 6.6).

8-week healing

-Ticare Inhex Quattro®

The new bone values were 38.8±13.7% and 28.7±6.4% at diaphysis and metaphysis sites ($p>0.05$). The old bone values were 4.8±3.5% and 2.1±0.4% at diaphysis and metaphysis sites, respectively ($p<0.05$). The soft tissue (bone marrow) values were 56.4±14.8% and 69.2±7.3% ($p>0.05$). Only soft tissue values showed a significant difference (Table 6.6).

-Ticare Inhex®

The new bone values were 34.0±9.5% and 29.9±8.9% at diaphysis and metaphysis sites (p>0.05). The old bone values were 1.9±2.0% and 0.5±0.7% at diaphysis and metaphysis sites, respectively (p>0.05). The soft tissue (bone marrow) values were 64.1±9.8% and 69.9±9.3% (p>0.05). There were no significant differences for these parameters at this stage (Table 6.6).

Table 6.5 Summary of proportion (%) of tissue components according implant macro-designs regarding topographic site, (n = 9) per each period of healing.

Macro-design	Diaphysis					Metaphysis					Differences
			New Bone	Old Bone	Soft Tissue			New Bone	Old Bone	Soft Tissue	
Inhex Quattro	2 weeks	Mean	18,3	8,0	77,0	2 weeks	Mean	14,4	7,2	78,4	NB: p=0,32
		SD	7,9	6,4	6,2		SD	10,1	5,3	11,7	OB: P=0,63
		Median	16,4	6,6	77,0		Median	13	6,4	81,3	ST: p=0,32
	4 weeks	Mean	22,7	3,2	77,0	4 weeks	Mean	18,2	1,2	80.6	NB: p=0,66
		SD	4,7	3,1	4,6		SD	8,3	1,3	8,8	OB: P=0,35
		Median	18,7	2,0	18,7		Median	17,7	0,6	82,3	ST: p=0,08
	8 weeks	Mean	38,8	4,8*	56,4	8 weeks	Mean	28,7	2,1*	69,2	NB: p=0,92
		SD	13,7	3,5	14,8		SD	6,4	0,4	7,3	OB: P=0,00
		Median	37,0	5,2	61,4		Median	29,8	1,3	70	ST: p=0,40
			New Bone	Old Bone	Soft Tissue			New Bone	Old Bone	Soft Tissue	Differences
Inhex	2 weeks	Mean	14,5	7,0	78,5	2 weeks	Mean	17,5	7,9	74,5	NB: p=0,55
		SD	8,1	5,0	7,5		SD	12,7	8,3	14,6	OB: P=0,53
		Median	16,4	6,6	77,0		Median	14,2	6,2	80,5	ST: p=0,67
	4 weeks	Mean	19,6	3,3*	74,0*	4 weeks	Mean	16	1,3*	82,7*	NB: p=0,06
		SD	8,3	3,5	9,4		SD	8,9	2,0	8,9	OB: P=0,03
		Median	24,4	1,8	70,6		Median	14,6	0,2	83,5	ST: p=0,03
	8 weeks	Mean	34,0	1,9	64,1	8 weeks	Mean	29,9	0,5	69,6	NB: p=0,07
		SD	9,5	2,0	9,8		SD	8,9	0,7	9,3	OB: P=0,29
		Median	35,7	1,5	63,8		Median	27,5	0	72,5	ST: p=0,19

U Mann Whitney-test: p<0,05
(*) P < 0.05 between diaphysis and metaphysis sites for either Inhex Quattro ® and Inhex ® implant macro-designs.

Multivariate analysis

It was observed that the implant position showed a statistical significance difference regarding BIC values at 4 and 8 weeks ($p<0.05$). Thus, a multivariate analysis was performed to assess the interaction between implant macro-design and position. The analysis failed to detect statistical significance for implant macro-designs and its interaction (design*position) over BIC values across healing stages ($p>0.05$).

A visual interaction is appreciated, suggesting that the position affects osseointegration values (Fig. 6.12). Also, is observed that Ticare Quattro® design showed a slight better BIC values at diaphysis sites across healing stages ($p>0.05$).

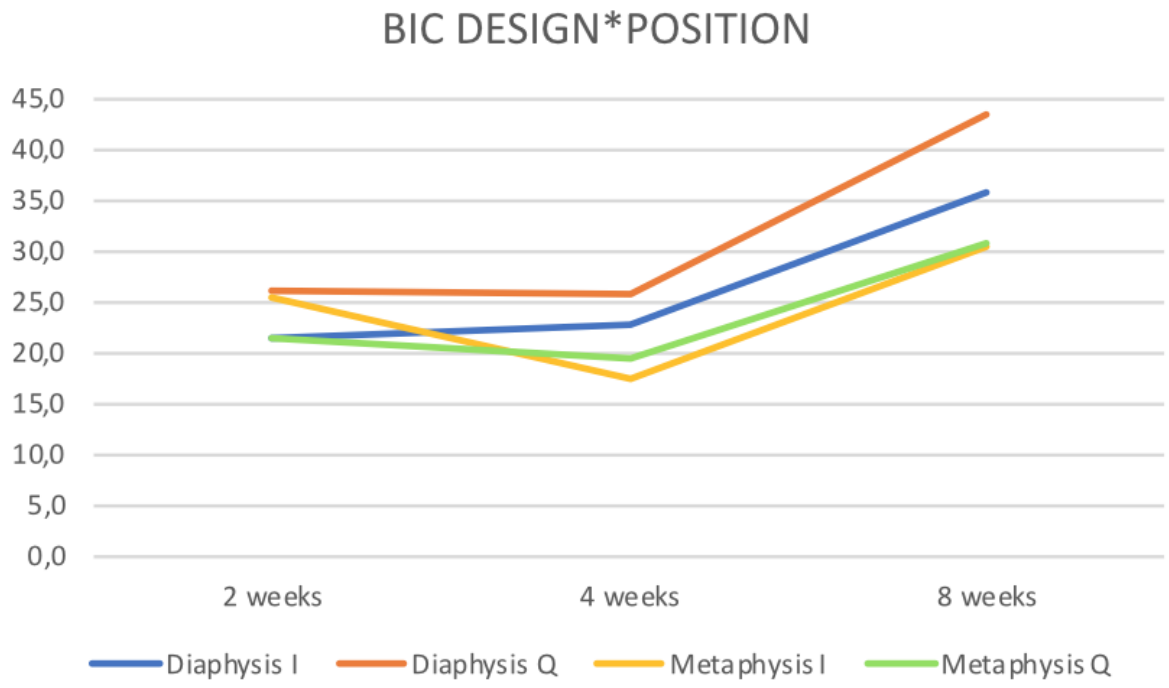

Figure 6.11 BIC values for both macro-designs according implantation site (diaphysis or metaphysis), to visually appreciate the interaction (Design*Position).

6.5 The bone-healing pattern at the cortical and marrow compartments in the diaphysis and metaphysis of rabbit´s tibiae

2-week healing

There were no significant differences among the parameters assessed between the cortical and marrow compartments in both diaphysis and metaphysis sites (Table 6.5; Figure 6.12 a, c). BIC values (Figure 6.12 b, d) were 30±9.9% versus 23.7±6.4% for diaphysis and metaphysis sites, respectively, in the cortical compartment (p=0.09), and 21.1±12.3% versus 13.9±8.0% in marrow compartment (p=0.07). Ground sections for the diaphysis and metaphysis at this stage are shown in Figure 6.13 a, b.

4-week healing

Significant differences were observed at this stage of healing for old bone at cortical compartment and for new bone and soft tissue in the marrow compartments between diaphysis and metaphysis sites (Table 6.5, Figure 6.12 a, c). No differences were detected for BIC values in the cortical compartment (Figure 6.12 b), that were 25.4±7.8% and 21.4±8.0% for diaphysis and metaphysis sites, respectively (p=0.26). However, a significant difference was found in the marrow compartment (Table 1; Figure 6.12 a, c), showing BIC values of 22.1±6.9% and 13.6±8.5 (p=0.01) for diaphysis and metaphysis sites, respectively (Figure 6.12 d). Ground sections for the diaphysis and metaphysis at this stage are presented in Figure 6.13 c, d.

8-week healing

On average, better values for new and old bone were observed in the cortical compartment; a significant difference was detected between the cortical and marrow compartments for these parameters in metaphysis sites (Table 6.5, Figure 3a,c). The mineralized bone-to-implant contact at this stage did not show significant differences within the cortical compartment between diaphysis and metaphysis implant sites, with BIC values 41.1 ± 6.8% and 39.9 ± 9.8%, respectively (p = 0.61). A similar trend was observed within the marrow compartments at diaphysis and metaphysis sites (Figure 3b,d). Ground sections for diaphysis and metaphysis at this stage are presented in Figure 4e,f.

Table 6.6 Proportion (%) of tissue components in contact with the implant surface for either the cortical or the marrow bony compartments at the various time periods in weeks (w). n = 9 per each period of healing.

Cortical compartment												
			New bone	Soft tissue	Old bone				New bone	Soft tissue	Old bone	Differences
2w	Cort-dia	Mean	17,8	70,0	12,2	2w	Cort-meta	Mean	15,1	76,3	8,5	NB: p=0,39
		SD	10,6	8,9	6,6			SD	5,8	6,4	6,5	ST: p=0,09
		Median	14,0	68,2	8,3			Median	14,8	78,9	6,2	OB: p=0,11
4w	Cort-dia	Mean	21,4	74,6	4,0*#	4w	Cort-meta	Mean	19,7*	78,6*	1,7#	NB: p=0,57
		SD	6,9	7,8	3,2			SD	8,3	8,0	1,5	ST: p=0,26
		Median	21,6	74,6	3,0			Median	17,3	79,3	1,5	OB: p=0,04
8w	Cort-dia	Mean	37,0*	58,9*	4,1	8w	Cort-meta	Mean	35,5*	61,3*	3,2*	NB: p=0,63
		SD	5,7	6,8	2,6			SD	8,7	9,8	3,4	ST: p=0,62
		Median	37,3	58,5	4,3			Median	33,8	60,9	2,6	OB: p=0,88
Marrow compartment												
			New bone	Soft tissue	Old bone				New bone	Soft tissue	Old bone	Differences
2w	Marrow-dia	Mean	13,8	78,9	7,3	2w	Marrow-meta	Mean	10,3	86,1	3,6	NB: p=0,18
		SD	9,2	12,3	8,9			SD	8,2	8,0	5,1	ST: p=0,07
		Median	13,2	82,8	2,9			Median	9,3	89,5	0,5	OB: p=0,23
4w	Marrow-dia	Mean	20,4#	77,9#	1,7*	4w	Marrow-meta	Mean	13,0*#	86,4*#	0,6	NB: p=0,02
		SD	6,8	6,9	2,3			SD	8,2	8,5	0,8	ST: p=0,01
		Median	19,7	79,4	0,4			Median	13,3	86,7	0,0	OB: p=0,16
8w	Marrow-dia	Mean	24,6*	73,6	1,8	8w	Marrow-meta	Mean	25,1*	74,7*	0,2*	NB: p=0,878
		SD	12,9	16,3	3,8			SD	9,6	9,7	0,4	ST: p=0,79
		Median	21,6	78,5	0,0			Median	23,2	75,9	0,0	OB: p=0,25

U Mann Whitney-test: p<0,05
*P < 0.05 between cortical and marrow compartment either at diaphysis (Cort-dia vs Marrow-dia) and metaphysis (Cort-meta vs Marrow-meta) topographic regions (vertical).
#P < 0.05 between diaphysis and metaphysis either at cortical (Cort-dia vs Cort-meta) or marrow compartment (Marrow-dia vs Marrow-meta) (horizontal).

Table 6.7 Summary of proportion (%) of bone to impant contact (BIC) according cortical and marrow compartments and topographic location at the various time periods. n = 9 per each period of healing.

Healing period	Statistic	BIC % Cortical compartment		Differences	Statistic	BIC % Marrow compartment		Differences
		Diaphysis	Metaphysis			Diaphysis	Metaphysis	
2 weeks	Mean	30,0	23,7	p=0.09	Mean	21,1	13,9	p=0.07
	SD	9,9	6,4		SD	12,3	8,0	
	Median	31,8	21,1		Median	17,2	10,5	
4 weeks	Mean	25,4	21,4	p=0.26	Mean	22,1*	13,6*	p=0.01
	SD	7,8	8,0		SD	6,9	8,5	
	Median	25,4	20,7		Median	20,6	13,3	
8 weeks	Mean	41,1	38,7	P=0.61	Mean	26,4	25,3	p=0,86
	SD	6,8	9,8		SD	16,3	9,7	
	Median	41,5	39,1		Median	21,6	24,2	

U Mann Whitney-test: p<0,05
*P < 0.05

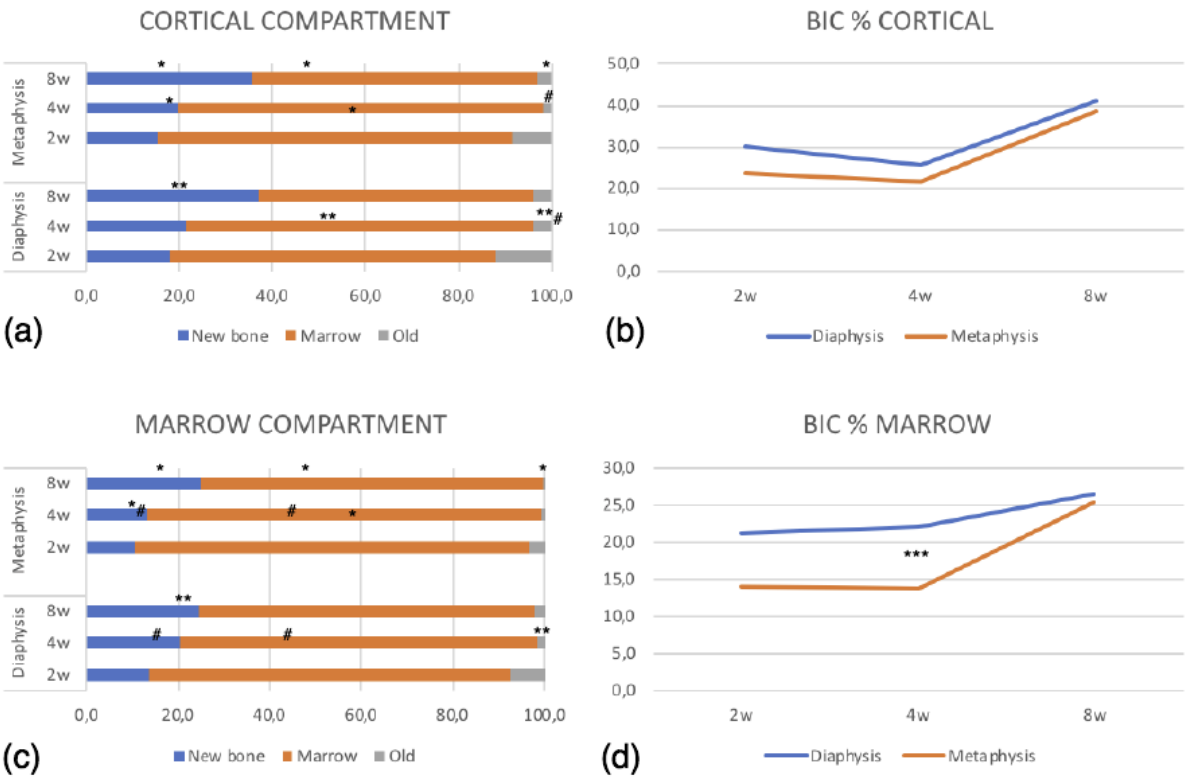

Figure 6.12 The total amount of new bone, marrow content, and old bone according to cortical (**a**) and marrow (**b**) compartment for implants placed via either diaphysis (n=9) or metaphysis (n=9) at different healing periods. Mineralized bone to implant contact (new + old) for cortical (**b**) and marrow (**d**) compartments at the various healing times. $p < 0.05$; between cortical and marrow compartments at metaphysis sites (*), at diaphysis sites (**) or (#) between diaphysis and metaphysis within cortical and marrow compartments and (***) for mineralized bone to implant contact, respectively. Comparisons are based on the same healing stage in weeks (w).

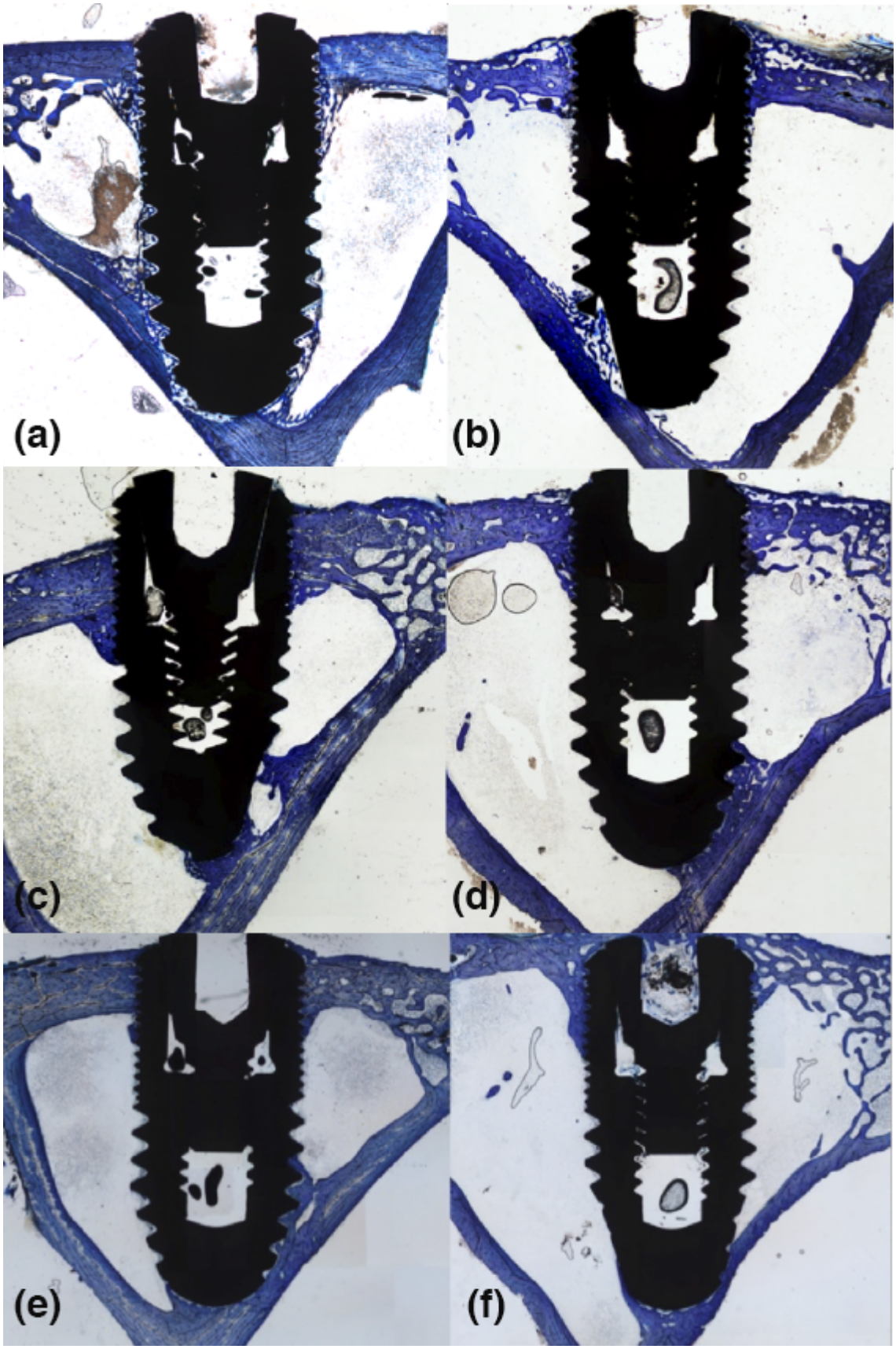

Figure 6.13 Ground section of bicortically-installed implants (Ticare Inhex® , Mozo Grau, Valladolid, Spain) at diaphysis (left side) and metaphysis (right side) sites at two (**a**,**b**), four (**c**,**d**) and eight (**e**,**f**) weeks of healing. An original magnification of ×2.5 and toluidine blue staining was used.

7. DISCUSSION

7.1 Effect of two distinct implant design with equal RBM surface treatment on osteointegration

The main aim of the present thesis is focused on the bone response over two different implant macro-designs with equal RBM surface treatment and the same length and diameter, bicortically installed in the tibia of the rabbit. It is performed with the aim of assessing the influence of macro-geometry on osseointegration. To isolate the possible effect of implant macro-geometry on bone formation, both implants had the same surface treatment.

In order to appreciate the behavior of both implant macro-designs in two different bone environments, they were placed in two topographic zones within the same tibia, one with a cortical layer and a medullar content (diaphysis) like a type II bone and the another more trabecular like a type III bone (metaphysis). The histomorphometric analysis at either 2, 4 and 8 weeks were similar ($p > 0.05$) for both implant designs. Moreover, comparing new bone percentages in relation to the topographic implant placement, after 4 and 8 weeks of healing, osseointegration was found to be slightly higher, but statistically not significant at the implants placed in the diaphysis compared to the metaphysis. These findings are contrary to those reported in a previous experiment in rabbits (Caneva et al. 2015). Observations that could be attributable to several factors, such as the implant thread design, the surface treatment tested and the implant osteotomy protocols, differing between studies. It is known that these factors could regulate the strain applied to hard tissue in proximity to the implant (Gottlow et al. 2012).

Old bone was resorbed, but was still present after 1 month of healing (<4%), with statistically significant better values in Quattro® group. This pattern of healing is in agreement with other studies performed in animals (Abrahamsson et al. 2004; Rossi et al. 2014b; Caneva et al. 2015) and humans (Lang et al. 2011). Noteworthy to mention, bone morphology in diaphysis is predominantly occupied by a marrow content in comparison to metaphysis that presents more trabecular bone. These findings are in agreement with the assumption that osseointegration is faster in zones where the bone apposition is not preceded by bone resorption (Abrahamsson et al. 2004).

It appears likely that bone formation started from the cortical compartments (in contact with mineralized parent bone) and, subsequently, proliferated toward into the marrow compartments. The implants were in close contact to pristine bone due to their bi-cortically stabilization, a condition that favors osseointegration on the implant surface, a pattern of healing that was

documented for osseointegration in different preclinical models (Botticelli et al. 2003; Araújo et al. 2006; Scala et al. 2012). The parent old bone in recipient site is responsible of mechanical interlocking, and thereafter it is relevant during implant stability dip, where takes place a cell mediated interfacial bone remodeling (Raghavendra et al. 2005).

This is typically described to occur in the area of contact between the pristine bone wall and implant surface, where remodeling arise in the proximity of microcracks followed by bone apposition in void spaces resulting in secondary stability (Gomes et al. 2013). The results from the present study are in agreement with other studies that showed that macro-design did not significantly affect the BIC rates under the absence of loading conditions (Leonard et al. 2009; Coelho et al. 2010). Also, a previous report suggests that implant macro-design features, such as thread pattern and thread pitch, can be responsible for differences in the amount of bone and degree of apposition toward the implant surface. Therefore, consideration of specific implant macro-design should be made relative to the biological and mechanical microenvironment (Vivan Cardoso et al. 2015). However, due to the absence of functional load, these parameters reflect the structural connection between implant and bone, and not the functional properties of the bone to implant interface (Leonard et al. 2009). There is scarce pre-clinical evidence regarding sequential healing of bicortically installed implants with two macro-designs and equal surface treatment, attempting to assess its interaction in two topographic sites.

Regarding the two distinct bone environments assessed, for this study there were considered as topographic sites (diaphysis or metaphysis) within rabbit tibiae. In average was observed better increasing values of new osseointegration across healing stages at diaphysis sites (that seems a type II bone density). Also, BIC values were significantly higher at 4 and eight weeks in diaphysis, compared to those implants installed in metaphysis (like a type III bone density). These observations could be in part explained because diaphysis is occupied by bone marrow in its middle section, so is presumably more favorable environment to a direct bone apposition onto implant surface, because it is not preceded by a resorption process (Abrahamsson et al. 2004), as occurs in trabecular bone (e.g. metaphysis). The Ticare Inhex® and Quattro® implant macro-designs showed better-increasing values at diaphysis sites, also Quattro® design showed better BIC values at diaphysis sites.

Despite that the interaction of factors was assessed, only the topographic site seems to contribute to the different values observed at 4 and 8 weeks. Regrettably, the test did not detect

significant differences, perhaps because the scarce sample number for this comparison conditionate a lack of statistical power in this analysis.

7.2 Bone healing patterns at cortical and marrow compartment

The bone-healing patterns at cortical and marrow compartments at equal surface bicortically installed implants in the diaphysis and metaphysis of rabbit tibiae was analyzed. The histomorphometric analyzes at 2, 4 and 8 weeks showed no differences ($p>0.05$) for either of the implant macro-designs. The new bone and BIC percentages in relation to the topographic implant placement after 4 and 8 weeks of healing showed that osseointegration tends to be slightly higher but statistically less significant for implants placed in the diaphysis than the metaphysis sites, with BIC values of 24.5±6.2% and 18.4±7.7% at 4 weeks; and 41.1±6.8% and 39.9±9.8% at 8 weeks.

As reported by previous studies, it is known that resorptive processes occur before new bone apposition in zones where the mineralized bone is present, conveying a slightly longer healing period to reach complete osseointegration (Berglundh et al. 2003; Abrahamsson et al. 2004). Indeed, in the present study, the new bone formation in the marrow compartment showed slightly better increasing values of 13.8, 20.4, and 24.6% at 2, 4 and 8 weeks at diaphysis sites, compared to 10.3, 13, and 25.1% at metaphysis sites. The same trend was observed in the cortical compartment with values 17.8, 21.4, and 37% at diaphysis sites, and 15.1, 19.7, and 35.5% in metaphysis sites. The old bone was resorbed but was still present (<2%) after 1 month in both topographical zones. The parent old bone values observed were slightly higher in diaphysis implant sites at 4 and 8 weeks compared to metaphysis sites in the present study sample. However, in this study it is possible to appreciate a contradiction of what was established by the study of Caneva et al. in 2015(Caneva et al. 2015)(Caneva et al. 2015)(Caneva et al. 2015)(Caneva et al. 2015). In this study, the new bone formation developed at a much higher speed at the implants placed in the metaphysis that those in the diaphysis.

The authors attributed the findings to the denser pattern of the trabecular bone in the metaphysis compared to the diaphysis tibiae, an event that may have empowered osseointegration. On the other hand, the bone formation that was supposed to be reinforced by the bone marrow did not work out, since this scarcely contributed to its formation in the middle section of the implants placed in the diaphysis compared to what was found in the coronal and apical sections. These observations could be attributable to several factors previously mentioned. Also, in the study of

Caneva et al. there were demarcated three sections (coronal, middle, and apical) to test the differences among compartments (Caneva et al. 2015). In the present study, the three sections were demarcated in the same manner, but the cortical compartment is considered as the sum of the cortical and apical regions as a whole, independently of the marrow compartment (middle). In both studies, the extreme regions of the implants were in close contact with pristine bone (bicortical stabilization), a condition that may have reinforced osseointegration on the implant surface (Caneva et al. 2015). Note to mention, diaphysis sites is predominantly occupied by a marrow content, a fact that could be agree with the premise that osseointegration is faster in areas where bone apposition is not precluded by bone resorption, as previous reported in dogs (Abrahamsson et al. 2004) and minipigs (Buser et al. 2004) animal models.

Also, it is possible to conclude that osseointegration seems to be favored by the existence of a blood clot, and prejudicated by the presence of yellow fatty bone marrow in the long bone model, such as sheep tibiae (Morelli et al. 2015). In this sense, Morelli et al. 2014 employed the sheep tibia model, where two osteotomies for implant installation are prepared in each tibia. On average, new bone apposition was better in the cortical compartment, as seen in the present study (Morelli et al. 2015). Moreover, it was observed that new bone apposition was faster in the fatty bone marrow group compared to blood clot groups at marrow compartments after 4 weeks. The authors concluded that osseointegration appeared to be favored by blood clots, because at 12 weeks of healing the test group showed better new bone values, statistically significant only at the marrow compartment (Morelli et al. 2015) , even though in this study the implants were not placed bicortically.

However, despite inter-species differences impeding direct comparisons, there is no certain data on the extent to which the rabbit tibia model, in its diaphysis or middle shaft, provides amounts of fatty bone marrow that may affect osseointegration after eight weeks of healing. So, it would be of interest to isolate its effect in a further study in order to confirm this hypothesis in the rabbit tibia model. It is for utmost importance to consider that present results only could be extrapolated to implants with the same surface roughness, its applicability is out range for other animal models because of the differences that were shown on healing patterns among species (e.g. dog, sheep, rabbit, rat). Further studies comparing equal surfaces treatment but with different manufacturing approaches are warrant, to elucidate if it replicates the patterns observed in the present work.

7.3 Efforts, limitations and future trends

This study was conducted in agreement with ARRIVE guidelines that encourages the good practices and quality of reporting in experimental animals and have an adequate sample size estimation to assess the predefined objectives, and was supervised by experts in the preclinical research. The novelty of the present work lies in the fact that there is no other study aiming to assess the impact of distinct implant macro-designs with equal moderately-rough RBM surface treatment in two different bone environments onto the osseointegration values and the healing patterns at the cortical and marrow compartments within the same rabbit tibiae. This allows us to isolate the macro-design effects on osseointegration, thus helping us separately evaluate the dynamics of the healing pattern in distinct bone densities. However, due to the absence of functional load, these parameters reflect the structural connection between implant and bone, and not the functional properties of the bone to implant interface.

There is scarce pre-clinical evidence regarding sequential healing of bicortically installed implants with two macro-designs and equal surface treatment, attempting to assess its interaction in two topographic sites. Despite that the interaction of factors was assessed, only the topographic site seems to contribute to values at 4 and 8 weeks. Regrettably, it is difficult to determine to which extent each implant macro-design contributes to these findings observed at the diaphysis or metaphysis sites. The scarce sample did not permit a proper statistical comparison. Note to mention, the findings of the interaction are merely exploratory and should be interpreted with caution. Thus, more studies are needed to explore the impact of different macro-designs with equal surface roughness of different manufacturing methods (e.g. SLA, anodized, etc) on osseointegration in rabbit model, and considering the impact of loading conditions. Also, there is no certain data on the extent to which the rabbit tibia model, in its diaphysis or middle shaft, provides amounts of fatty bone marrow that may affect osseointegration after eight weeks of healing. In this sense, a concern to be further elucidated is to determine if the values observed at diaphysis sites on healing patterns are related to bone marrow composition of rabbit tibia, or merely explained by chance. Further studies are warranted with a greater sample size to answer these aspects, but this is a tough challenge, taking into consideration the ethical and economic aspects that may be involved in consideration of the replacement, refinement, or reduction (3Rs) criteria for the use of animals in research.

8. CONCLUSIONS

8. Conclusions

The following conclusions can be drawn from the present thesis:

I. The sequential osseointegration pattern of RBM surfaces is successful in the rabbit model.

II. The implant macro-designs does not significantly affect the osseointegration process in the absence of loading across healing stages.

III. Bone morphometry and density may affect the bone apposition onto the implant surface. The apposition rates were slightly better in diaphysis compared to metaphysis topographic sites. The BIC values were significantly higher at 4 and 8 weeks in diaphysis sites.

IV. There is no interaction between implant macro-design and topographic site as shown by the multivariate analysis. Though, it was observed that Ticare Quattro® implant macro-design showed a slightly better BIC values at diaphysis sites across the healing stages.

V. The new bone apposition was better in the cortical- compared to the marrow- compartment. The apposition rates were slightly better at both cortical and marrow compartments in diaphysis compared to metaphysis sites.

9. REFERENCES

Abrahamsson I, Berglundh T, Linder E, et al (2004) Early bone formation adjacent to rough and turned endosseous implant surfaces. An experimental study in the dog. Clin Oral Implants Res 15:381–392. doi: 10.1111/j.1600-0501.2004.01082.x

Abuhussein H, Pagni G, Rebaudi A, Wang HL (2010) The effect of thread pattern upon implant osseointegration: Review. Clin Oral Implants Res 21:129–136. doi: 10.1111/j.1600-0501.2009.01800.x

Adell R, Hansson BO, Brånemark PI, Breine U (1970) Intra-osseous anchorage of dental prostheses. Scand J Plast Reconstr Surg Hand Surg 4:19–34. doi: 10.3109/02844317009038440

Albrektsson T, Eriksson AR, Friberg B, et al (1993) Histologic investigations on 33 retrieved Nobelpharma implants. Clin Mater 12:1–9. doi: 10.1016/0267-6605(93)90021-X

Araújo MG, Wennström JL, Lindhe J (2006) Modeling of the buccal and lingual bone walls of fresh extraction sites following implant installation. Clin Oral Implants Res 17:606–14. doi: 10.1111/j.1600-0501.2006.01315.x

Asagiri M, Takayanagi H (2007) The molecular understanding of osteoclast differentiation. Bone 40:251–264. doi: 10.1016/j.bone.2006.09.023

Barfeie A, Wilson J, Rees J (2015) Implant surface characteristics and their effect on osseointegration. Br Dent J 218:E9. doi: 10.1038/sj.bdj.2015.171

Bartold PM, Kuliwaba JS, Lee V, et al (2011) Influence of surface roughness and shape on microdamage of the osseous surface adjacent to titanium dental implants. Clin Oral Implants Res 22:613–618. doi: 10.1111/j.1600-0501.2010.02024.x

Bashutski JD, D'Silva NJ, Wang H-L (2009) Implant Compression Necrosis: Current Understanding and Case Report. J Periodontol 80:700–704. doi: 10.1902/jop.2009.080581

Bellido T (2014) Osteocyte-driven bone remodeling. Calcif. Tissue Int. 94:25–34

Bentolila V, Boyce TM, Fyhrie DP, et al (1998) Intracortical remodeling in adult rat long bones after fatigue loading. Bone 23:275–281. doi: 10.1016/S8756-3282(98)00104-5

Berglundh T, Abrahamsson I, Lang NP, Lindhe J (2003) De novo alveolar bone formation adjacent to endosseous implants: A model study in the dog. Clin Oral Implants Res 14:251–262. doi: 10.1034/j.1600-0501.2003.00972.x

Beutel BG, Danna NR, Granato R, et al (2016) Implant design and its effects on osseointegration over time within cortical and trabecular bone. J Biomed Mater Res - Part B Appl Biomater 104:1091–1097. doi: 10.1002/jbm.b.33463

Bosshardt DD, Salvi GE, Huynh-Ba G, et al (2011) The role of bone debris in early healing adjacent to hydrophilic and hydrophobic implant surfaces in man. Clin Oral Implants Res 22:357–364. doi: 10.1111/j.1600-0501.2010.02107.x

Botticelli D, Berglundh T, Buser D, Lindhe J (2003) Appositional bone formation in marginal defects at implants: An experimental study in the dog. Clin Oral Implants Res 14:1–9. doi: 10.1034/j.1600-0501.2003.140101.x

Botticelli D, Berglundh T, Persson LG, Lindhe J (2005) Bone regeneration at implants with turned or rough surfaces in self-contained defects. An experimental study in the dog. J Clin Periodontol 32:448–455. doi: 10.1111/j.1600-051X.2005.00693.x

Botticelli D, Lang NP (2017) Dynamics of osseointegration in various human and animal models - a comparative analysis. Clin Oral Implants Res 28:742–748. doi: 10.1111/clr.12872

Boyce BF, Yoneda T, Lowe C, et al (1992) Requirement of pp60c-srcexpression for osteoclasts to form ruffled borders and resorb bone in mice. J Clin Invest 90:1622–1627. doi: 10.1172/JCI116032

Brunski JB (1988) Biomaterials and biomechanics in dental implant design. Int J Oral Maxillofac Implants 3:85–97

Burr DB, Forwood MR, Fyhrie DP, et al (1997) Bone microdamage and skeletal fragility in

osteoporotic and stress fractures. J Bone Miner Res 12:6–15. doi: 10.1359/jbmr.1997.12.1.6
Burr DB, Turner CH, Naick P, et al (1998) Does microdamage accumulation affect the mechanical properties of bone? J Biomech 31:337–345. doi: 10.1016/S0021-9290(98)00016-5
Buser D, Broggini N, Wieland M, et al (2004) Enhanced bone apposition to a chemically modified SLA titanium surface. J Dent Res 83:529–533. doi: 10.1177/154405910408300704
Caneva M, Lang NP, Calvo Guirado JL, et al (2015) Bone healing at bicortically installed implants with different surface configurations. An experimental study in rabbits. Clin Oral Implants Res 26:293–299. doi: 10.1111/clr.12475
Cardoso L, Herman BC, Verborgt O, et al (2009) Osteocyte Apoptosis Controls Activation of Intracortical Resorption in Response to Bone Fatigue. J Bone Miner Res 24:597–605. doi: 10.1359/jbmr.081210
Chamay A, Tschantz P (1972) Mechanical influences in bone remodeling. Experimental research on Wolff's law. J Biomech 5:173–180. doi: 10.1016/0021-9290(72)90053-X
Chowdhary R, Halldin A, Jimbo R, Wennerberg A (2015) Influence of Micro Threads Alteration on Osseointegration and Primary Stability of Implants: An FEA and In Vivo Analysis in Rabbits. Clin Implant Dent Relat Res 17:562–569. doi: 10.1111/cid.12143
Chowdhary R, Jimbo R, Thomsen CS, et al (2014) The osseointegration stimulatory effect of macrogeometry-modified implants: A study in the rabbit. Clin Oral Implants Res 25:1051–1055. doi: 10.1111/clr.12212
Coelho PG, Bonfante EA, Pessoa RS, et al (2011) Characterization of five different implant surfaces and their effect on osseointegration: a study in dogs. J Periodontol 82:742–50. doi: 10.1902/jop.2010.100520
Coelho PG, Suzuki M, Guimaraes MVM, et al (2010) Early bone healing around different implant bulk designs and surgical techniques: A study in dogs. Clin Implant Dent Relat Res 12:202–208. doi: 10.1111/j.1708-8208.2009.00153.x
Currey JD (1969a) The mechanical consequences of variation in the mineral content of bone. J Biomech 2:1–11. doi: 10.1016/0021-9290(69)90036-0
Currey JD (1969b) The relationship between the stiffness and the mineral content of bone. J Biomech 2:477–480. doi: 10.1016/0021-9290(69)90023-2
Currey JD (2004) Tensile yield in compact bone is determined by strain, post-yield behaviour by mineral content. J Biomech 37:549–556. doi: 10.1016/j.jbiomech.2003.08.008
Currey JD, Brear K, Zioupos P (1996) The effects of ageing and changes in mineral content in degrading the toughness of human femora. J Biomech 29:257–260. doi: 10.1016/0021-9290(95)00048-8
Davies J (2003) Understanding peri-implant endosseous healing. J Dent Educ 67:932–949
Davies JE (1998) Mechanisms of endosseous integration. Int J Prosthodont 11:391–401
Davies JE, Hosseini MH (2000) Histodynamics of Endosseous Wound Healing. Bone Eng 1–14
Delgado-Ruiz RA, Abboud M, Romanos G, et al (2015) Peri-implant bone organization surrounding zirconia-microgrooved surfaces circularly polarized light and confocal laser scanning microscopy study. Clin Oral Implants Res 26:1328–1337. doi: 10.1111/clr.12461
Ernst S, Stübinger S, Schüpbach P, et al (2015) Comparison of two dental implant surface modifications on implants with same macrodesign: An experimental study in the pelvic sheep model. Clin Oral Implants Res 26:898–908. doi: 10.1111/clr.12411
Esposito M, Grusovin MG, Willings M, et al (2008) The effectiveness of immediate, early, and conventional loading of dental implants: a Cochrane systematic review of randomized controlled clinical trials. Int J Oral Maxillofac Implants 22:893–904
Falco A, Berardini M, Trisi P (2018) Correlation Between Implant Geometry, Implant Surface, Insertion Torque, and Primary Stability: In Vitro Biomechanical Analysis. Int J Oral Maxillofac Implants 33:824–830. doi: 10.11607/jomi.6285

Favero R, Botticelli D, Antunes AA, et al (2016a) Sequential Healing at Calcium- versus Calcium Phosphate-Modified Titanium Implant Surfaces: An Experimental Study in Dogs. Clin Implant Dent Relat Res 18:369–378. doi: 10.1111/cid.12311

Favero R, Lang NP, Salata LA, et al (2016b) Sequential healing events of osseointegration at UnicCa® and SLActive® implant surfaces: An experimental study in the dog. Clin Oral Implants Res 27:203–210. doi: 10.1111/clr.12591

Freitas AC, Bonfante EA, Giro G, et al (2012) The effect of implant design on insertion torque and immediate micromotion. Clin Oral Implants Res 23:113–118. doi: 10.1111/j.1600-0501.2010.02142.x

Gehrke SA, Pérez-Albacete Martínez C, Piattelli A, et al (2017) The influence of three different apical implant designs at stability and osseointegration process: experimental study in rabbits. Clin Oral Implants Res 28:355–361. doi: 10.1111/clr.12807

Gomes JB, Campos FE, Marin C, et al (2013) Implant Biomechanical Stability Variation at Early Implantation Times in Vivo: An Experimental Study in Dogs. Int J Oral Maxillofac Implants 28:e128–e134. doi: 10.11607/jomi.2885

Gottlow J, Barkamo S, Sennerby L (2012) An Experimental Comparison of Two Different Clinically Used Implant Designs and Surfaces. Clin Implant Dent Relat Res 14:e204-12. doi: 10.1111/j.1708-8208.2012.00439.x

Halldin A, Jimbo R, Johansson CB, et al (2011) The effect of static bone strain on implant stability and bone remodeling. Bone 49:783–789. doi: 10.1016/j.bone.2011.07.003

Halldin A, Jimbo R, Johansson CB, et al (2014) Implant Stability and Bone Remodeling after 3 and 13 Days of Implantation with an Initial Static Strain. Clin Implant Dent Relat Res 16:383–393. doi: 10.1111/cid.12000

Horne WC, Sanjay A, Bruzzaniti A, Baron R (2005) The role(s) of Src kinase and Cbl proteins in the regulation of osteoclast differentiation and function. Immunol Rev 208:106–125. doi: 10.1111/j.0105-2896.2005.00335.x

Huang HL, Chang YY, Lin DJ, et al (2011) Initial stability and bone strain evaluation of the immediately loaded dental implant: An in vitro model study. Clin Oral Implants Res 22:691–698. doi: 10.1111/j.1600-0501.2010.01983.x

Ikeda F, Nishimura R, Matsubara T, et al (2006) Activation of NFAT Signal In Vivo Leads to Osteopenia Associated with Increased Osteoclastogenesis and Bone-Resorbing Activity. J Immunol 177:2384–2390. doi: 10.4049/jimmunol.177.4.2384

Isidor F (2006) Influence of forces on peri-implant bone. Clin Oral Implants Res 17:8–18. doi: 10.1111/j.1600-0501.2006.01360.x

Ivanoff CJ, Gröndahl K, Sennerby L, et al (1999) Influence of variations in implant diameters: a 3- to 5-year retrospective clinical report. Int J Oral Maxillofac Implants 14:173–180

Ivanoff CJ, Sennerby L, Lekholm U (1996) Influence of mono- and bicortical anchorage on the integration of titanium implants. A study in the rabbit tibia. Int J Oral Maxillofac Surg 25:229–235. doi: 10.1016/S0901-5027(96)80036-1

Ivanovski S, Hamlet S, Salvi GE, et al (2011) Transcriptional profiling of osseointegration in humans. Clin Oral Implants Res 22:373–381. doi: 10.1111/j.1600-0501.2010.02112.x

Javed F, Romanos GE (2010) The role of primary stability for successful immediate loading of dental implants. A literature review. J Dent 38:612–620. doi: 10.1016/j.jdent.2010.05.013

Jaworski ZF (1981) Physiology and pathology of bone remodeling. Cellular basis of bone structure in health and in osteoporosis. Orthop Clin North Am 12:485–512

Jimbo R, Janal MN, Marin C, et al (2014a) The effect of implant diameter on osseointegration utilizing simplified drilling protocols. Clin Oral Implants Res 25:1295–1300. doi: 10.1111/clr.12268

Jimbo R, Tovar N, Marin C, et al (2014b) The impact of a modified cutting flute implant design on

osseointegration. Int J Oral Maxillofac Surg 43:883–888. doi: 10.1016/j.ijom.2014.01.016
Jurdic P, Saltel F, Chabadel A, Destaing O (2006) Podosome and sealing zone: Specificity of the osteoclast model. Eur J Cell Biol 85:195–202. doi: 10.1016/j.ejcb.2005.09.008
Kang H-G, Jeong Y-S, Huh Y-H, et al (2018) Impact of Surface Chemistry Modifications on Speed and Strength of Osseointegration. Int J Oral Maxillofac Implants 33:780–787. doi: 10.11607/jomi.5871
Kilkenny C, Browne WJ, Cuthill IC, et al (2010) The ARRIVE Guidelines Checklist Animal Research : Reporting In Vivo Experiments. Br J Pharmacol 8:8–9. doi: 10.1371/journal.pbio.1000412
Klein-Nulend J, Bacabac RG, Bakker AD (2012) Mechanical loading and how it affects bone cells: The role of the osteocyte cytoskeleton in maintaining our skeleton. Eur Cells Mater 24:278–291. doi: vol024a20 [pii]
Koh J-W, Yang J-H, Han J-S, et al (2009) Biomechanical evaluation of dental implants with different surfaces: Removal torque and resonance frequency analysis in rabbits. J Adv Prosthodont 1:107–12. doi: 10.4047/jap.2009.1.2.107
Kubatzky KF, Kloos B, Hildebrand D (2013) Signaling cascades of Pasteurella multocida toxin in immune evasion. Toxins (Basel). 5:1664–1681
Lang NP, Salvi GE, Huynh-Ba G, et al (2011) Early osseointegration to hydrophilic and hydrophobic implant surfaces in humans. Clin Oral Implants Res 22:349–356. doi: 10.1111/j.1600-0501.2011.02172.x
Lanyon LE (1996) Using functional loading to influence bone mass and architecture: objectives, mechanisms, and relationship with estrogen of the mechanically adaptive process in bone. Bone 18:37S-43S. doi: 10.1016/8756-3282(95)00378-9
Le Guéhennec L, Soueidan A, Layrolle P, Amouriq Y (2007) Surface treatments of titanium dental implants for rapid osseointegration. Dent Mater 23:844–854. doi: 10.1016/j.dental.2006.06.025
Leonard G, Coelho P, Polyzois I, et al (2009) A study of the bone healing kinetics of plateau versus screw root design titanium dental implants. Clin Oral Implants Res 20:232–239. doi: 10.1111/j.1600-0501.2008.01640.x
Lioubavina-Hack N, Lang NP, Karring T (2006a) Significance of primary stability for osseointegration of dental implants. Clin Oral Implants Res 17:244–250. doi: 10.1111/j.1600-0501.2005.01201.x
Lioubavina-Hack N, Lang NP, Karring T (2006b) Significance of primary stability for osseointegration of dental implants. Clin Oral Implants Res 17:244–250. doi: 10.1111/j.1600-0501.2005.01201.x
Listgarten MA, Buser D, Steinemann SG, et al (1992) Light and transmission electron microscopy of the intact interfaces between non-submerged titanium-coated epoxy resin implants and bone or gingiva. J Dent Res 71:364–71. doi: 10.1177/00220345920710020401
Liu C, Carrera R, Flamini V, et al (2018) Effects of mechanical loading on cortical defect repair using a novel mechanobiological model of bone healing. Bone 108:145–155. doi: 10.1016/j.bone.2017.12.027
Mainetti T, Lang NP, Bengazi F, et al (2016) Sequential healing at implants installed immediately into extraction sockets. An experimental study in dogs. Clin Oral Implants Res 27:130–138. doi: 10.1111/clr.12533
Mainetti T, Lang NP, Bengazi F, et al (2015) Immediate loading of implants installed in a healed alveolar bony ridge or immediately after tooth extraction: an experimental study in dogs. Clin Oral Implants Res 26:435–441. doi: 10.1111/clr.12389
Marchisio PC, Cirillo D, Naldini L, et al (1984) Cell-substratum interaction of cultured avian osteoclasts is mediated by specific adhesion structures. J Cell Biol 99:1696–705
Marco F, Milena F, Gianluca G, Vittoria O (2005) Peri-implant osteogenesis in health and

osteoporosis. Micron 36:630–44. doi: 10.1016/j.micron.2005.07.008
Maruyama T (2011) [Development of the skeletal system in utero]. Clin Calcium 21:1299–305. doi: CliCa110912991305
Mason DJ, Huggett JF (2002) Glutamate transporters in bone. J Musculoskelet Neuronal Interact 2:406–14
Mason DJ, Suva LJ, Genever PG, et al (1997) Mechanically regulated expression of a neural glutamate transporter in bone: A role for excitatory amino acids as osteotropic agents? Bone 20:199–205. doi: 10.1016/S8756-3282(96)00386-9
Matsugaki A, Isobe Y, Saku T, Nakano T (2015) Quantitative regulation of bone-mimetic, oriented collagen/apatite matrix structure depends on the degree of osteoblast alignment on oriented collagen substrates. J Biomed Mater Res Part A 103:489–499. doi: 10.1002/jbm.a.35189
Meyer U, Joos U, Mythili J, et al (2004) Ultrastructural characterization of the implant/bone interface of immediately loaded dental implants. Biomaterials 25:1959–1967. doi: 10.1016/j.biomaterials.2003.08.070
Morelli F, Lang NP, Bengazi F, et al (2015) Influence of bone marrow on osseointegration in long bones: an experimental study in sheep. Clin Oral Implants Res 26:300–306. doi: 10.1111/clr.12487
Müeller W-D, Gross U, Fritz T, et al (2003) Evaluation of the interface between bone and titanium surfaces being blasted by aluminium oxide or bioceramic particles. Clin Oral Implants Res 14:349–56
Nakano T, Kaibara K, Tabata Y, et al (2002) Unique alignment and texture of biological apatite crystallites in typical calcified tissues analyzed by microbeam X-ray diffractometer system. Bone 31:479–87
Noble BS, Stevens H, Loveridge N, Reeve J (1997) Identification of apoptotic changes in osteocytes in normal and pathological human bone. Bone 20:273–82
Norton M (2013) Primary stability versus viable constraint--a need to redefine. Int J Oral Maxillofac Implants 28:19–21
O'Brien FJ, Taylor D, Lee TC (2005) The effect of bone microstructure on the initiation and growth of microcracks. J Orthop Res 23:475–480. doi: 10.1016/j.orthres.2004.08.005
Osborn J, Newesley H (1980) Dynamics aspects of the implant bone interface. In: Heimke G (ed) Dental implants - Materials and Systems, Carl Hanse. München, pp 111–123
Parfitt AM (1994) Osteonal and hemi-osteonal remodeling: the spatial and temporal framework for signal traffic in adult human bone. J Cell Biochem 55:273–86. doi: 10.1002/jcb.240550303
Park JY, Gemmell CH, Davies JE (2001) Platelet interactions with titanium: modulation of platelet activity by surface topography. Biomaterials 22:2671–82
Petrie CS, Williams JL (2005) Comparative evaluation of implant designs: influence of diameter, length, and taper on strains in the alveolar crest. A three-dimensional finite-element analysis. Clin Oral Implants Res 16:486–94. doi: 10.1111/j.1600-0501.2005.01132.x
Piattelli M, Scarano A, Paolantonio M, et al (2002) Bone response to machined and resorbable blast material titanium implants: an experimental study in rabbits. J Oral Implantol 28:2–8. doi: 10.1563/1548-1336(2002)028<0002:BRTMAR>2.3.CO;2
Raghavendra S, Wood MC, Taylor TD, et al (2005) Early wound healing around endosseous implants: a review of the literature. Int J Oral Maxillofac Implants 20:425–31. doi: 10.1016/S0084-3717(08)70105-3
Riggs CM, Lanyon LE, Boyde A (1993) Functional associations between collagen fibre orientation and locomotor strain direction in cortical bone of the equine radius. Anat Embryol (Berl) 187:231–8
Rodan GA, Harada S (1997) The missing bone. Cell 89:677–80
Rossi F, Lang NP, De Santis E, et al (2014a) Bone-healing pattern at the surface of titanium

implants: an experimental study in the dog. Clin Oral Implants Res 25:124–131. doi: 10.1111/clr.12097
Rossi F, Lang NP, De Santis E, et al (2014b) Bone-healing pattern at the surface of titanium implants: an experimental study in the dog. Clin Oral Implants Res 25:124–131. doi: 10.1111/clr.12097
Rubin CT, Lanyon LE (1987) Kappa Delta Award paper. Osteoregulatory nature of mechanical stimuli: function as a determinant for adaptive remodeling in bone. J Orthop Res 5:300–10. doi: 10.1002/jor.1100050217
Salvi GE, Bosshardt DD, Lang NP, et al (2015) Temporal sequence of hard and soft tissue healing around titanium dental implants. Periodontol 2000 68:135–152. doi: 10.1111/prd.12054
Salvi GE, Lang NP (2001) Changing paradigms in implant dentistry. Crit Rev Oral Biol Med 12:262–72
Sasaki M, Kuroshima S, Aoki Y, et al (2015) Ultrastructural alterations of osteocyte morphology via loaded implants in rabbit tibiae. J Biomech 48:4130–4141. doi: 10.1016/j.jbiomech.2015.10.025
Scala A, Botticelli D, Faeda RS, et al (2012) Lack of influence of the Schneiderian membrane in forming new bone apical to implants simultaneously installed with sinus floor elevation: An experimental study in monkeys. Clin Oral Implants Res 23:175–181. doi: 10.1111/j.1600-0501.2011.02227.x
Schenk RK, Buser D (1998) Osseointegration: a reality. Periodontol 2000 17:22–35
Schroeder A, Pohler O, Sutter F (1976) [Tissue reaction to an implant of a titanium hollow cylinder with a titanium surface spray layer]. Schweizerische Monatsschrift fur Zahnheilkd = Rev Mens suisse d'odonto-stomatologie 86:713–27
Schroeder A, Stich H, Straumann F, Sutter F (1978) [The accumulation of osteocementum around a dental implant under physical loading]. Schweizerische Monatsschrift fur Zahnheilkd = Rev Mens suisse d'odonto-stomatologie 88:1051–8
Schroeder A, van der Zypen E, Stich H, Sutter F (1981) The reactions of bone, connective tissue, and epithelium to endosteal implants with titanium-sprayed surfaces. J Maxillofac Surg 9:15–25
Sela MN, Badihi L, Rosen G, et al (2007) Adsorption of human plasma proteins to modified titanium surfaces. Clin Oral Implants Res 18:630–8. doi: 10.1111/j.1600-0501.2007.01373.x
Shalabi MM, Gortemaker A, Van't Hof MA, et al (2006) Implant surface roughness and bone healing: a systematic review. J Dent Res 85:496–500. doi: 10.1177/154405910608500603
Skedros JG, Bloebaum RD, Mason MW, Bramble DM (1994a) Analysis of a tension/compression skeletal system: possible strain-specific differences in the hierarchical organization of bone. Anat Rec 239:396–404. doi: 10.1002/ar.1092390406
Skedros JG, Mason MW, Bloebaum RD (1994b) Differences in osteonal micromorphology between tensile and compressive cortices of a bending skeletal system: indications of potential strain-specific differences in bone microstructure. Anat Rec 239:405–13. doi: 10.1002/ar.1092390407
Skerry TM, Bitensky L, Chayen J, Lanyon LE (1989) Early strain-related changes in enzyme activity in osteocytes following bone loading in vivo. J Bone Miner Res 4:783–8. doi: 10.1002/jbmr.5650040519
Soriano P, Montgomery C, Geske R, Bradley A (1991) Targeted disruption of the c-src proto-oncogene leads to osteopetrosis in mice. Cell 64:693–702. doi: 10.1016/0092-8674(91)90499-O
Southam JC, Selwyn P (1970) Structural changes around screws used in the treatment of fractured human mandibles. Br J Oral Surg 8:211–221. doi: 10.1016/S0007-117X(70)80082-8
Spriano S, Yamaguchi S, Baino F, Ferraris S (2018) A critical review of multifunctional titanium

surfaces: New frontiers for improving osseointegration and host response, avoiding bacteria contamination. Acta Biomater 79:1–22. doi: 10.1016/j.actbio.2018.08.013

Staedt H, Palarie V, Staedt A, et al (2017) Primary Stability of Cylindrical and Conical Dental Implants in Relation to Insertion Torque—A Comparative Ex Vivo Evaluation. Implant Dent 26:250–255. doi: 10.1097/ID.0000000000000531

Steigenga J, Al-Shammari K, Misch C, et al (2004) Effects of Implant Thread Geometry on Percentage of Osseointegration and Resistance to Reverse Torque in the Tibia of Rabbits. J Periodontol 75:1233–1241. doi: 10.1902/jop.2004.75.9.1233

Takahashi N, Ejiri S, Yanagisawa S, Ozawa H (2007) Regulation of osteoclast polarization. Odontology 95:1–9. doi: 10.1007/s10266-007-0071-y

Takayanagi H (2007) Osteoimmunology: shared mechanisms and crosstalk between the immune and bone systems. Nat Rev Immunol 7:292–304. doi: 10.1038/nri2062

Terheyden H, Lang NP, Bierbaum S, Stadlinger B (2012) Osseointegration - communication of cells. Clin Oral Implants Res 23:1127–1135. doi: 10.1111/j.1600-0501.2011.02327.x

Traini T, Degidi M, Caputi S, et al (2005a) Collagen Fiber Orientation in Human Peri-Implant Bone Around Immediately Loaded and Unloaded Titanium Dental Implants. J Periodontol 76:83–89. doi: 10.1902/jop.2005.76.1.83

Traini T, Degidi M, Strocchi R, et al (2005b) Collagen fiber orientation near dental implants in human bone: do their organization reflect differences in loading? J Biomed Mater Res B Appl Biomater 74:538–46. doi: 10.1002/jbm.b.30245

Traini T, Neugebauer J, Thams U, et al (2009) Peri-implant bone organization under immediate loading conditions: collagen fiber orientation and mineral density analyses in the minipig model. Clin Implant Dent Relat Res 11:41–51. doi: 10.1111/j.1708-8208.2008.00086.x

Traini T, Pecora G, Iezzi G, Piattelli A (2006) Preferred Collagen Fiber Orientation in Human Peri-implant Bone After a Short- and Long-term Loading Period: A Case Report. J Oral Implantol 32:177–181. doi: 10.1563/285.1

van Oers RFM, Ruimerman R, Tanck E, et al (2008) A unified theory for osteonal and hemi-osteonal remodeling. Bone 42:250–259. doi: 10.1016/j.bone.2007.10.009

Verborgt O, Gibson GJ, Schaffler MB (2000) Loss of osteocyte integrity in association with microdamage and bone remodeling after fatigue in vivo. J Bone Miner Res 15:60–7. doi: 10.1359/jbmr.2000.15.1.60

Vivan Cardoso M, Vandamme K, Chaudhari A, et al (2015) Dental Implant Macro-Design Features Can Impact the Dynamics of Osseointegration. Clin Implant Dent Relat Res 17:639–45. doi: 10.1111/cid.12178

Warreth A, Polyzois I, Lee CT, Claffey N (2009) Generation of microdamage around endosseous implants. Clin Oral Implants Res 20:1300–1306. doi: 10.1111/j.1600-0501.2009.01808.x

Weinbaum S, Cowin SC, Zeng Y (1994) A model for the excitation of osteocytes by mechanical loading-induced bone fluid shear stresses. J Biomech 27:339–360. doi: 10.1016/0021-9290(94)90010-8

Wennerberg A, Albrektsson T (2009) Effects of titanium surface topography on bone integration: a systematic review. Clin Oral Implants Res 20:172–184. doi: 10.1111/j.1600-0501.2009.01775.x

Wolff J (1986) The Law of Bone Remodelling. Springer Berlin Heidelberg, Berlin, Heidelberg

Xiong J, Piemontese M, Onal M, et al (2015) Osteocytes, not osteoblasts or lining cells, are the main source of the RANKL required for osteoclast formation in remodeling bone. PLoS One 10:e0138189. doi: 10.1371/journal.pone.0138189

Yeo I-S (2014) Reality of dental implant surface modification: a short literature review. Open Biomed Eng J 8:114–9. doi: 10.2174/1874120701408010114

Yeo I-S, Han J-S, Yang J-H (2008) Biomechanical and histomorphometric study of dental implants

with different surface characteristics. J Biomed Mater Res B Appl Biomater 87:303–11. doi: 10.1002/jbm.b.31104

Zaidi M, Blair HC, Moonga BS, et al (2003) Osteoclastogenesis, bone resorption, and osteoclast-based therapeutics. J Bone Miner Res 18:599–609. doi: 10.1359/jbmr.2003.18.4.599

Zhang K, Barragan-Adjemian C, Ye L, et al (2006) E11/gp38 Selective Expression in Osteocytes: Regulation by Mechanical Strain and Role in Dendrite Elongation. Mol Cell Biol 26:4539–4552. doi: 10.1128/MCB.02120-05

Zizic TM, Marcoux C, Hungerford DS, et al (1985) Corticosteroid therapy associated with ischemic necrosis of bone in systemic lupus erythematosus. Am J Med 79:596–604

10. LIST OF FIGURES AND TABLES

10.1 List of figures

Figure 4.1 Schematic representation of the osteocyte trapped within lacunae in mineralized bone matrix "light blue" linked with surface cells "osteoblasts" through canaliculi. Image Adapted from Davies et al. (Davies 1998). 54
Figure 4.2 Illustration of a functional active osteoclast. Mature osteoclasts are large multi-nucleated cells that cover a big area on the bone to degrade the bone matrix. The apical membrane faces the bone and the sealing zone generates an isolated region. A ring of aggregated F-actin assures the strong attachment of the osteoclast to its substrate. The resorptive area is acidified by secretion of HCL to demineralize the bone matrix. Organic components are degraded by Cathepsin K. Osteoclasts express tartrate-resistant acid phosphatase (TRAP), which is commonly used as a marker for osteoclasts. Image adapted from (Kubatzky et al. 2013). 56
Figure 4.3 Osteoconduction is mainly influenced by the titanium surface treatment. Thus, depending of the degree of roughness, may capable to retain in more or less extent the blood clot and consequently the stabilization of fibrin matrix (yellow fibers) toward the implant surface after platelets (purple spheres) activation. This fibrin matrix does work as a provisional extracellular matrix, that encourages the cell migration, releasing growth factors, fomenting the angiogenesis. .58
Figure 4.4 The "De Novo" bone formation. (a) Organic matrix secreted by osteoblast without collagen fiber, but rich in bone sialoproteins such osteopontin (OPN) and proteoglycans; OPN is secreted by immune cells like T lymphocytes, macrophages and monocytes. It is early expressed by osteoprogenitors cells, their presence is linked to pre-osteoblast differentiation. The proteoglycans is a fundamental component of extracellular matrix, it "fills" the intercellular spaces, and there are involved with Ca+ cations union and forms complex links with other proteins as type I collagen. (b) Ca+ ions nucleation. (c) Collagen synthesis, it is ensembled as woven bone, although at this instance collagen fibers are not completely mineralized. (d) Collagen mineralization, arose the cement line, that differentiate the mineralized from non-mineralized compartment, evidenced by cement line. Adapted from Davies and Hosseini 2000. 59
Figure 5.1 Randomization and allocation concealment scheme. 67
Figure 5.2 Ticare Inhex® (a): the implant body had a little conicity and a large area of micro-threads at the coronal portion, and higher number of triangular threads per unit length and with little thread depth compared to Quattro® model. Moreover, the implant had a double self-tapping at the apical portion. **Ticare Inhex Quattro® (b):** the implant body had a marked conicity. Fewer micro-threads at the coronal portion and a lower number of macro-threads were present compared to Ticare Inhex® implants. The threads were squared in the middle part of the implant and become triangular and deeper at the apex. Aggressive self-tapping at the apex. 68
Figure 5.3 Surgical procedures in rabbit tibia. (a) Surgical flap debridement. (b) Implant bed drilling at diaphysis (D) and metaphysis sites (M). (c) Implant inserted within implant bed. (d) Topographic sites used for implantation. (e) Implant installed and cover screw placement. 69
Figure 5.4 Ground section of rabbit tibia in diaphysis position at 4 weeks of healing. The implant is divided in 3 equal sections (coronal, middle, apical) for BIC measurement. Two points were traced: (B) Most coronal part of bone to implant contact. (A) Base of the implant. The Implant surface outside to the cortical bone is not considered in analysis (red arrows). Original magnification x2. Toluidine blue staining. 71
Figure 6.1 Optical micrograph of woven bone (WB) in a rabbit model at 2 weeks of healing. The image depict an uncontrolled and disorganized bone growth as consequence of organic bone matrix (OBM) deposition by osteoblast, note the irregular distribution of fibrous matrix in a diffuse woven bone and the presence of some osteocytes embedded within lacunae (L). Toluidine blue staining. .75
Figure 6.2 Optical micrograph at 2 weeks in-vivo in a rabbit model. It is observed the non-mineralized woven bone (WB) within healing chamber, also some osteoblast (cube-shaped cells)

secreting organic bone matrix perceived by the light blue color (OBM) and some lacunae in the proximity (L) suggesting the presence of osteoblast trapped in bone matrix to become converted as osteocytes. The image depicted at this stage suggesting a high activity of the cellular content. Toluidine blue staining.....76
Figure 6.3 Optical micrograph at 2 weeks of healing in a rabbit model. It could be appreciated how the bone-implant interface, advert visually a mechanical interlocking between parent bone of implant site and implant surface, responsible for the primary stability. At this period the presence of a microcrack (MC) in proximity to implant thread (yellow arrow), as well as old bone particles (BP) within healing chamber, shed light that yield of bone strength overpass the physiological limit due to the high stress in this area. It is denoted by an active remodeling establishment within healing chamber and microcrack proximity (red arrow), compatible with an interfacial bone remodeling. Toluidine blue staining.....76
Figure 6.4 Optical micrographs at 4 weeks in-vivo in a rabbit model, it is observed how the woven bone (WB) is progressively replaced by a more organized lamellar bone (LB) surrounding primary osteonic structures (O), also some osteoblast (cube-shaped cells) secreting organic bone matrix within osteon lumen in a circumferential manner. There are some lacunae within lamellar bone distributed in concentric manner. Toluidine blue staining.....77
Figure 6.5 Optical micrograph at 4 weeks of healing in a rabbit model. It is evident a remodeling across healing chambers, remodeling sites occurs in the proximity of microcracks (red arrows). The resorbed area will be replaced by woven (WB) bone which reestablishes the contact to implant surface (secondary stability), subsequently to arise the will be the new primary osteons (O) with some osteocytes trapped within lacunae (L). Tissue remodeling has occurred at the interface where cell-mediated processes resorbed the region encompassed between the green dashed line and the implant. Toluidine blue staining. 77
Figure 6.6 Optical micrographs at 8 weeks in-vivo in a rabbit model. **(a)** The bone remodeling still occurs within healing chamber in the proximity of implant surface, it is denoted by the presence of woven bone (WB) with some osteoblasts (OB) depositing organic bone matrix (OBM) characterized by a light blue staining, and lacunae (L) with trapped osteocytes. The WB is surrounded by lamellar bone showing primary osteonic structures (O) which revealed that onset of woven bone remodeling toward lamellar configuration surrounding blood vessels, outlined by reversal "cement lines" (CL) that differentiate the mineralized from non-mineralized compartment. **(b)** It could be clearly observed the presence of primary and secondary osteonic structures (O) with their owns haversian´s system canals (HVS). At this stage the mature bone its capable to resist load bearing. Toluidine blue staining.....78
Figure 6.7 Optical micrograph at 8 weeks in-vivo in a rabbit model. It is evidenced a mixed bone morphology with regions of woven (WB) characterized by a "more intense" staining color and lamellar bone (LB) "less intense" staining color, surrounding osteonic structures (O). There is a new bone formation in contact implant surface (IS) at expense of lamellar bone remodeling, it is visible the presence of osteocytes in LB (black asterisk) and trapped in lacunae's (L) as well, behind the organic bone matrix (OBM) deposition by osteoblast cells (OB) disposed circumferentially within osteon lumen (yellow arrow), and denoted by the light blue color (red arrow). Toluidine blue staining. 79
Figure 6.8 Optical micrograph of the lamellar bone (LB) in a rabbit model at 8 weeks of healing. The histological image showed remodeling units "osteons" showing concentric layers of lamellae (LL) around a Haversian canals (HVC) (vascular support). 79
Figure 6.9 The total amount of new bone and old bone (**a**) and BIC values (new+old) according to implant implant macro designs, Ticare Inhex or Ticare Quattro (**b**) at different healing periods. Significant differences between implant macro-designs (*); ($p < 0.05$). 80

Figure 6.10 The total amount of new bone and old bone (**a**) and BIC values (new+old) according to implant position (diaphysis or metaphysis) at different healing periods. Significant differences between implant macro-designs (*) and between diaphysis and metaphysis (**); ($p < 0.05$). 82
Figure 6.11 BIC values for both macro-designs according implantation site (diaphysis or metaphysis), to visually appreciate the interaction (Design*Position). 87
Figure 6.12 The total amount of new bone, marrow content, and old bone according to cortical (**a**) and marrow (**b**) compartment for implants placed via either diaphysis (n = 9) or metaphysis (n = 9) at different healing periods. Mineralized bone to implant contact (new + old) for cortical (**b**) and marrow (**d**) compartments at the various healing times. $p < 0.05$; between cortical and marrow compartments at metaphysis sites (*), at diaphysis sites (**) or (#) between diaphysis and metaphysis within cortical and marrow compartments and (***) for mineralized bone to implant contact, respectively. Comparisons are based on the same healing stage in weeks (w). 90
Figure 6.13 Ground section of bicortically-installed implants (Ticare Inhex® , Mozo Grau, Valladolid, Spain) at diaphysis (left side) and metaphysis (right side) sites at two (**a**,**b**), four (**c**,**d**) and eight (**e**,**f**) weeks of healing. An original magnification of ×2.5 and toluidine blue staining was used. 91

10.2 List of tables

Table 6.1 Summary of proportion (%) of tissues components assessed in contact with the implant surface for both implant macro-designs at the various time periods, n = 9 per each period of healing. 81
Table 6.2 Summary of proportion (%) of bone to impant contact (BIC) of implant macro-designs at the various time periods. n = 9 per each period of healing. 81
Table 6.3 Summary of proportion (%) of tissues components assessed in contact with the implant surface according topographic location at the various time periods. n = 9 per each period of healing. 83
Table 6.4 Summary of proportion (%) of bone to impant contact (BIC) according topographic location at the various time periods. n = 9 per each period of healing. 83
Table 6.5 Summary of proportion (%) of tissues components according implant macro-designs regarding topographic site, (n = 9) per each period of healing. 86
Table 6.6 Proportion (%) of tissue components in contact with the implant surface for either the cortical or the marrow bony compartments at the various time periods in weeks (w). n = 9 per each period of healing. 89
Table 6.7 Summary of proportion (%) of bone to impant contact (BIC) according cortical and marrow compartments and topographic location at the various time periods. n = 9 per each period of healing.....90

11. SCIENTIFIC PUBLICATIONS

11.1 Scientific documents derived from the present thesis

- Soto-Peñaloza D, Caneva M, Viña-Almunia J, Martín-de-Llano JJ, Peñarrocha-Oltra D, Peñarrocha-Diago M. Bone-Healing Pattern on the Surface of Titanium Implants at Cortical and Marrow Compartments in Two Topographic Sites: an Experimental Study in Rabbits. Materials (Basel). 2018 Dec 27;12(1). pii: E85.doi: 10.3390/ma12010085.

- Soto-Peñaloza D, Caneva M, Viña-Almunia J, Martin-de-Llano JJ, García-Mira B, Peñarrocha-Oltra D, Botticelli D, Peñarrocha-Diago M. Effect on osseointegration of two implant macro-designs:A histomorphometric analysis of bicortically installed implants in different topographic sites of rabbit's tibiae. Med Oral Patol Oral Cir Bucal. 2019 Jul 1;24(4):e502-e510. doi: 10.4317/medoral.22825.

12. ENGLISH ABSTRACT

12. ABSTRACT

Scientific background and study aims

The use of dental implants as an alternative for mouth rehabilitation has proven its efficacy showing high survival rates. A key aspect of dental implant osseointegration is related to adequate primary stability, ensured by the mechanical interlocking at the bone to implant interface and depends in part by the implant geometry, surface roughness and surgical technique for implant bed preparation. Several factors are involved in the interaction between the implant surface and the surrounding parent bone during osseointegration. One of them is the implant macro-design, that may provide different shear stress depending on the bone density of the insertion site. According to its features, implant macro-design could affect in more or less extent on the stress yielded on bone, triggering a host response inducing vascular and cellular events, that cause a cell mediated interfacial bone remodeling. It consists of the resorption of mineralized bone “cortical bone” and consequently a "primary stability dip", that concurs simultaneously with a new bone apposition towards the implant surface as an increase of the biologic- “secondary stability”. Different implant thread designs and thread pitches were proposed to improve the osseointegration. In this sense implant geometry prove to affect the bone-to-implant contact (BIC) values. Modified macro-geometry and different microgeometries of implants has shown to have a stimulatory effect on osseointegration, suggesting its features should be made related to the biological and mechanical micro-environment. Moreover, other features such as the healing chamber design and apical configurations have proven to improve osseointegration.

Dental implants macro-design often are supplemented with titanium surface modification in such a way to improve their bioactivity and clot retention capacity during bone healing. These modifications increase the three-dimensional surface area and confer different topographical characteristics for cell homing. The surface roughness is quantified and reported as Ra or Sa, depending on if the parameter is classified as two-dimensional or three-dimensional respectively. It provide an enhanced activation of platelets, cell adhesion and protein adsorption toward implant surface, with effects on osseointegration process in terms of BIC and implant stability during early healing stages, through an increase of osteogenic activity and osteoconductivity of titanium. Several methods for implant surface treatments (e.g., etched surfaces, sandblasted and acid etched surfaces, hydroxyapatite-coated surfaces, grit-blasted surfaces, laser ablation, fluoride treatment) have been proposed. Among them, the resorbable blasted media (RBM) surface is obtained through the grit-

blasting of calcium phosphate bioceramic (CaP) particles at high velocity, in which the particle size determines the roughness degree as a particle-free titanium surface. The RBM surfaces showed BIC values that were comparable to other blasting surfaces, such as titanium dioxide (TiO2) or aluminum oxide (Al2O3) and similar biomechanical strength and removal torque measurements were obtained by calcium- and magnesium- enhanced implants.

Recent evidence reinforces the concept that the implant geometry and the density of the bone are key factors involved in the degree of primary stability. However, osseointegration is strongly influenced by the implant surface, which plays a role during the early phase of healing through resorptive and appositional events.

At this regard, different topographic sites confer different healing patterns, such as occurring at the cortical and the marrow compartments at both flat- (dog jaw) and long- bones (sheep tibia). This behavior is observed in rabbit tibiae as well, and despite inherent experimental model differences, the effects of equal implant geometries have been tested, but at different implant surface modifications, and evidencing the effect of surface treatment on the BIC values reached. Therefore, it is presumable that both the cortical and marrow compartments provide distinct biological and physical features at bone-to-implant interfacial remodeling and direct bone apposition toward the implant surface. Their nature demarcates the transition from primary to secondary/biological stability after an implant stability dip in the osseointegration process. However, there is a scarcity of data based on bi-cortically placed dental implants with different macro-designs and equal surface roughness, and a lack of studies regarding bone-healing pattern on implant surfaces at different bone compartments and bone environments are still missing.

Based on the above mentioned aspects, and the gap of information at this regard, the general aim of this thesis was a more consistent understanding of osseointegration values (new bone, old bone, bone marrow and BIC [new bone + old bone]) of two different implant macro-designs, with equal RBM surface treatment in different topographic sites in rabbit tiabiae (diaphysis or metaphysis). Thus, the following objectives were disaggregated from this primary objective, to exploit in more detail the study sample, as shown below:

VI. To document the sequential healing during osseointegration of implants with RBM surface treatment at 2, 4 and 8 weeks in a rabbit model.

VII. To evaluate the effect of two different implant macro-designs on the sequential osseointegration values at 2, 4 and 8 weeks.

VIII. To evaluate the effect of different bone topographic site of rabbit´s tibiae on osseointegration process.

IX. To evaluate the effect of implant macro-design regarding the topographic site at rabbit`s tibiae, on osseointegration.

X. To evaluate the bone-healing pattern at the cortical and marrow compartments in the diaphysis and metaphysis of rabbit´s tibiae.

Material and methods

The study protocol was approved by the Ethics Committee of Valencia University, Valencia, Spain (Protocol ref.: A1432625410189), which followed the guidelines established by the Council Directive of the European Union (53/2013; February 1, 2013) for animal care and experimentation in agreement with the ethical and legal conditions established by Royal Decree 223, March 14 and October 13, 1988.

-*Study design*

A experimental pre-clinical study involved twenty-seven males, albino New Zealand rabbits, 24 weeks of mean age and weighing 3–4 kg. The animals were segmented into three groups composed of 9 animals each and sacrificed at 2, 4 and 8 weeks, respectively. Implants were put into the animals in a random allocation, a resulting in the imposition of four dental implants in each rabbit; two in each tibia, one in the diaphysis, and the other in the metaphysis. Before surgery, the animals were put in one of the three groups by random allocation, each group representing a healing period. Two implants each with a different macro-design were installed in each tibia. The position of each implant, i.e., the diaphysis or metaphysis, was randomly assigned. The aleatory choice was carried out electronically (www.randomization.com) by an independent author neither involved in the selection of the animals nor in the surgical procedures. Two distinct implant macro-designs were used, Ticare® implants (Mozo-Grau, Valladolid, Spain) made of commercially available pure grade-IV titanium treated with resorbable blast media (RBM) (implant surface blasted with calcium phosphate bioceramics particles, resulting in a moderately rough (Ra = 1.53 ± 0.24) surface) were used. All implants had a dimension of 3.75 mm of diameter and 8 mm of length and a conical connection with a 45° polish neck with a self-tapping feature closer to the apex.

Ticare Inhex® : the implant body had a little conicity and a large area of micro-threads at the coronal portion, and higher number of triangular threads per unit length and with little thread depth compared to Quattro® model. Moreover, the implant had a double self-tapping at the apical portion.

Ticare Inhex Quattro® : the implant body had a marked conicity. Fewer micro-threads at the coronal portion and a lower number of macro-threads were present compared to Ticare Inhex®

implants. The threads were squared in the middle part of the implant and become triangular and deeper at the apex. Aggressive self-tapping at the apex.

-Clinical procedures

The rabbits were anesthetized with intramuscular injection of Ketamine (22mg/kg) and xylazine (2.5 mg/kg) were administered at 50% and intravenous injection of Propofol (1.5mg/kg) and maintained with 2% of isoflurane. Before surgery, the skin at the proximal tibia was shaved and disinfected with Betadine. A preoperative antibiotic Enrofloxacin 5mg/Kg (ALSIR® 2,5%, Esteve Veterinaria, Barcelona, Spain) was administered subcutaneously, and 3 ml of articaine at 2% with 0.01 mg/ml epinephrine infiltrative anesthesia was also administered intramuscularly in the surgical area of each leg. The skin of both tibiae was incised in the proximal region (Fig. 1c). Two experimental sites were identified in each tibia (Fig. 1d). The recipient sites were prepared using drills with increasing diameter under irrigation with sterile saline according manufacturer. A distance of about 8-10 mm was maintained between the two osteotomies. Two implants with different macro-design were randomly installed in each tibia, and were screwed until the implant shoulder was leveled with the bone surface. The apex of the implants was placed in close contact with or into the cortical bone opposing the coronal cortical compartment, aiming to obtain a bicortical anchorage. The cover screws were placed on the implants, and the flaps were subsequently sutured in layers with resorbable sutures to allow a submerged healing (Vicryl 5/0, Ethicon, Sommerville, NJ, USA), and Nylon 3/0 (Ethilon 3/0, Ethicon, Sommerville, NJ, USA).

-Pre- and Post-operative care, housing and husbandry

All animals were kept in individual cages during its acclimatization period before intervention (2 weeks) and during post-operative care at the Animal Room Service Unit, University of Valencia, Spain, in purpose-designed and acclimatized rooms at 21ºC with 12 h dark/light ambiance. The animals were fed with a standard diet and had free access to water. The analgesic pattern consisted in 2.5mg/kg of morphine intraoperative, 0.02 mg/kg buprenodale, buprex, 0.2 mg/kg meloxicam (every 12 hours during 3 days) and antibiotic therapy with Enrofloxacin 2.5 mg/Kg (ALSIR® 2,5%, Esteve Veterinaria, Barcelona, Spain) (every 24 hours during 7 days) post-operatively.

-Euthanasia

Nine rabbits of each three groups were euthanized after 2, 4 and 8 weeks, respectively. The same sedation and anesthesia protocols, such as for the surgery, were applied and the euthanasia induction was performed with 50mg/kg intravenous sodium pentobarbital. A small electric saw was used to obtain the sections of the tibia containing each implant.

-Histological preparation

Implant samples were dehydrated by sequential solvent exchange and embedded in methyl methacrylate containing poly-(methyl methacrylate). After adding benzoyl peroxide (1 g/100 mL), samples were polymerized and were then sawed using a diamond wheel on a precision table top cut-off machine Accutom-5 (Struers, Copenhagen, Denmark) and then were wet ground and polished using a LaboPol-21 system (Struers, Copenhagen, Denmark) and SiC foils. Approximately 80 μm thin sections were obtained. The samples were stained at 55 °C with toluidine blue for 30 min, washed with tap water for 2 minutes and let dry.

-Histological examination

Overlapping calibrated digital images of the tissues surrounding the whole implant surface (about 20 images/implant) were recorded with a bright field Leica DM4000 B microscope (Leica Microsystems GmbH, Wëtzlar, Germany) and DFC420 digital camera using a 5× objective and the Leica Applications Suite version 4.4.0 software. Individual images were merged to compose each implant side using the Photoshop program (Adobe Photoshop CC 2015.0.0, Adobe Systems Incorporated, San José, CA, USA, http://www.adobe.com/Photoshop). The image processing program ImageJ 1.48 (National Institutes of Health, Bethesda, MD, USA; http://imagej.nih.gov/ij) was used for histological measurements. Lines were drawn by hand on calibrated images showed on the computer screen at a 400× magnification by an independent and calibrated assessor not involved in study. The BIC was evaluated as the sum of new and old bone, and percentages in relation to the length of the implant surface examined calculated. The apical portion of the implant that extruded beyond the compact cortical layer was excluded from the analyses.

-Data analysis

Differences between implant designs across the healing periods were analyzed with the Mann–Whitney U-test for independent variables. Differences between implants placed in the diaphysis and metaphysis were also performed using a Wilcoxon rank-sum test. A multivariate general lineal model analysis was performed to explore the interaction between the two independent variables (design/position) over BIC values at different healing stages. Each factor with two categories: design (Ticare Inhex® /Ticare Quattro®) and position (diaphysis/metaphysis). This approach was chosen because previous reports observed that the positions of the implants can be used as independent replicates regarding outcome variable, since bone quality varies between implantation sites (topographic sites) at same degree as between experimental units. The level of significance was set at α=0.05.

Results

To isolate the possible effect of implant macro-geometry on bone formation, both implants had the same surface treatment. In order to appreciate the behavior of both implant macro-designs in two different bone environment, they were placed in two topographic zones within the same tibia, one with a cortical layer and a medullar content (diaphysis) like a type II bone and the another more trabecular like a type III bone (metaphysis).

The purpose of the study was to evaluate the effect of two different implant macro-designs but equal surface roughness on the sequential osseointegration at bicortically installed implants in the rabbit tibia. Data of 27 experimental animals with four implants each were analyzed. The areas between the threads were filled with woven bone at two weeks. Remodeling processes were observed after 4 and 8 weeks of healing, as shown by the lighter-staining of the lamellar bone compared to the darker-staining of the woven bone.

At 2 weeks of healing a similar degree of new osseointegration was observed in both macro-designs, being 16.0±7.5% for Ticare Inhex® , and 16.3±7.2% for Quattro® implants. The old bone percentages observed were around 7.4% and 7.6% for Ticare Inhex® and Quattro® implants, respectively. Regarding implant position (diaphysis or metaphysis), there were no significant differences among the assessed parameters at this stage. Similar BIC values were observed between implant macro-designs and regarding topographic site placement being 23.5±14.4% and 23.9±13.3% for Ticare Inhex® and Quattro® implant designs, respectively. None of the differences for both macro-design and topographic sites was statistically significant.

At 4 weeks of healing, the values of new osseointegration at this time of healing were 19.4±7.3% and 18.9±4.7% for the Ticare Inhex® and Quattro® designs, respectively. Old bone percentages at this stage were 2.3±2.2% and 2.4±1.6%, respectively. Grouping the data according to the implant position in the diaphysis and metaphysis, there was no significant difference for new osseointegration (p=0.10). However, a significant difference found for old bone and soft tissue values at this stage. Similar BIC values (old + new bone) were observed between implant macro-designs, but regarding topographic site placement better BIC values for diaphysis 24,5±6,2% than metaphysis 18,4±7,7 % at this stage (p=0,05).

At 8 weeks of healing, the new bone increased, reaching percentages of 33.2±7.6% and 33.4±7.7% for Ticare Inhex® and Quattro® implant designs, respectively. No statistically significant differences were found between the two groups. Old bone was still present, however at very low percentages, being 1.2±1.1% and 3.3±1.1% for Ticare Inhex® and Quattro® designs, respectively (p=0.001). The new bone percentages in the diaphysis was 36.4±10.5% while in the

metaphysis was 29.3±6.2%. No statistically significant differences were found. The BIC values observed between implant macro-designs do not showed a significant difference, even though slight better BIC values in favor Ticare Quattro® compared to Inhex® design were found, being 36.7±7.7 % and 34.4±7.8, respectively. However, regarding the topographic site placement, a better BIC value for diaphysis (39.5±11.1%) than metaphysis sites (30.6±6.2%) ($p=0.05$) was seen at this stage of healing.

In the multivariate analysis it was observed that the implant position showed a statistical significance regarding BIC values at 4 and 8 weeks ($p<0.05$). However, the analysis fails to detect statistical significance for implant macro-designs and its interaction (design*position) over BIC values across healing stages. Is observed that Ticare Quattro® design showed a slight better BIC values at diaphysis sites across healing stages ($p>0.05$).

Another objective was to evaluate the bone-healing pattern at the cortical and marrow compartments at equal RBM surfaces of bicortically installed implants in the diaphysis and metaphysis of rabbit tibia. The bone healing stages follow the intramembranous-type and appositional ossification mode patterns. The latter could be observed where intimate contact between the implant surface and newly formed bone from the implant bed occurred. On average, better osseointegration values were identified in the cortical compartments, and slightly higher but no statistically significant values at the diaphysis sites. Regarding the marrow compartment, better apposition rates of new bone were observed at two and four weeks at the diaphysis sites.

At 2 weeks of healing, there were not significant differences among the parameters assessed between the cortical and marrow compartments in both the diaphysis and metaphysis sites. The BIC values were around 30 ± 9.9% versus 23.7 ± 6.4% for diaphysis and metaphysis sites respectively in the cortical compartment ($p=0.09$), and 21.1 ± 12.3 versus 13.9 ± 8.0 in marrow compartment ($p=0.07$).

At 4 weeks of healing, significant differences were observed for old bone at cortical compartment and for new bone and soft tissue in the marrow compartments between diaphysis and metaphysis sites. No differences were detected for BIC values in the cortical compartment that were around 25.4 ± 7.8% and 21.4 ± 8.0% for diaphysis and metaphysis sites, respectively ($p=0.26$). However, a significant difference was found in the marrow compartment, showing BIC values of 22.1± 6.9 and 13.6 ± 8.5 ($p=0.01$) for diaphysis and metaphysis sites, respectively.

At 8 weeks of healing, on average, better values for new and old bone were observed in the cortical compartment; a significant difference was detected between the cortical and marrow compartments for these parameters in metaphysis sites. The mineralized bone-to-implant contact at this stage did

not show significant differences within the cortical compartment between diaphysis and metaphysis implant sites, with BIC% values 41.1 ± 6.8% and 39.9 ± 9.8%, respectively (p=0.61). A similar trend was observed within the marrow compartments at diaphysis and metaphysis sites.

Discussion

Study outcomes

The main aim of the present doctoral dissertation was to assess the impact of two distinc implant macro-designs bicortically installed in two bone envirorments (diaphysis or metaphysis) within rabbit tibiae. Moreover, the bone healing patterns at cortical and marrow compartments in diaphysis and metaphysis sites were analyzed.

Summary of main findings

The study was performed with the aim of assessing the influence of macro-geometry on osseointegration. To isolate the possible effect of implant macro-geometry on bone formation, both implants had the same surface treatment. In order to appreciate the behavior of both implant macro-designs in two different bone environment, they were placed in two topographic zones within the same tibia, one with a cortical layer and a medullar content (diaphysis) like a type II bone and the another more trabecular like a type III bone (metaphysis). In the present study, the new bone regarding the topographic site of implantation after 2, 4 and eight weeks of healing, was found to be slightly higher, at the implants in the diaphysis compared to the metaphysis, but without reach statistical significance differences ($p>0.05$). The BIC values observed between implant macro-designs do not showed a significant difference, even though slight better BIC values in favor Ticare Quattro® compared to Inhex® design were found. However, regarding the topographic site placement, a better BIC value for diaphysis than metaphysis sites were seen at 4 and 8 weeks of healing ($p=0.05$). A multivariate general lineal model analysis was performed to explore the interaction between the two independent variables (design/position) over BIC values at different healing stages. It was observed that the implant position showed a statistical significance regarding BIC values at 4 and 8 weeks ($p<0.05$). However, the analysis fails to detect statistical significance for implant macro-designs and its interaction (design*position) over BIC values across healing stages. Is observed that Ticare Quattro® design showed a slight better BIC values at diaphysis sites across healing stages ($p>0.05$).

On the other hand, the bone-healing pattern at cortical and marrow compartments at diaphysis and metaphysis sites was studied. The new bone formation in the marrow compartment showed slightly better increasing values of 13.8%, 20.4, and 24.6% at two, four and eight weeks at diaphysis sites,

compared to 10.3%, 13%, and 25.1% at metaphysis sites. The same trend was observed in the cortical compartment with values around 17.8%, 21.4%, and 37% at diaphysis sites, and 15.1%, 19.7%, and 35.5% in metaphysis sites. The old bone was resorbed but was still present (<2%) after 1 month in both topographical zones. The parent old bone values observed were slightly higher in diaphysis implant sites at four and eight weeks compared to metaphysis sites in the present study sample. The BIC values not showed significant differences, except for marrow compartment at four weeks of healing, showing BIC values of 22.1± 6.9 and 13.6 ± 8.5 (p=0.01) for diaphysis and metaphysis sites, respectively.

Disscussion with previous literature

The histomorphometric analysis at either 2, 4 and 8 weeks were similar (P > 0.05) for both implant macro-designs. Moreover, comparing new bone percentages in relation to the topographic implant placement, after 4 and 8 weeks of healing, osseointegration was found to be slightly higher, but statistically not significant at the implants placed in the diaphysis compared to the metaphysis. These findings are contrary to those reported in a previous experiment in rabbits from Caneva et al. in 2017. Observations that could be attributable to several factors, such as the implant thread design, the surface treatment tested and the implant osteotomy protocols, differing between studies. It is known that these factors could regulate the strain applied to hard tissue in proximity to the implant. Old bone was resorbed, but was still present after 1 month of healing (<4%), with statistical significant better values in Quattro® group. This pattern of healing is in agreement with other studies performed in animals and humans. Noteworthy to mention, bone morphology in diaphysis is predominantly occupied by a marrow content in comparison to metaphysis that presents more trabecular bone. These findings are in agreement with the assumption that osseointegration is faster in zones where the bone apposition is not preceded by bone resorption as previous observed in a dog model by Abrahamsson et. al in 2003 and confirmed in miniature pigs by Buser et al. in 2004. It appears likely that bone formation started from the cortical compartments (in contact with mineralized parent bone) and, subsequently, proliferated toward into the marrow compartments. It is known that resorptive processes occur before new bone apposition in zones where the mineralized bone is present, conveying a slightly longer healing period to reach complete osseointegration.

The implants in the present study were in close contact to pristine bone due to its bicortically stabilization, a condition that favors osseointegration on the implant surface. A pattern of healing that were documented for osseointegration in different pre-clinical models. The parent old bone in

recipient site is responsible of mechanical interlocking, and thereafter it is relevant during implant stability dip, where takes place a cell mediated interfacial bone remodeling. This is typically described to occur in the area of contact between the pristine bone wall and implant surface, where remodeling arise in the proximity of microcracks followed by bone apposition in void spaces resulting in secondary stability.

The results from the present study are in agreement with other studies such as Leonard et al. in 2009; that showed that macro-design did not significantly affect the BIC rates under the absence of loading conditions. However, the scientific literature does not differentiate the discrepancies regarding implant positioning within rabbit tibiae, a factor that may probably contribute to results due to the different bone density. At this regard, a previous report suggests that implant macro-design features, such thread pattern and thread pitch, can be responsible for differences in the amount of bone and degree of apposition toward the implant surface. Therefore, consideration of specific implant macro-design should be made relative to the biological and mechanical microenvironment, as suggested by Vivan-Cardoso et al. in 2015.

In keeping with the observations mentioned above, the healing pattern at cortical and marrow compartments was further analyzed in the two bone environments (diaphysis and metaphysis) within rabbit tibiae. Indeed, in the present study, the new bone formation in the marrow compartment showed slightly better increasing values at diaphysis implantation sites, values of 13.8%, 20.4, and 24.6% at two, four and eight weeks at diaphysis sites, compared to 10.3%, 13%, and 25.1% at metaphysis sites. The same trend was observed in the cortical compartment with values around 17.8%, 21.4%, and 37% at diaphysis sites, and 15.1%, 19.7%, and 35.5% in metaphysis sites. Is observed that parent old bone values observed were slightly higher in diaphysis implant sites at four and eight weeks compared to metaphysis sites in the present study sample. In the context of topographic sites of implantation, our results found to be contradictory to those reported in a previous study from Caneva et al. in 2017, where the new bone formation developed at a much higher speed at the implants placed in the metaphysis that those in the diaphysis. Though, these differences could be attributable to various factors, as mentioned previously. The authors attributed the findings to the denser pattern of the trabecular bone in the metaphysis compared to the diaphysis tibiae, an event that may have empowered osseointegration. On the other hand, the bone formation that was supposed to be reinforced by the bone marrow did not work out, since this scarcely contributed to its formation in the middle section of the implants placed in the diaphysis compared to what was found in the coronal and apical sections.

Methodological differences could be mentioned for this aspect; In the study of Caneva et al. in 2017, there were demarcated three sections (coronal, middle, and apical) to test the differences among compartments in the rabbit tibiae. In the present study, the three sections were demarcated in the same manner, but the cortical compartment is considered as the sum of the cortical and apical regions as a whole, independently of the marrow compartment (middle). Although, in both studies, the extreme regions of the implants were in close contact with pristine bone due its bicortical stabilization.

On the other hand, it is possible to conclude that osseointegration seems to be favored by the existence of a blood clot, and prejudicated by the presence of the yellow fatty bone marrow in the long bone model, such as sheep tibiae. In this sense, Morelli et al. in 2014 employed the sheep tibia model, where two osteotomies for implant installation are prepared in each tibia. At the control sites, no further treatments were performed while, at the test sites, bone marrow was removed from the osteotomy site with a curette to an extent that exceeded the implant dimensions. As a result, the apical portion of the implants at the control sites was in contact with bone marrow while, at the test sites, it was in contact with the blood clot. On average, new bone apposition was better in the cortical compartment, as seen in the present study. Moreover, it was observed that new bone apposition was faster in the fatty bone marrow group compared to blood clot groups at marrow compartments after 4 weeks but without reach statistical significance. However, these authors further concluded that osseointegration appeared to be favored by blood clots, because at 12 weeks of healing the test group showed better new bone values, statistically significant only at the marrow compartment, even though in this study the implants were not placed bicortically. However, despite inter-species differences impeding direct comparisons.

Efforts, limitations and recommendations for future search

This study was conducted in agreement with ARRIVE guidelines that encourages the good practices and quality of reporting in experimental animals. The novelty of the present work lies in the fact that there is no other study aiming to assess the impact of distinct implant macro-designs with equal moderately-rough RBM surface treatment in two different bone environments onto the osseointegration values and the healing patterns at the cortical and marrow compartments within the same rabbit tibiae. This allows us to isolate the macro-design effects on osseointegration, thus helping us separately evaluate the dynamics of the healing pattern in distinct bone densities. However, due to the absence of functional load, these parameters reflect the structural connection between implant and bone, and not the functional properties of the bone to implant interface.

There is scarce pre-clinical evidence regarding sequential healing of bicortically installed implants with two macro-designs and equal surface treatment, attempting to assess its interaction in two topographic sites. Despite that the interaction of factors was assessed, only the topographic site seems to contribute to values at 4 and 8 weeks. Regrettably, it is difficult to determine to which extent each implant macro-design contributes to these findings observed at the diaphysis or metaphysis sites. The scarce sample did not permit a proper statistical comparison. Note to mention, the findings of the interaction are merely exploratory and should be interpreted with caution. Thus, more studies are needed to explore the impact of different macro-designs with equal surface roughness of different manufacturing methods (e.g. SLA, anodized, etc) on osseointegration in rabbit model, and considering the impact of loading conditions. Also, there is no certain data on the extent to which the rabbit tibia model, in its diaphysis or middle shaft, provides amounts of fatty bone marrow that may affect osseointegration after eight weeks of healing. Thus, it would be of interest to isolate its effect in a further study in the rabbit tibia model. Further studies are warranted with a greater sample size to answer these aspects, but this is a tough challenge, taking into consideration the ethical and economic aspects that may be involved in consideration of the replacement, refinement, or reduction (3Rs) criteria for the use of animals in research.

Conclusions

In summary this thesis concluded that:

I. The sequential osseointegration pattern of RBM surfaces is successful in the rabbit model.

II. The implant macro-designs does not significantly affect the osseointegration process in the absence of loading across healing stages.

III. Bone morphometry and density may affect the bone apposition onto the implant surface. The apposition rates were slightly better in diaphysis compared to metaphysis topographic sites. The BIC values were significantly higher at 4 and 8 weeks in diaphysis sites.

IV. There is no interaction between implant macro-design and topographic site as shown by the multivariate analysis. Though, it was observed that Ticare Quattro® implant macro-design showed a slightly better BIC values at diaphysis sites across the healing stages.

V. The new bone apposition was better in the cortical- compared to the marrow- compartment. The apposition rates were slightly better at both cortical and marrow compartments in diaphysis compared to metaphysis sites.